Propagation de fissures chargées en tension dans des matériaux fortement hétérogènes

Manish Vasoya

UNIVERSITÉ PIERRE ET MARIE CURIE

École Doctorale $n°391$ (SMAER)

Laboratoire FAST - l'Institut Jean le Rond d'Alembert

THESE

pour obtenir le titre de Docteur de l'Université Pierre et Marie Curie - Paris 6
Spécialité : **Mécanique**

présentée par

Manishkumar Laxmanbhai VASOYA

Study on Tensile Failure of Highly Heterogeneous Brittle Materials

Soutenue le November 27, 2014
devant le jury composé de Madame et Messieurs :

M. Mokhtar Adda-Bedia	Président
M. Christophe Josserand	Examinateur
Mme. Véronique Lazarus	Directrice de thèse
M. Jean-Baptiste Leblond	Co-directeur
M. Laurent Ponson	Co-directeur
M. Julien Réthoré	Rapporteur
M. Martin Shanahan	Membre invité
M. Damien Vandembroucq	Rapporteur
M. John Willis	Examinateur

Dedicate to my teachers, my parents and Bindiya.

Acknowledgements

Working on this topic for the Ph.D. has been a wonderful and often overwhelming experience. It is hard to say whether is has been grappling with the topic itself which has been the real learning experience, or grappling with how to write papers, give talks, stay up until the birds start singing, and stay focus ...

In any case, I am indebted to many people for making the time working in my side during these enriching three years of my life with an unforgettable experience.

First and foremost, I would like to acknowledge my thesis advisors, Véronique Lazarus, Laurent Ponson and Jean-Baptiste Leblond. To work with you has been a real pleasure to me, with heaps of fun and excitement. You have been a steady influence throughout my Ph.D. career; you all have oriented and supported me with promptness and care, and have always been patient and encouraging in times of new ideas and difficulties. Véronique for your depth views on theory and mechanical aspects in numerical part and Laurent for yours on physical and experimental aspects and Prof. Leblond for your all inspiration and depth theoretical knowledge in this field.

I would like to thank the scientific jury members of my thesis: M. Adda-Bedia, C. Josserand, J.R. Willis, and especially J. Réthore and D. Vandembroucq who have reported their comments on the thesis. I would like to M. Shanahan being in the jury as invited member.

I would like to thank all the colleagues, professors, researcher and administrators at the "Institut Jean le Rond d'Alembert" and " Laboratoire FAST", where most of the work has been carried. In particular, I am deeply thankful to Prof. D. Kondo for providing a solution for extension of my work contact for last month. I would like to thanks all intern students of Laurent who working with me in the peeling experiments: Aparna, Claudy, Farman. I would like to thanks Vincent Demery and Julien Chopin (Postdocs with Laurent ponson) for all support and discussion during our meetings.

Special heartfelt thanks go to my officemates at these both laboratories: Agnes (first officemate at d'alembert), Lauren, Bharat and Awadhesh (keeping the noise of "hindi" in the cafeteria), Nicolas and Ilango (for all helps and explanations in university administrative paper works), Sarah, Symphony. I would like to thank to my early buddies when I arrived in France: Dr. Arup Das, Sandeep and Komlanvi madou.

Going back to the past of my academic journey: I would like to thank to all my teachers since my school days: teachers at Patel Boarding Rajkot, a boarding school where I spent beautiful five-years of my life, teachers during graduation at Nirma Univeristy and during master at IIT Delhi. Especially to Dr. Piat at KIT, Germany and Prof. Mahajan at IIT Delhi: my master thesis advisors, for all their inspirations and supports since I have taken the decision for pursuing the PhD and go for research profession.

I am eternally indebted to my parents, parents-in-law, my brother and three sisters, and my brother-in-law, for their love and affection. Finally, I would like to thank Bindiya - the joy and soul of my life.

yadā yadā hi dharmasya
glānirbhavti bhārata |
ābhyutthānam adharmasya
tadātmānam srjāmyham ||

It is Faith (or dharma) which teaches renunciation and is responsible for the elevation and well-being of human beings. Whenever in the passage of time, faith is weakened or is under attack - and whenever faithlessness spreads without control - it is then that I (supreme God) re-incarnate myself with all my powers to restore faith.

– Bhagavad Gita, Chapter 4, Verse: 7-8

Contents

List of Figures

General introduction

Predicting the role played by small scale heterogeneities on the macroscopic response of materials is an important challenge in mechanics. In fracture problems, heterogeneities and defects can play a central role: In some specific cases, when crack initiation dominates the fracture process, the strength to failure of a solid is not ruled by an average of its local properties, but rather by the response of small parts, that act as "weak links" and are responsible for the failure of the whole solid (Weibull, 1939). In other cases, when material failure involves the propagation of a free-discontinuity (interface) like a crack, some rare specific heterogeneities located at the crack tip can have a dominant effect on the macroscopic material strength. For these reasons, the passage from micro to macro in fracture problems governed by the propagation of a crack can be highly complex. The central objective of this work is to develop tools relevant to such a passage and quantify the effects of the small scale heterogeneities on the macroscopic failure response of a material.

We shall address this problem for a planar crack propagation in the presence of strong toughness heterogeneities for which new and interesting mechanisms take place. The presence of a strong heterogeneity may induce large front perturbations (see Fig. Int. (a)) from which non-linear geometrical mechanisms can emerge. Another mechanism is the occurrence of an unstable crack growth where material failure is localized on some specific part of the fracture front (see *e.g.* the fingering instability in Fig. Int. (b)).

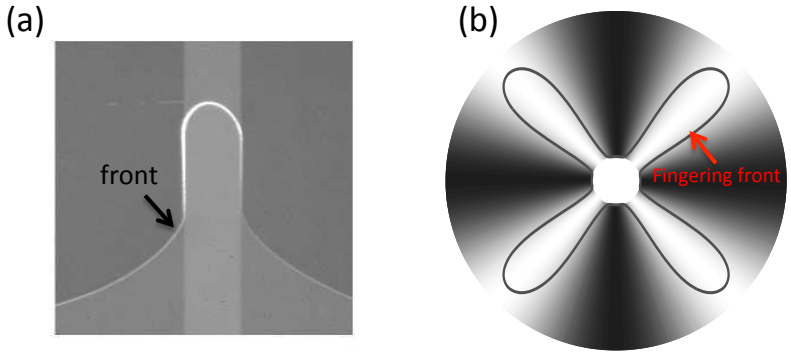

Figure Int.: Crack fronts propagating in a heterogeneous medium (a) Experimental example of a crack interacting with a single strong heterogeneity (Chopin, 2010); (b) Numerical example of a front propagating by fingering.

Describing quantitatively the large front deformation under the effect of strong toughness heterogeneities and their implication on the effective fracture behavior is the aim of this work. More precisely, we will start by extending current linear theories of crack front

deformation in order to describe non-linear effects arising in the presence of rather strong heterogeneities. For achieving a critical comparison with experimental examples, the extended theories will be tested on heterogeneous systems using peeling experiments. Finally, we address the problem numerically to explore the effect of arbitrarily strong heterogeneities. This work is divided in two preliminary chapters plus two parts, the first part concerning analytical developments and experiments, while the second part deals with the numerical works.

As a preliminary, **chapter 1** gives the context and motivation of this study: we briefly present the concepts relevant to fracture process in homogeneous brittle materials. We then present more recent developments useful to describe the fracture of heterogeneous materials and some important challenges in this field. In **chapter 2**, as a prerequisite we describe the theoretical framework of fracture mechanics for a perturbed crack front which will be used throughout in this manuscript.

Part I which is made of chapters 3, 4 and 5, is devoted to the analytical extension of the current linear theories, discussed in chapter 2, to second-order in the crack front perturbation. This is done for two model geometries: a half-plane crack in an infinite body **(chapter 3)** and a half-plane crack lying on the mid-plane of an infinite plate **(chapter 4)**. The theoretical predictions drawn from these developments are then confronted to peeling experiments in **chapter 5**.

Part II which is made of chapters 6 and 7, is devoted to the resolution of the problem of crack propagation in the presence of heterogeneities for arbitrary large toughness variations. The method (described in **chapter 6**) is based on the iteration of the perturbative approach, presented in chapter 2. It is applied, in **chapter 7**, to the study of a penny-shaped crack propagating in some model heterogeneous toughness field.

Chapter 1

Context and motivation

Crack propagation is the main mechanism of failure of materials. Based on an energy approach developed all over the twentieth century, Linear Elastic Fracture Mechanics (LEFM) brings nowadays a solid theoretical framework to describe how cracks propagate in homogeneous brittle materials. However, this approach says little about the fracture of heterogeneous solids, despite the key role played by material heterogeneities on the propagation of a crack. After a pedagogical introduction of classical approach to fracture of homogeneous media, we will describe recent developments in the study of fracture of heterogeneous materials in the context of weak heterogeneities before to introduce the current challenges on the problem of crack propagation in presence of strong heterogeneities, in particular the prediction of effective macroscopic fracture properties from microscopic heterogeneities.

1.1 Fracture of brittle materials: The central role of flaws and cracks

To discuss the role of defects and cracks on the response of solids, let us consider first the idealized case of a flawless solid presented on Fig.1.1 (a) and estimate its strength. When submitted to an external tensile stress σ, the atomic bonds get stretched over a length $\Delta a = a_0 \frac{\sigma}{E}$ where, a_0 is the their original spacing and E is the YoungÕs modulus of the material. Quantum-mechanical calculations done by Marder and Fineberg (1996) showed that when Δa becomes 20% of the original spacing a_0 between atoms, the bond breaks. This corresponds to a critical stress σ_c at material failure of the order of $E/5$. This estimation is compared with the experimental strengths of materials in Table 1.1. This oversimplified model predict a strength

Table 1.1: Comparison between theoretical and experimental strengths of materials.

Materials	Young's modulus E (GPa)	Theoretical strength $E/5$ (GPa)	Experimental strength (GPa)
Iron	160	32	0.85
Copper	190	38	0.49
Silicon	180	36	0.62
Glass	70	14	0.02

σ_c which is about two orders of magnitude larger than the experimental observations. The

reason behind this huge discrepancy is the existence of numerous defects in real materials.

1.1.1 Concept of stress concentration at crack tips

In order to improve the description of the material provided above, we introduce an elliptical cavity (Fig. 1.1 (b)) and investigate the effect on the material strength. Inglis (1913) analyzed the stress field in a such geometry. We note the semi-axes of the elliptical cavity by b and c. Under the application of an external uniform stress σ as schemated in Fig. 1.1 (b) on the body

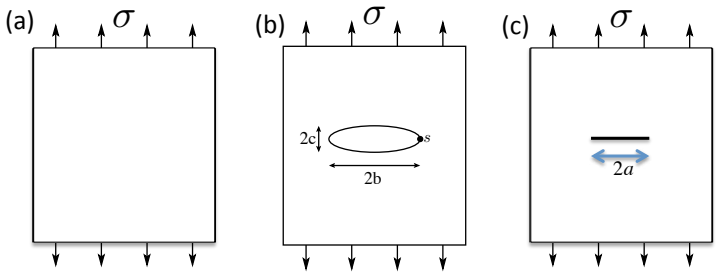

Figure 1.1: Models of material description for fracture problems: (a) an idealized model without any defect, (b) a solid containing an elliptical hole with semi-axes b and c, and (c) a solid containing a Griffith (slit) crack with length $2a$, subjected to uniform tensile stress σ

boundaries, Inglis showed that the actual stress acting locally at point s where the radius of curvature $\rho_s = c^2/b$ is minimal is amplified and follows

$$\frac{\sigma_s}{\sigma} = 1 + 2\sqrt{\frac{b}{\rho_s}}. \tag{1.1}$$

The resulting *stress concentration* in the vicinity of this defect may explain the discrepancy between practical and theoretical strengths of materials. However, for the limiting case $b/\rho_s \to \infty$ equivalent to a slit crack (Fig. 1.1 (c)) in an ideal elastic homogeneous solid, the amplification factor of Eq. (1.1) is diverging. This description predict not only *zero* strength of material but seems also contrary to the fact that larger cracks propagate generally more easily than smaller ones. This inconsistency motivates an other approach based on energy-balance rather than on the crack-tip stresses.

1.1.2 Concept of energy balance during crack propagation

Here we present the energy approach proposed by Griffith (1920). The main idea is to look at the variation of the stored elastic energy in a loaded elastic solid when a crack propagates over an infinitesimal distance. This rate of energy released, which is a finite quantity even in the slit crack geometry (Fig. 1.1 (c)) where the stress diverges, provides a driving force for crack advance. In qualitative terms, for crack extension to occur under the influence of an applied stress, the decrease in mechanical energy must compensate the increase in surface energy due to crack extension δa. Noting δU_M the mechanical energy of the body released during this process, the energy balance then reads as

$$\delta U_M = 2\gamma_s \delta a \tag{1.2}$$

where γ_s –known as the specific surface energy – is an intrinsic quantity of a material. It describes the energy required to create two new surfaces of unit area by taking into account the atomic bond energy. Accordingly, to the applied stress level at the material boundary, the energy balance of Eq. (1.2) gives a critical condition for the crack propagation in terms of rate at which mechanical energy is flowing in the crack tip region. It is accordingly convenient to define a quantity called the energy-release-rate (ERR),

$$G \equiv -\lim_{\delta a \to 0} \frac{\delta U_{\mathrm{M}}}{\delta a} = -\frac{\partial U_{\mathrm{M}}}{\partial a} \tag{1.3}$$

where the minus sign denotes decrease in the total mechanical energy. The unit of G is J.m^{-2}, and coincides with the units of a surface energy. With this, the so called Griffith's criterion for crack propagation follows

$$\begin{cases} G & < & G_c & \text{Stable crack} \\ G & = & G_c & \text{Propagating crack} \end{cases} \tag{1.4}$$

where G_c – known as the fracture energy or fracture toughness – is equal to $2\gamma_s$ in the case of an ideally brittle material. Very recently, this relation between the surface energy and the fracture energy was verified in cleavage experiment performed on silicon crystal (Gleizer and Sherman, 2014). However, the large majority of materials do not behave on an ideally brittle manner and their failure is accompanied by some additional dissipation (plasticity, visco-elasticity, damage). The ERR is then increased due to blunting at the crack tip, resulting from various dissipative mechanisms accompanying bond breaking. As suggested by Orowan (1955) and Irwin (1958), the Griffith's criterion reformulated by incorporating the dissipative energy γ_d due to these additional mechanisms follows

$$G_c = 2\left(\gamma_s + \gamma_d\right). \tag{1.5}$$

Table 1.2 compares fracture to surface energy for different brittle materials. Even though these

Table 1.2: Comparison between contributions due to surface energy $2\gamma_s$ and dissipative energy $2\gamma_d$ in the fracture energy G_c.

Materials	G_c (J.m^{-2})	$2\gamma_s$ (J.m^{-2})	$\frac{\gamma_d}{\gamma_s} = \frac{G_c}{2\gamma_s} - 1$
Silicon – Si(110) Gleizer and Sherman (2014); Pérezss and Gumbsch (2000)	3.5	3.46	0.01
Diamond – C (111) Lawn (1993)	15	12	0.25
Sapphire – Al_2O_3 ($\bar{1}010$) Lawn (1993)	25	8	2.12
Silica – SiO_2 (Glass) Lawn (1993)	8	2	3

materials are nominally brittle, the fraction of dissipation energy is not negligible and in some

cases dominants over the surface energy conditions. Therefore, the effective fracture toughness of the material is not always governed by the pure contribution of surface energy. One of the key factors that are responsible for generating dissipation near the crack tip, might be the small scale material heterogeneities that exist near the crack tip. Some strong heterogeneity then might trap the crack front. As a result, large deformations may localized there which result in some dissipations and affect the macroscopic effective fracture toughness.

Now we have derived a global criterion for crack propagation, we would like to come back to the properties of the local stress field in the crack tip vicinity.

1.1.3 Local stress field near the crack tip

Near the crack tip, the stress field can be decomposed in three components, called Mode I, Mode II and Mode III, as sketched in Fig. 1.2. Mode I causes the crack to open orthogonally to the crack plane. Mode II causes the crack surfaces to slide relative to each other in the the crack propagation direction. Mode III causes the crack surface to slide relative to each other in the 3 – direction. With these definitions the solution of the crack tip fields can be broken down into three problems. Modes I and II are found by the solution of either a plane stress or plane strain problem and Mode III by the solution of an anti-plane shear problem.

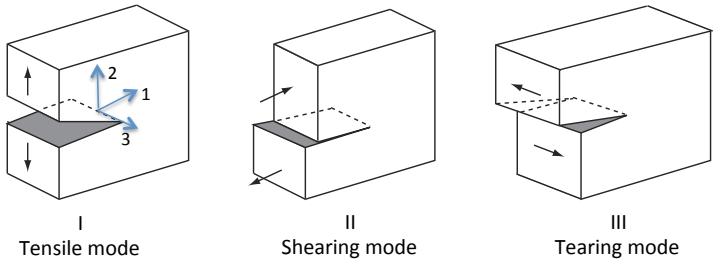

Figure 1.2: The three modes of fracture.

Let us focus further on a pure mode I loading that will be the main focus in this work. In his fundamental contribution to the analysis of stresses in the vicinity of a crack, Irwin (1958) calculated the stress distribution in the rectangular coordinate system of Fig. 1.3 :

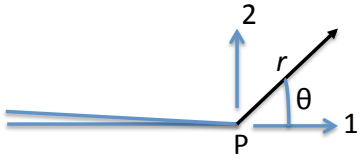

Figure 1.3: Rectangular co-ordinate system at the crack tip P.

$$\sigma_{ij}(\rho,\theta) = \frac{K_I}{\sqrt{2\pi r}} f_{ij}^I(\theta) \tag{1.6}$$

where f_{ij}^I are universal functions; (r,θ) are polar co-ordinates of point ahead of crack tip where the stress is being observed; $i,j = 1,2$ and K_I is the so-called stress intensity factor (SIF).

This quantity depends both on the geometry of the system and the external loading. Note that non-diverging terms contribute also to the stress field near the crack tip. However, our interest lies here in singularity term given in Eq. (1.6), since they dominant both the stress level sufficiently close to the tip and the crack behavior.

Mode II and mode III loadings lead to the same form of stress field as given in Eq. (1.6) but with stress intensity factors K_{II}, K_{III} and functions $f_{ij}^{II}, f_{ij}^{III}$ that varies with the fracture mode. In the case of a slit crack in an elastic solid, the stress field for mixed modes is given by the sum of the three contributions of each mode taken individually.

In the mode I, SIF $K_I \equiv K$ and energy-release-rate G are linked by Irwin (1958)'s formula:

$$G = \frac{K^2}{E} \tag{1.7}$$

so that, Griffith (1920)'s criterion (1.4) is equivalent to Irwin (1958)'s criterion which states that the crack propagates if the stress intensity factor K at the crack tip exceeds the local toughness K_c:

$$\begin{cases} K & < & K_c & \text{Stable crack} \\ K & = & K_c & \text{Propagating crack} \end{cases} \tag{1.8}$$

where the toughness is defined as $K_c = \sqrt{G_c E}$.

1.1.4 Existence of a process zone

To summarize, the basic essence of the LEFM is that it provides a criterion of crack propagation based on energy balance that links the available macroscopic energy – that depends only on the imposed boundary conditions and the sample geometry – to microscopic energy required to create two new surfaces. Unfortunately, this is also the limitation of this macroscopic approach. The divergence of the stress field at the crack tip is physically unacceptable. Most materials develop plastic deformation or damage when the intrinsic strength σ_c of material is exceeded in the region near the crack tip. On one hand, this provides an explanation to the release of the crack tip stresses. On the other hand, it explains the additional dissipation highlighted by the large experimental values of fracture energy $G_c > 2\gamma_s$ (Table 1.2). These dissipative mechanisms take place in a *process-zone* of size l_{pz} near the crack tip. Qualitatively, this size is comprehended to the maximum distance from the crack tip where the tensile stress imposed by the presence of the crack is sufficient to induce irreversible deformations (Fig. 1.4). A rough approximation can then be obtained using the relation $\sigma_c \sim K_c/\sqrt{l_{pz}}$. A more refined model was proposed by Barenblatt (1962) based on a cohesive zone approach with constant cohesive strength σ_c. The predicted value follows $l_{pz} = \frac{\pi}{8}(K_c/\sigma_c)^2$.

Therefore, the elastic stress analysis becomes increasingly inaccurate as this process zone at the crack tip becomes sufficiently large and linear elastic fracture mechanics (LEFM) is no longer useful for predicting the crack evolution. However, LEFM reconciles such non-linear processes under the assumption of the so-called *small scale yielding* : the size l_{pz} of the *process zone* is assumed to be smaller than any structural length of the system, for example the crack size a (Fig. 1.4). Under this condition, instead of relating the ERR G to the local quantity SIF K that is ill-defined, it now interprets as the flow of energy going to the crack tip region that can, still be defined using local stress field near the crack tip using the concept of $J-$integral. This path-independent $J-$ integral, introduced by Cherepanov (1967) and Rice (1968) can be

used to calculate crack driving force G from the presence of some localized process zone at the tip under small scale yielding conditions.

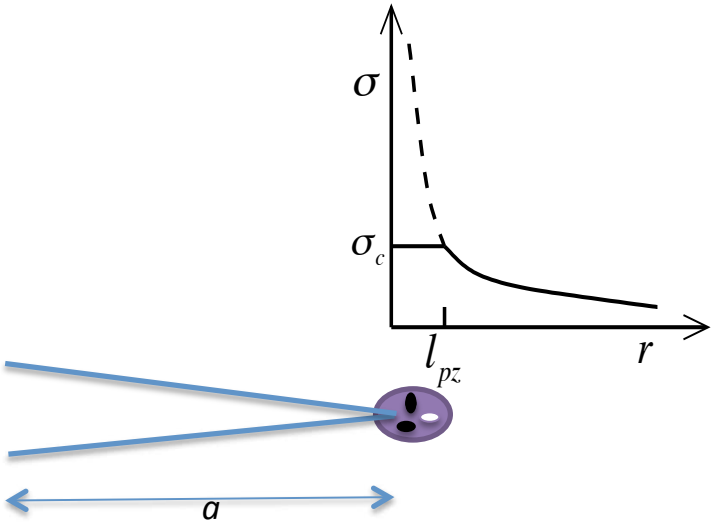

Figure 1.4: Schematic representation of the process zone around the crack tip surrounded by a material behaving elastically.

Finally, it is useful to note that the approach discussed so far is restricted to ideal homogeneous media. As soon as one considers real materials, small scale heterogeneities can have dramatic effects that are not described by the theory presented so far. This is the central point of the following section.

1.2 Fracture of heterogeneous materials

As explained in the previous section, LEFM provides a powerful framework to study the problem of a crack propagating in an ideal homogeneous elastic medium. However this approach does not address the effects due to microscopic material heterogeneities - that can have huge consequences on the response of a crack. Therefore, the concepts presented until now leave many fundamental questions open: What sets the value of the fracture toughness of a material? In the context of perfectly brittle materials, can we predict the macroscopic toughness from their microscopic features? Let us now look in more detail at the role played by material heterogeneities on the propagation of a crack and the effective material toughness.

1.2.1 On the key role of the heterogeneous fracture properties on crack propagation

Because of the presence of the stress singularity at the crack tip, material heterogeneity, even very localized in a small zone, can have macroscopic consequences on the crack propagation. This effect is characteristic of failure problems: Because of the stress concentration, the crack enhances the effects of mechanisms localized at its tip. In other words, rare specific heterogeneity can have a giant effect on the macroscopic failure behavior.

To illustrate these effects, let us consider a 2D material characterized by a one-dimensional layered heterogeneity as represented in Fig. 1.5. This composite material is made of two compounds a and b characterized by their toughness K_c^a and K_c^b, respectively ($K_c^a < K_c^b$). Let's consider the specific case when these compounds are oriented transversely to the crack line (Fig. 1.5 (a)). To make the crack propagate through the whole material, one must apply a loading $K_I^{applied}$ at least equal to K_c^b otherwise the crack is "pinned" in the blue region. Therefore, the macroscopic response of this model heterogeneous material is solely governed by the tough phase b, irrespective of the toughness of the phase a. In the case when these compounds oriented parallel to the crack line (Fig. 1.5 (b)), the macroscopic response of this model heterogeneous material is mainly governed by the phase in which the crack is lying. As presented in Fig. 1.5 (b), crack lies in weak phase a, the macroscopic response is governed by phase a only. With

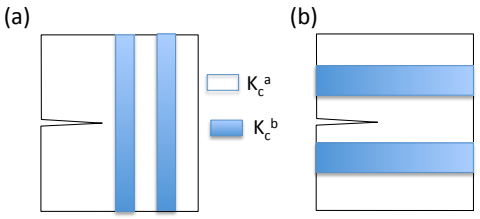

Figure 1.5: Representation of a 2D layered material made of two compounds with different toughness: (a) Compounds oriented transversely to the crack line, (b) Compounds oriented parallel to the crack line.

these two examples in mind, let's now consider a material made of N different parallel layers of toughness K_c^i with parallel orientation with respect to the crack. The macroscopic failure response is then governed either by the maximum value of K_c^i or its minimum value so that a very small part of the heterogeneous materials rules its whole behavior. Therefore, the way of doing a homogenization in fracture problems must be tackled carefully and is very different from other homogenization problems like in elasticity, electrostatics, magnetism and other problems that are addressed by variational principles that consist in finding relevant effective parameters by the principle of minimization of the stored potential energy in the system (Nemat-Nasser and Hori, 1999). After these examples on how small scale heterogeneities can dramatically change the whole response of a solid, we now discuss the 3D situation where a planar crack propagates in some heterogeneous fracture plane.

1.2.2 Involvements of the different length scales

Fig. 1.6 (a) shows a schematic representation of planar crack propagating in a medium with heterogeneity of size ξ[1]. Compare to 2D example presented in Fig. 1.4, the circular process zone is now a cylinder of radius of l_{pz}, elongated along the crack front. Before pursuing, let us make some remarks on the length scales involved in this 3D problem. There is one more material length scale ξ involved here along with the two length scales introduced previously in the context of homogeneous medium, namely the process zone size l_{pz} and a structural length like the crack size a. This length scale due to heterogeneity plays a crucial role from two points of view : (i) If ξ is comparable with the process zone size l_{pz}, the framework of LEFM does

[1]We define here as the typical length scale over which fracture energy G_c is varying. In the reminder of this work, we will restrict our discussion to smoothly varying G_c along the propagation direction.

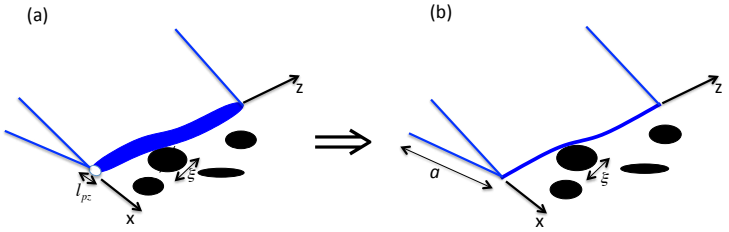

Figure 1.6: Representation of a 3D crack of size a with (a) the process zone of size l_{pz} at crack tip, and (b) its equivalent representation in the limit of *small scale yielding*, propagating in a medium with heterogeneities of size ξ.

not remain valid anymore to quantify the effects of small scale heterogeneities, and one needs to look for another framework to tackle the problem; (ii) if this size is large enough compare to l_{pz} but smaller than a structural length a ($l_{pz} \ll \xi \ll a$), the framework of LEFM can be properly used: We can study crack propagation by replacing the crack front with its cylindrical process zone by a crack front described as a line (Fig. 1.6 (b)). At these neglected intermediate scales (of order between tens of nanometers to hundreds of microns), material heterogeneities can have dramatic effects on the macroscopic failure response of a material. In order to have a clear conceptual and theoretical framework to explore these effects, we confine ourselves to the case where $l_{pz} \ll \xi \ll a$ for which LEFM works properly.

1.2.3 Homogenization over the small scale heterogeneities

In the limit of quasi-static crack propagation, recently, Hossain *et al.* (2014) have derived the effective toughness of heterogeneous media loaded in Mode-I loading conditions. Their main formulation is based on what they called "surfing boundary conditions". The main idea lies in defining an effective homogeneous medium with an effective property that describes the results of a macroscopic experiment without having to resolve the microscopic details. In order to do that, one needs to define a problem in which the crack growth is steady at the macroscopic scale, but crack sets are completely free to evolve in any manner that they choose at the microscopic scale. They have achieved this by solving the microscopic problem subject to the surfing boundary condition. They have explored their formulation mainly in studying the crack propagation in the 2D examples that we have discussed in previous section in the context of toughness heterogeneity. They have also studied the example of heterogeneity in the elastic constants. Their calculations found that the effective toughness of heterogeneous media is solely governed by the peak value of toughness field.

In this work, we are going to study the corresponding 3D fracture problem. We will restrict ourselves to the case of toughness heterogeneities while keeping homogeneous elastic properties. The problem with heterogeneities in the elastic constants will be remained to one of the perspective of this work. The basic difference from that 2D example is that, now crack can have more than one interaction with heterogeneities at the same time. Deformations of the front line is, thus, going to be the main mechanism to select local properties. With this new mechanism in the problem, our key objective is here to explore in different situations how the complex front evolution selects local fracture properties and sets the overall effective material toughness. In order to do that, at first, one needs to calculate the front deformations when trapped by heterogeneities. A basic mechanism playing a role here is that elasticity tries to

keep the front line flat while heterogeneities try to deform it. Thus, the distribution of driving forces along the crack front and front geometry are coupled and both are unknown a *priori*. Our basic approach to address the problem is based on perturbation method developed by Rice (Rice, 1985, 1989) that gives a *priori*, the variations in the driving force along the crack front due to small otherwise arbitrary perturbations of crack front geometry.

1.2.4 Weakly heterogeneous toughness fields: In the limit of small front deformations

Let us look at the propagation of a crack in some specific cases of weakly heterogeneous toughness fields, as schematized on Fig. 1.7. Depending on the fluctuations in fracture toughness along the propagation direction, different cases can be distinguished (Roux *et al.*, 2003): (i) if the fluctuations of the toughness in the propagation directions are very small or negligible (Fig. 1.7 (a)), the crack front propagates smoothly so that the driving force G reaches the local fracture toughness at each position along the crack front ($G = G_c$). In this case, heterogeneous material can be safely replaced by an equivalent homogeneous one with effective toughness equal to its mean value $< G_c >$; (ii) In contrast if the spatial fluctuations along the propagation direction are strong (Fig. 1.7 (b)), there might be jumps during the crack propagation: crack front gets pinned on higher toughness points for a while, and once loading increases enough, the crack front get depinned and jumps to another tough point without visiting domains of weaker toughness. Therefore, the condition $G = G_c$ might not always admit a solution and the effective toughness is governed by the pinned points: hence it is larger than the spatial average of the local fracture energy (Patinet *et al.*, 2013; Demery *et al.*, 2014). However, note that these results hold in the limit of very small front deformations.

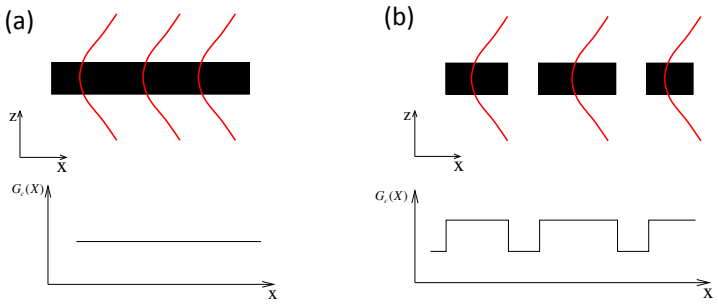

Figure 1.7: Representation of the propagation of a crack (in *red*) in (a) a toughness field (tougher zones are in *black*) that is invariant along the left to right propagation direction (*weak pinning*), and (b) a toughness field that is variant along the propagation direction (*strong pinning*).

1.3 Objective of this thesis

The key objective of this thesis is to explore new effects arising for strongly heterogeneous toughness fields. In particular, since stronger heterogeneities would not affect much the strong pinning regime, we will focus on the effect of strong heterogeneities in the weak pinning regime. Does the equation $G = G_c$ still admits any solution in terms of crack front geometry? How to predict the evolution of front geometry during its propagation? How does it set the effective

fracture properties of the materials? These are the main key issues that will be tackled in this manuscript. In order to address them, we will use the theoretical framework of fracture mechanics with perturbed crack front that we describe in the next chapter.

Chapter 2

Some prerequisites on perturbative approaches in brittle fracture

The aim of this chapter is to expound some necessary definitions and classical results of LEFM with perturbed crack front. As explained in the previous chapter, attention is restricted to the sole case of a planar crack subjected to some tensile mode I loading.

2.1 Basic definition of the mode I stress intensity factor

Consider (Figure 2.1) a planar crack with arbitrary contour embedded in some arbitrary isotropic elastic body symmetric about the crack plane, loaded in pure mode I through some symmetric system of prescribed forces and/or displacements. Let $Oxyz$ denote the global reference co-ordinate system, and s some curvilinear abscissa along $\mathcal{F}$. At each point s of $\mathcal{F}$, define a local basis of vectors $(\overrightarrow{e}_1(s), \overrightarrow{e}_2(s), \overrightarrow{e}_3(s))$ as follows:

- $\overrightarrow{e}_1(s) \equiv \overrightarrow{e}_1$ is orthogonal to the crack plane.
- $\overrightarrow{e}_2(s)$ is in the crack plane and orthogonal to $\mathcal{F}$.
- $\overrightarrow{e}_3(s)$ is in the crack plane and tangent to $\mathcal{F}$.

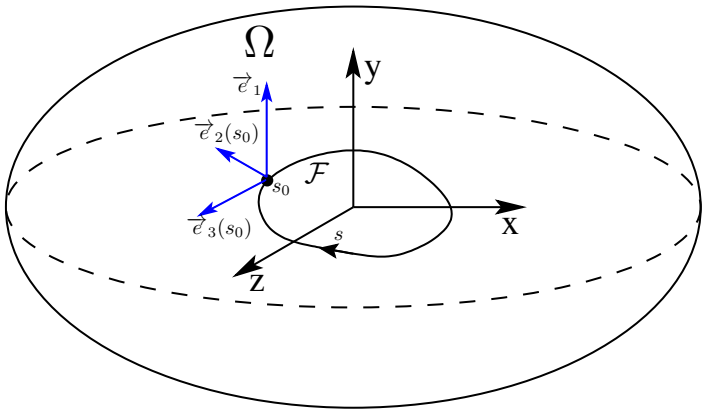

Figure 2.1: A three-dimensional planar crack $\mathcal{F}$ embedded in an arbitrary body Ω

The mode I SIF K at the point s is then defined by the following asymptotic forms of the tensile stress just ahead of the crack front and the crack opening displacement just behind it :

$$\sigma_{11}(s,\rho) \equiv \sigma(s,\rho) \sim \frac{K}{\sqrt{2\pi\rho}}; \quad [\![u_1(s,\rho)]\!] \equiv [\![u(s,\rho)]\!] \sim 8\frac{1-\nu^2}{E}K(s)\sqrt{\frac{\rho}{2\pi}}. \tag{2.1}$$

In these expressions $\boldsymbol{\sigma}(s,\rho)$ denotes the stress tensor at the distance ρ ahead of the point s, in the direction of the vector $\overrightarrow{e}_2(s)$; $[\![\mathbf{u}(s,\rho)]\!]$ denotes the displacement discontinuity across the crack plane at the distance ρ behind the point s, in the direction of the vector $-\overrightarrow{e}_2(s)$; E denotes Young's modulus and ν Poisson's ratio.

2.2 Coplanar perturbation of a crack

The aim of this section is to give the first-order variations of the stress intensity factor and the *fundamental kernel* (FK) due to small in-plane perturbations of the crack front (Fig. 2.2). Such formulae have been developed by Rice (1989) using Bueckner (1970)'s weight-function theory, and generalized to general loading conditions by Leblond *et al.* (1999), Favier *et al.* (2006).

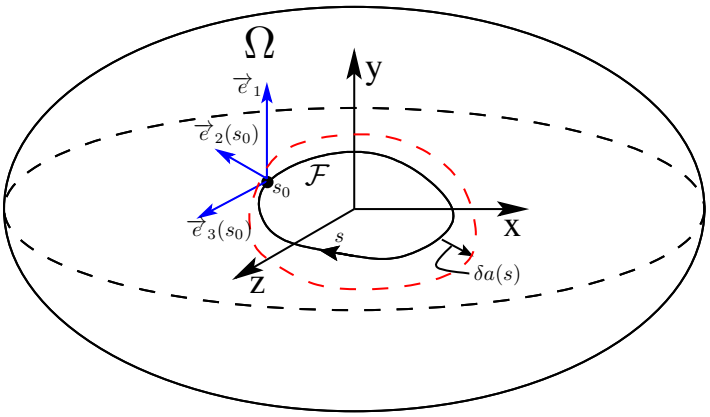

Figure 2.2: A planar mode I crack with a slightly perturbed front in an arbitrary body.

2.2.1 Definition and elementary properties of crack-face weight functions

The mode I crack-face weight function (CFWF), denoted by $k(x,z;s)$, verifies the following properties, the first of which is in fact a definition (Rice, 1989) :

- If the loading consists of opposite surface tractions $T(x,\pm 0,z) = \pm T(x,z)$ exerted on the upper $(+)$ and lower $(-)$ crack surfaces at the location $(x,\pm 0,z)$, then the mode I SIF K induced at the location s along $\mathcal{F}$ is

$$K(s) = \int_{\text{crack}} k(x,z;s)T(x,z)\mathrm{d}x\mathrm{d}z. \tag{2.2}$$

  Considering the special case of a pair of unit point forces exerted at the location $(x,\pm 0,z)$, one sees that $k(x,z;s)$ may be interpreted as the SIF generated at point s of the crack

front $\mathcal{F}$ by such forces. Thus the function $k(x, z; s)$ depends on the crack front geometry but has no dependence upon the original loading other than on which portions of the body and its boundary have forces versus displacements prescribed.

- If the crack front location is altered by a small distance $\delta a(s)$, as in Fig. 2.2, under fixed loading conditions, then the variation of the crack opening displacement at location (x, z) is, to first order in $\delta a(s)$,

$$\delta[\![u(x,z)]\!] = 2\frac{1-\nu^2}{E}\int_{\mathcal{F}} k(x,z;s)K(s)\delta a(s)\mathrm{d}s. \tag{2.3}$$

A special limit of the CFWF will play a major role in the sequel. Let us choose two point locations s and s' along $\mathcal{F}$, and a point $(x, \pm 0, z)$ on the crack faces behind the point s at a distance $\rho = \rho(x, z)$ along the direction of the vector $-\overrightarrow{e}_2(s)$. The function $k(x, z; s')/\sqrt{\rho(x, z)}$ is known to have a well-defined limit for $\rho(x, z) \to 0$ (Rice, 1989). One may then define a regular function $W(s, s')$ by the formula

$$W(s,s') \equiv \pi\sqrt{\frac{\pi}{2}}D^2(s,s') \lim_{\rho(x,z)\to 0} \frac{k(x,z;s')}{\sqrt{\rho(x,z)}} \tag{2.4}$$

where $D^2(s, s')$ denotes the cartesian distance between the points s and s'. The function $W(s, s')$ thus depends on the crack front geometry, just like the CFWF, but has no dependence upon the loading other than on which portions of the body and its boundary have forces versus displacements prescribed. It may also be shown, using Betti's theorem, to be symmetric (Rice, 1989).

We shall also use the notation

$$Z(s,s') \equiv \frac{W(s,s')}{2\pi D^2(s,s')}. \tag{2.5}$$

Just like $W(s, s')$, $Z(s, s')$ depends on the crack front geometry but has no dependence upon the loading other than on which portions of the body and its boundary have forces versus displacements prescribed. Also, since $W(s, s) = 1$ it behaves like $1/D^2(s, s')$ when the points s and s' become close.

In the sequel, the wording "fundamental kernel" (FK) will designate the functions W or Z indifferently.

2.2.2 First order variation of the stress intensity factor

Assume that the crack front is perturbed, under constant loading, by a small distance $\delta a(s)$ within the crack plane in the direction perpendicular to the front (Fig. 2.2). Assume further that $\delta a(s_1) = 0$ at some point s_1.

Consider a point (x, z) at a small distance $\rho(x, z)$ from the point s_1 of the crack front $\mathcal{F}$ along the vector $-\overrightarrow{e}_2(s_1)$. The variation of $[\![u(x, z)]\!]$ is then given by Eq. $(2.1)_2$:

$$\delta[\![u(x,z)]\!] \sim 8\frac{1-\nu^2}{E}\delta K(s)\sqrt{\frac{\rho(x,z)}{2\pi}}. \tag{2.6}$$

Using this equation along with Eqs. (2.3), (2.4) and (2.5), dividing both sides of the resulting equation by $\sqrt{\rho(x, z)}$ and taking the limit $\rho(x, z) \to 0$, one gets Rice (1989)'s *first formula*

which provides the infinitesimal variation $\delta K(s_1)$ of the SIF to first order in the crack front perturbation $\delta a(s)$:

$$\delta K(s_1) = PV \int_{\mathcal{F}} Z(s_1, s) K(s) \delta a(s) \mathrm{d}s \tag{2.7}$$

where the symbol PV denotes the Cauchy principal value of the integral, which is taken over the crack front $\mathcal{F}$.

Note that the asymptotic behaviour of the FK Z mentioned above ensures that the integral in Eq. (2.7) does make sense as a Cauchy principal value if (1) $\delta a(s_1) = 0$, and (2) $\mathrm{d}[\delta a(s)]/\mathrm{d}s$ is Hölder continuous at $s = s_1$.

There is an issue with the practical applicability of Eq. (2.7), since it does not provide $\delta K(s)$ at points s where $\delta a(s) \neq 0$. However, Rice (1989) has pointed out that it is always possible to decompose the given perturbation $\delta a(s)$ in the following form

$$\delta a(s) = \delta_* a(s) + [\delta a(s) - \delta_* a(s)] \tag{2.8}$$

where $\delta_* a$ is another perturbation such that $\delta_* a(s_1) = \delta a(s_1)$, so that the second term, in brackets, vanishes as required for to be applicable Eq. (2.7). Such a decomposition is interesting, of course, only if special motions $\delta_* a(s)$ of crack front exist for which the variation $\delta_* K(s_1)$ may be calculated independently. Then

$$\delta K(s_1) = \delta_* K(s_1) + PV \int_{\mathcal{F}} Z(s_1, s) K(s) \left[\delta a(s) - \delta_* a(s)\right] \mathrm{d}s \tag{2.9}$$

where $\delta_* K(s_1)$ represents the perturbation of $K(s_1)$ arising from the perturbation $\delta_* a$. An interesting special case consists of a $\delta_* a(s)$ representing a *uniform* advance of the crack front $\mathcal{F}$ by the amount $\delta a(s_1)$, for which the corresponding first order variation of the SIF, $[\delta K(s_1)]_{\delta a(s) \equiv \delta a(s_1)\ \forall s}$ is often known explicitly. From this choice of $\delta_* a$ Eq. (2.9) becomes

$$\delta K(s_1) = [\delta K(s_1)]_{\delta a(s) \equiv \delta a(s_1)\ \forall s} + PV \int_{\mathcal{F}} Z(s_1, s) K(s) \left[\delta a(s) - \delta a(s_1)\right] \mathrm{d}s. \tag{2.10}$$

It is useful to rewrite this formula in terms of the function W :

$$\delta K(s_1) = [\delta K(s_1)]_{\delta a(s) \equiv \delta a(s_1)\ \forall s} + \frac{1}{2\pi} PV \int_{\mathcal{F}} \frac{W(s_1, s)}{D^2(s_1, s)} K(s) \left[\delta a(s) - \delta a(s_1)\right] \mathrm{d}s. \tag{2.11}$$

Another possibility is to choose $\delta_* a$ corresponding to an overall translatory motion of the crack front. In the special cases, for example a circular crack in an infinite body subject to prescribed forces only, such motion leave the SIF unaffected so that $\delta_* K(a_1) = 0$.

2.2.3 First order variation of the fundamental kernel

In addition, just by applying Eq. (2.9) to the special case of a loading system consisting of a pair of opposite unit point forces exerted on the upper (+) and lower (−) crack surfaces, one may derive *Rice (1989)'s second formula* which provides the infinitesimal variation of the FK in the following form:

$$\delta Z(s_1, s_2) = \delta_* Z(s_1, s_2) + PV \int_{\mathcal{F}} Z(s_1, s) Z(s, s_2) [\delta a(s) - \delta_* a(s)] \mathrm{d}s \tag{2.12}$$

or equivalently

$$\delta W(s_1,s_2) = \delta_* W(s_1,s_2) + \frac{D^2(s_1,s_2)}{2\pi} PV \int_{\mathcal{F}} \frac{W(s_1,s)}{D^2(s_1,s)} \frac{W(s,s_2)}{D^2(s,s_2)} [\delta a(s) - \delta_* a(s)] \mathrm{d}s \qquad (2.13)$$

where $\delta_* Z(s_1,s_2)$ or $\delta_* W(s_1,s_2)$ is the variation of the FK due to any other crack perturbation $\delta_* a(s)$ such that

$$\delta_* a(s_1) = \delta a(s_1) \text{ and } \delta_* a(s_2) = \delta a(s_2). \qquad (2.14)$$

Note that there are in fact two principal values here, one at $s = s_1$ and the other at $s = s_2$. Eq. (2.12) is interesting, again, only if one can find special motions $\delta_* a(s)$ (satisfying the constraints (2.14)) of the crack front for which the variation $\delta_* Z(s_1,s_2)$ may be calculated independently. Such a motion can always be found by combining a translatory motion, a rotation and a homothetical transformation bringing two distinct points s_1 and s_2 from their initial positions to their final positions. In some special cases, for instance that of a semi-infinite crack in an infinite body subjected to prescribed forces only, such a combination leaves the FK unaffected so that $\delta_* Z(s_1,s_2) = 0$. In some other cases like planar circular cracks embedded in an infinite body loaded by remote stress, one has $\delta_* W(s_1,s_2) = 0$ since W is dimensionless and the problem is unchanged by the transformations. In finite bodies, such cases are no longer the case in general but there are some special cases where certain perturbations $\delta_* a(s)$ generate a zero $\delta_* Z$ or $\delta_* W$.

2.3 Concluding remarks

With this framework of LEFM with perturbed crack front, in the sequel we will use the formula updating the SIF K and FK Z or W in iterative way to explore the effects due to large front deformations induced in the presence of strong heterogeneities.

Part I

A second-order analytical study of crack front deformations by heterogeneities for small toughness contrasts

Introduction

Almost two decades ago, based on Bueckner (1970)'s *weight-function* theory, Rice (1985) derived the first-order expression of the variation of the mode I stress intensity factor (SIF) induced by some small, but otherwise arbitrary coplanar perturbation of the front of a semi-infinite tensile crack in an infinite body. This expression was the first analytical development of the type. This expression has then been extensively used as a cornerstone for predicting planar crack growth evolution through a single defect, or a periodic or random array of such defects (Schmittbuhl *et al.*, 1995; Bonamy *et al.*, 2008; Gao and Rice, 1989; Bower and Ortiz , 1991; Li and Keer, 1992), and deciphering the puzzling geometrical properties of planar cracks observed in experiments (Delaplace *et al.*, 1999; Santucci *et al.*, 2010; Bonamy and Bouchaud, 2011; Budzik *et al.*, 2013; Xia *et al.*, 2012).

However, Rice (1985)'s first-order formula relies on the assumption that crack front perturbations are of small wavelength compared to the specimen dimensions, which is questionable in some experiments (Schmittbuhl *et al.*, 2003). This was the motivation for Legrand *et al.* (2011)'s recent extension of Rice (1985)'s formula to the case of coplanar perturbation of an emerging tensile crack lying on the mid-plane of a semi-infinite plate, thus accounting for the effect of the finite dimensions of the specimen. Patinet *et al.* (2013) showed that the new formula did significantly improve the agreement between experimental and computed shapes of crack fronts deformed by the presence of obstacles.

However, both Rice (1985)'s and Legrand *et al.* (2011)'s formulae are only accurate to first order in the perturbation of the front, limiting their application to weak variations of toughness. To explore the non-linear response of cracks pinned by defects of larger contrasts, Leblond *et al.* (2012) extended Rice (1985)'s first-order formula to the second order in the case of a semi-infinite crack propagating in an infinite body. Leblond *et al.* (2012)'s treatment relied on application of some general results of Rice (1989) presented in chapter 2. Their formula for the perturbed SIF was found to differ from the earlier ones, themselves in conflict, of Adda-Bedia *et al.* (2006) and Katzav *et al.* (2007), derived by a more complex method. Direct numerical computations of the SIF along perturbed crack fronts by the finite element method confirmed the correctness of Leblond *et al.* (2012)'s new formula. However Leblond *et al.* (2012) retained Adda-Bedia *et al.* (2006)'s and Katzav *et al.* (2007)'s assumption that the unperturbed SIF, for the straight configuration of the crack front, was independent of the position of this front within the crack plane. Further extensions are therefore necessary. This part is organised as follows:

Chapter 3

As a first-step this chapter is devoted to extend the work of Leblond *et al.* (2012) on second-order perturbation of a semi-infinite crack in an infinite body to the case where the unperturbed SIF is dependent on the position of the crack front within the crack plane (*i.e.* $\mathrm{d}K^0/\mathrm{d}a \neq 0$). This hypothesis of $\mathrm{d}K^0/\mathrm{d}a \neq 0$ permits to unambiguously calculate the shape of the front deformed by inhomogeneities of toughness, up to second order in the fluctuation of fracture toughness. Using this equilibrium shape of the crack front, as a first application we show that the effective fracture toughness experienced by a crack propagating in a randomly heterogeneous, but statistically homogeneous material is slightly less than the average value of the local toughness. As a second application, we study the influence of the shape of the toughness map on the crack front deformations by calculating the equilibrium shape of a crack front penetrating into (i) a single obstacle of infinite length in the direction of propagation, (ii) a periodic array of such obstacles, (iii) a sinusoidal distribution of such obstacles, up to second order in the contrast of toughness between the matrix and the obstacle(s). One major outcome is that in all cases, the first-order approximation overestimates the deformations of the front.

Chapter 4

This chapter is devoted to further extension of second-order perturbation with $\mathrm{d}K^0/\mathrm{d}a \neq 0$, for a semi-infinite crack in an infinite body to the case of the finite body and particular to a plates of arbitrary thickness. The case of a single, harder, infinitely elongated obstacle is considered to highlight the finite thickness effect. We find notably that the thiner the sample, the small the deformation of the front. This case is further addressed to experiments in the next chapter.

Chapter 5

For achieving a critical comparison of the model with experimental examples, this chapter is devoted to the experimental study on half-plane cracks propagating in heterogeneous materials. We perform these experiments following the setup designed by Xia *et al.* (2012) in which a thin film is being peeled of from the rigid substrate with patterned interface with controlled field of fracture energy. We explore the process of front pinning in specimens of thickness comparable with the obstacle size. The geometry of the experimental pinned front is compared with the results of our calculations for various toughness contrasts of the obstacles, providing a critical test of the theory and its range of applicability. This comparison qualifies the limits in the approach in terms of toughness contrast and of crack width.

Chapter 3

Second-order perturbation of a semi-infinite mode I crack in an infinite body

The aim of this chapter[1] is to derive the second-order variation of the SIF induced by some small, but otherwise arbitrary coplanar perturbation of the front of a semi-infinite tensile crack in an infinite body subjected to some symmetric Mode I loading. In particular, we will extend the results of Leblond *et al.* (2012) to the case where the unperturbed SIF depends upon the position of the (straight) crack front within the crack plane. The chapter is organized as follows:

- Section 3.1 presents the basic problem definition with the necessary notations.
- As a preliminary, Section 3.2 presents the first-order solution for a slightly perturbed crack front.
- We then calculate, in Section 3.3, the second-order expression of the SIF for the same cracked geometry. This is done by applying Rice (1989)'s formula for the infinitesimal variation of the SIF to some pre-perturbed configuration of the front upon which is superposed some infinitesimal proportional perturbation. One thus gets an expression of the derivative of the SIF with respect to the amplitude of the perturbation accurate to first order in this amplitude, which yields the second-order expression of this SIF upon integration. We finally perform a Fourier transform of this second-order expression in the direction of the crack front.
- Section 3.4 then considers the case of a crack propagating according to Griffith's criterion along a fracture plane having a given heterogeneous distribution of toughness. Assuming the ERR to be equal to its critical value at every point of the crack front, we apply the results just obtained to the determination of the shape of this front up to second order in the fluctuations of toughness.
- As a first application, Section 3.5 presents the calculation of the "apparent macroscopic toughness" experienced by a crack propagating in a material having a random distribution of toughness at the micro scale.

[1] The results presented in this chapter constitute the bulk of the material published in Vasoya *et al.* (2013).

- As a second application, Section 3.6 finally considers the case of a crack penetrating into a single obstacle of infinite length in the direction of propagation, or some periodic distribution of such obstacles and the case of sinusoidal distribution of the toughness. The equilibrium shape of the front is calculated up to second order in the contrast of toughness between the matrix and the obstacle(s).

3.1 Problem definition

Consider (Fig. 3.1) a semi-infinite tensile crack located in some infinite body subjected to prescribed forces only (no prescribed displacements). Assume that the (planar) crack front is slightly curved, its equation in the crack plane Oxz being of the form

$$x(z) = a + \delta a(z) = a + \epsilon\phi(z) \tag{3.1}$$

where a denotes the distance from the axis Oz to some "reference straight front", ϵ a small but not necessarily infinitesimal parameter, and $\phi(z)$ a given, fixed, smooth function. The position of the front is thus characterized by the parameters a and ϵ, and the position of a current point along it by the parameter z.

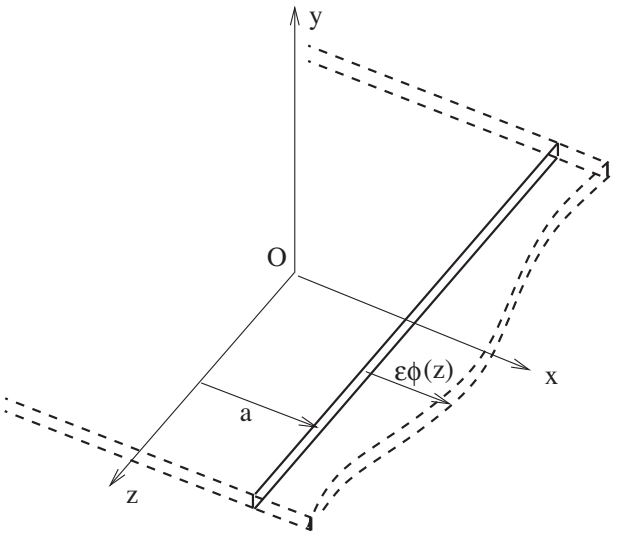

Figure 3.1: A semi-infinite crack with a slightly perturbed front in an infinite body

The SIF for a given, fixed loading, and the FK for this cracked geometry are denoted $K(a, \epsilon; z_1)$ and $Z(\epsilon; z_1, z_2)$ respectively. (The FK is independent of the position of the unperturbed crack front a because as explained in chapter 1, it depends only on the geometry and hence is insensitive to translatory motions of the crack front in the direction x). Our interest here lies in both the second-order expression of $K(a, \epsilon; z_1)$ and the first-order expression of $Z(\epsilon; z_1, z_2)$ with respect to ϵ:

$$\left\{ \begin{array}{lcl} K(a, \epsilon; z_1) & \equiv & K^0(a) + \epsilon K^1(a; z_1) + \epsilon^2 K^2(a; z_1) + O(\epsilon^3) \\ Z(\epsilon; z_1, z_2) & \equiv & Z^0(z_1, z_2) + \epsilon Z^1(z_1, z_2) + O(\epsilon^2). \end{array} \right. \tag{3.2}$$

It is assumed in Eq. $(3.2)_1$ that the loading has a translatory invariance in the direction z of the crack front, so that the unperturbed SIF $K^0(a)$ depends on the position a of the (straight) front but not on the position of the point of observation along it.

3.2 Zeroth and first-order solutions

- *At order 0 in* ϵ, no general expression can be provided for the unperturbed SIF $K^0(a)$, since it depends on the loading. On the other hand the expression of the unperturbed FK $Z^0(z_1, z_2)$ is known to be (Rice, 1985, 1989):

$$Z^0(z_1, z_2) = \frac{1}{2\pi(z_1 - z_2)^2}. \tag{3.3}$$

- *At order 1*, $K^1(a; z_1)$ is obtained through direct application of Rice (1989)'s first formula (2.10) to the straight configuration of the front with the perturbation $\delta a(z) = \epsilon\phi(z)$; this is possible since the FK appearing in this formula is known explicitly for this configuration. Thus

$$K^1(a; z_1) = \frac{\mathrm{d}K^0}{\mathrm{d}a}(a)\,\phi(z_1) + K^0(a)\,PV\int_{-\infty}^{-\infty} Z^0(z_1, z)\,[\phi(z) - \phi(z_1)]\,\mathrm{d}z. \tag{3.4}$$

  The first term in the right-hand side here results from identification of the quantity $[\delta K(s_1)]_{\delta a(s)\equiv\delta a(s_1),\forall s}$ of Eq. (2.10) to $\dfrac{\mathrm{d}K^0}{\mathrm{d}a}(a)\epsilon\phi(z_1)$, since it represents the variation of the SIF resulting from a uniform shift of the straight crack front by a distance $\epsilon\phi(z_1)$ in the direction x.

  The expression of $Z^1(z_1, z_2)$ may be obtained by combining Rice (1989)'s second formula (2.12), applied to the straight configuration of the front, and Eq. (3.3). To make the procedure work, one needs to decompose the arbitrary perturbation $\epsilon\phi(z)$ in the same way as in Eq. (2.8), *i.e.* as $\epsilon\phi(z) = [\epsilon\phi(z) - \epsilon\phi_*(z)] + \epsilon\phi_*(z)$. In the specific case considered here, the ancillary perturbation $\epsilon\phi_*(z)$ may be taken as a suitable combination of a translatory motion and a rotation:

$$\phi_*(z) \equiv \phi(z_1) + \frac{\phi(z_2) - \phi(z_1)}{z_2 - z_1}(z - z_1) = \phi(z_2) + \frac{\phi(z_1) - \phi(z_2)}{z_1 - z_2}(z - z_2). \tag{3.5}$$

  Such a motion brings no change to the FK since it leaves the geometry unmodified, so that the term $\delta_* Z(z_1, z_2)$ in Eq. (2.12) is zero. The ancillary perturbation $\epsilon\phi_*(z)$ may be eliminated in the resulting formula through suitable transformations. The final result is (Leblond *et al.*, 2012):

$$\begin{aligned} Z^1(z_1, z_2) \;=\; & \frac{1}{4\pi^2(z_1 - z_2)^2} PV\int_{-\infty}^{+\infty} \left[\left(\frac{1}{z - z_1} + \frac{1}{z - z_2}\right)\phi'(z)\right. \\ & \left. + \frac{2}{z_1 - z_2}\left(\frac{1}{z - z_2} - \frac{1}{z - z_1}\right)\phi(z)\right]\mathrm{d}z. \end{aligned} \tag{3.6}$$

3.3 Second-order variations of the stress intensity factor and the energy-release-rate

We now wish to derive the expression of $K^2(a;z_1)$ for a semi-infinite crack with a slightly perturbed front in an infinite body. This will be done by considering two configurations of the front, whose respective positions $x(z), (x+\delta x)(z)$ along the axis Ox are given by the equations

$$\left\{\begin{array}{l} x(z) = a + \epsilon\phi(z) \\ (x+\delta x)(z) = a + (\epsilon+\delta\epsilon)\phi(z) \end{array}\right. \tag{3.7}$$

where ϵ is a small quantity and $\delta\epsilon$ an infinitesimal one; the first configuration is thus obtained from the straight one ($x=a$) by adding the perturbation $\epsilon\phi(z)$, and the second one from the first by adding a secondary perturbation $\delta\epsilon\phi(z)$ having the same function $\phi(z)$, but some infinitesimal amplitude $\delta\epsilon$. This will allow us to derive an expression of the derivative $\partial K(a,\epsilon;z_1)/\partial\epsilon$ accurate to first order in ϵ, and the second-order expression of $K(a,\epsilon;z_1)$ will follow through integration. On the one hand, the variation $\delta K(z_1)$ of the SIF between the two configurations is given by

$$\delta K(z_1) \equiv K(a,\epsilon+\delta\epsilon;z_1) - K(a,\epsilon;z_1) \equiv \frac{\partial K}{\partial\epsilon}(a,\epsilon;z_1)\delta\epsilon. \tag{3.8}$$

On the other hand this variation is given by Rice (1989)'s first formula (2.10)[1]:

$$\delta K(z_1) = [\delta K(z_1)]_{\delta x(z)\equiv\delta x(z_1),\forall z} + PV\int_{-\infty}^{+\infty} Z(\epsilon;z_1,z)K(a,\epsilon;z)[\delta\epsilon\phi(z) - \delta\epsilon\phi(z_1)]\mathrm{d}z. \tag{3.9}$$

Now since $[\delta K(z_1)]_{\delta x(z)\equiv\delta x(z_1),\forall z}$ represents the variation of the SIF arising from a *uniform* shift $\delta\epsilon\phi(z_1)$ of the crack front, it is given by

$$[\delta K(z_1)]_{\delta x(z)\equiv\delta x(z_1),\forall z} \equiv K(a+\delta\epsilon\phi(z_1),\epsilon;z_1) - K(a,\epsilon;z_1) \equiv \frac{\partial K}{\partial a}(a,\epsilon;z_1)\delta\epsilon\phi(z_1). \tag{3.10}$$

Combining equations (3.8), (3.9) and (3.10) and dividing by $\delta\epsilon$, and then using the expansions (3.2) of $K(a,\epsilon;z_1)$ and $Z(\epsilon;z_1,z)$ and the expression (3.4) of $K^1(a;z_1)$, one gets

$$\begin{aligned}
\frac{\partial K}{\partial\epsilon}(a,\epsilon;z_1) &= \frac{\partial K}{\partial a}(a,\epsilon;z_1)\phi(z_1) + PV\int_{-\infty}^{+\infty} Z(\epsilon;z_1,z)K(a,\epsilon;z)\left[\phi(z)-\phi(z_1)\right]\mathrm{d}z \\
&= \left[\frac{\mathrm{d}K^0}{\mathrm{d}a}(a) + \epsilon\frac{\partial K^1}{\partial a}(a;z_1)\right]\phi(z_1) + PV\int_{-\infty}^{+\infty}\left[Z^0(z_1,z)+\epsilon Z^1(z_1,z)\right] \\
&\quad \times\left[K^0(a)+\epsilon K^1(a;z)\right]\left[\phi(z)-\phi(z_1)\right]\mathrm{d}z + O(\epsilon^2) \\
&= \frac{\mathrm{d}K^0}{\mathrm{d}a}(a)\phi(z_1) + K^0(a)PV\int_{-\infty}^{+\infty} Z^0(z_1,z)\left[\phi(z)-\phi(z_1)\right]\mathrm{d}z \\
&\quad +\epsilon\left\{\frac{\mathrm{d}^2K^0}{\mathrm{d}a^2}(a)\phi^2(z_1) + \frac{\mathrm{d}K^0}{\mathrm{d}a}(a)PV\int_{-\infty}^{+\infty} Z^0(z_1,z)\left[\phi^2(z)-\phi^2(z_1)\right]\mathrm{d}z\right. \\
&\quad +K^0(a)PV\int_{-\infty}^{+\infty}\int_{-\infty}^{+\infty} Z^0(z_1,z)Z^0(z,z')\left[\phi(z)-\phi(z_1)\right]\left[\phi(z')-\phi(z)\right]\mathrm{d}z\mathrm{d}z' \\
&\quad \left.+K^0(a)PV\int_{-\infty}^{+\infty} Z^1(z_1,z)\left[\phi(z)-\phi(z_1)\right]\mathrm{d}z\right\} + O(\epsilon^2).
\end{aligned} \tag{3.11}$$

[1] This formula is applied using the infinitesimal distance between the fronts and the infinitesimal length element measured perpendicularly to and along the axis Oz, respectively, instead of the true ones measured perpendicularly to and along the primarily perturbed front. The errors made are of second order in ϵ and therefore negligible in the calculation of the first-order expression of $\partial K(a,\epsilon;z_1)/\partial\epsilon$.

Integration of this expression with respect to ϵ then yields Eq. $(3.2)_1$, $K^1(a;z_1)$ being given by Eq. (3.4) and $K^2(a;z_1)$ by

$$\begin{aligned} K^2(a;z_1) &= \frac{1}{2}\frac{\mathrm{d}^2K^0}{\mathrm{d}a^2}(a)\phi^2(z_1) + \frac{1}{2}\frac{\mathrm{d}K^0}{\mathrm{d}a}(a)PV\int_{-\infty}^{+\infty} Z^0(z_1,z)\left[\phi^2(z)-\phi^2(z_1)\right]\mathrm{d}z \\ &\quad + \frac{K^0(a)}{2}\left\{PV\int_{-\infty}^{+\infty}\int_{-\infty}^{+\infty} Z^0(z_1,z)Z^0(z,z')\left[\phi(z)-\phi(z_1)\right]\left[\phi(z')-\phi(z)\right]\mathrm{d}z\mathrm{d}z'\right. \\ &\quad \left. + PV\int_{-\infty}^{+\infty} Z^1(z_1,z)\left[\phi(z)-\phi(z_1)\right]\mathrm{d}z\right\} \end{aligned} \tag{3.12}$$

or equivalently, account being taken of the expressions (3.3) and (3.6) of Z^0 and Z^1 :

$$\begin{aligned} K^2(a;z_1) &= \frac{1}{2}\frac{\mathrm{d}^2K^0}{\mathrm{d}a^2}(a)\phi^2(z_1) + \frac{1}{2\pi}\frac{\mathrm{d}K^0}{\mathrm{d}a}(a)\,PV\int_{-\infty}^{-\infty}\frac{\phi(z)\phi'(z)}{z-z_1}\,\mathrm{d}z \\ &\quad + \frac{K^0(a)}{8\pi^2}\,PV\int_{-\infty}^{+\infty}\int_{-\infty}^{+\infty}\left[\left(\frac{1}{z'-z_1}+\frac{2}{z'-z}\right)\phi'(z')\right. \\ &\quad \left. + \frac{2}{z-z_1}\left(\frac{1}{z'-z_1}-\frac{1}{z'-z}\right)\phi(z')\right]\frac{\phi(z)-\phi(z_1)}{(z-z_1)^2}\,\mathrm{d}z\mathrm{d}z'. \end{aligned} \tag{3.13}$$

Integrations by parts have been performed here, with respect to z in the integral involving $\phi^2(z)-\phi^2(z_1)$, and with respect to z' in that involving $[\phi(z)-\phi(z_1)]\,[\phi(z')-\phi(z)]$. In the limit $\dfrac{\mathrm{d}K^0}{\mathrm{d}a}\to 0$, Eq. (3.13) becomes equivalent to equation (14) of Leblond *et al.* (2012).
It is worth noting that for the sinusoidal perturbation

$$\phi(z)\equiv\cos(kz)\quad(k>0), \tag{3.14}$$

equation (3.13) yields, after some calculations,

$$K^2(a;z) = \frac{1}{2}\frac{\mathrm{d}^2K^0}{\mathrm{d}a^2}(a)\cos^2(kz) - \frac{1}{4}\frac{\mathrm{d}K^0}{\mathrm{d}a}(a)\,k\cos(2kz) - \frac{K^0(a)}{8}\,k^2\sin^2(kz), \tag{3.15}$$

this same result has been arrived at by Willis (2013), by a completely different method.

3.3.1 Formulae in Fourier's space

Expressions of the Fourier transforms of the formulae obtained in the direction of the crack front will be needed in the sequel. The definition adopted here for the Fourier transform $\widehat{\psi}(k)$ of an arbitrary function $\psi(z)$ is

$$\psi(z)\equiv\int_{-\infty}^{+\infty}\widehat{\psi}(k)e^{ikz}\mathrm{d}k\quad\Leftrightarrow\quad\widehat{\psi}(k)\equiv\frac{1}{2\pi}\int_{-\infty}^{+\infty}\psi(z)e^{-ikz}\mathrm{d}z. \tag{3.16}$$

Stress intensity factor:

The expression $(3.2)_1$ of the SIF reads in Fourier's space,

$$\widehat{K}(a,\epsilon;k)\equiv K^0(a)\delta(k)+\epsilon\widehat{K^1}(a;k)+\epsilon^2\widehat{K^2}(a;k)+O(\epsilon^3) \tag{3.17}$$

where δ denotes Dirac's distribution (or generalised function), and $\widehat{K^1}(a;k)$ and $\widehat{K^2}(a;k)$ are the Fourier transforms of $K^1(a;z)$ and $K^2(a;z)$.

The expression of the Fourier transform $\widehat{K^1}(a;k)$ is then (Lazarus, 2011):

$$\widehat{K^1}(a;k) = K^0(a)\left[\frac{\mathrm{d}K^0}{K^0\mathrm{d}a}(a) - \frac{|k|}{2}\right]\widehat{\phi}(k). \tag{3.18}$$

The expression of the Fourier transform of $K^2(a;z_1)$ consists of several terms. The Fourier transform of the term involving $\phi^2(z_1)$ is proportional to the convolution product of the function $\widehat{\phi}$ and itself. To get that of the term involving $PV\int_{-\infty}^{+\infty}\frac{\phi(z)\phi'(z)}{z-z_1}\mathrm{d}z$, the simplest method is to express $\phi(z)$ as an integral involving $\widehat{\phi}(k)$, and $\phi'(z)$ as another one involving $\widehat{\phi}(k')$; the problem then reduces to calculating the integral

$$\begin{aligned} PV\int_{-\infty}^{+\infty}\frac{e^{i\lambda z}}{z-z_1}\mathrm{d}z &= e^{i\lambda z_1}PV\int_{-\infty}^{+\infty}\frac{e^{i\lambda(z-z_1)}}{z-z_1}\mathrm{d}z = e^{i\lambda z_1}\mathrm{sgn}(\lambda)PV\int_{-\infty}^{+\infty}\frac{e^{i\lambda u}}{u}\mathrm{d}u \\ &= i\pi\ \mathrm{sgn}(\lambda)e^{i\lambda z_1}. \end{aligned} \tag{3.19}$$

Finally the calculation of the Fourier transform of the double integral is more complex but basically reduces to that of the same integral; it is detailed in the work of Leblond *et al.* (2012). The final result reads:

$$\widehat{K^2}(a;k_1) = K^0(a)\int_{-\infty}^{+\infty} R(a;k,k_1-k)\,\widehat{\phi}(k)\,\widehat{\phi}(k_1-k)\,\mathrm{d}k \tag{3.20}$$

where

$$\begin{aligned} R(a;k,k') \equiv\ & \frac{1}{2}\frac{\mathrm{d}^2K^0}{K^0\mathrm{d}a^2}(a) - \frac{1}{4}\frac{\mathrm{d}K^0}{K^0\mathrm{d}a}(a)|k+k'| + \frac{1}{16}\Big\{\mathrm{sgn}(kk')(k+k')^2 \\ & + \left[\mathrm{sgn}(k) - \mathrm{sgn}(k')\right]|k+k'|(k-k') - k^2 - k'^2\Big\}. \end{aligned} \tag{3.21}$$

Energy-release-rate:

The expansion of the Fourier transform $\widehat{G}(a,\epsilon;k)$ of the ERR $G(a,\epsilon;z)$ follows from Irwin's formula and the expressions (3.18) and (3.20) of $\widehat{K^1}(a;k)$ and $\widehat{K^2}(a;k)$:

$$\widehat{G}(a,\epsilon;k) \equiv G^0(a)\delta(k) + \epsilon\widehat{G^1}(a;k) + \epsilon^2\widehat{G^2}(a;k) + O(\epsilon^3) \tag{3.22}$$

where $G^0(a)$ is the unperturbed ERR, and

$$\left\{\begin{aligned} \widehat{G^1}(a;k) &= G^0(a)\left[\frac{\mathrm{d}G^0}{G^0\mathrm{d}a}(a) - |k|\right]\widehat{\phi}(k) \\ \widehat{G^2}(a;k_1) &= G^0(a)\int_{-\infty}^{+\infty} S(a;k,k_1-k)\,\widehat{\phi}(k)\,\widehat{\phi}(k_1-k)\,\mathrm{d}k \end{aligned}\right. \tag{3.23}$$

with

$$\begin{aligned} S(a;k,k') \equiv\ & \frac{1}{2}\frac{\mathrm{d}^2G^0}{G^0\mathrm{d}a^2}(a) - \frac{1}{4}\frac{\mathrm{d}G^0}{G^0\mathrm{d}a}(a)\left(|k+k'| + |k| + |k'|\right) \\ & + \frac{1}{8}\Big\{\mathrm{sgn}(kk')(k+k')^2 + \left[\mathrm{sgn}(k) - \mathrm{sgn}(k')\right]|k+k'|(k-k') - \left(|k| - |k'|\right)^2\Big\}. \end{aligned} \tag{3.24}$$

3.4 The equilibrium shape of the front of a crack

3.4.1 Generalities

We shall now apply the preceding results to the study of coplanar propagation of the crack, governed by Griffith's criterion with a heterogenous fracture toughness $G_c(x,z)$ given by

$$G_c(x,z) \equiv \overline{G_c}\,[1+\epsilon g_c(x,z)] \tag{3.25}$$

where $\overline{G_c}$ is a "mean toughness", ϵ a small parameter and $g_c(x,z)$ a given function describing the toughness fluctuations. For a given loading, provided that G is equal to G_c at every point of the crack front, the distribution of toughness determines the shape of this front in the form

$$x = a + \epsilon\phi^1(a;z) + \epsilon^2\phi^2(a;z) + O(\epsilon^3) \tag{3.26}$$

where a, $\phi^1(a;z)$ and $\phi^2(a;z)$ are a parameter and functions to be determined.

3.4.2 First- and second-order expressions of the crack front shape

To determine a, $\phi^1(a;z)$ and $\phi^2(a;z)$, it is useful to rewrite, for a crack front shape of type (3.1),Eqs. (3.23) in the form

$$\widehat{G^1}(a;k) \equiv \widehat{\mathcal{G}^1}\left[a;\{\widehat{\phi}\}\right](k) \quad ; \quad \widehat{G^2}(a;k) \equiv \widehat{\mathcal{G}^2}\left[a;\{\widehat{\phi}\}\right](k). \tag{3.27}$$

These somewhat formal equalities express the fact that the functions $\widehat{G^1}(a;.)$ and $\widehat{G^2}(a;.)$ are linear and quadratic functionals, respectively, of the Fourier transform $\widehat{\phi}$ of the "perturbation function" ϕ.

With these notations, for the crack front shape depicted by Eq.equation (3.26), corresponding to the perturbation function $\epsilon\phi \equiv \epsilon\phi^1 + \epsilon^2\phi^2$, the expansion (3.22) of $\widehat{G}(a,\epsilon;k)$ takes the form

$$\begin{aligned}\widehat{G}(a,\epsilon;k) &= G^0(a)\,\delta(k) + \epsilon\widehat{\mathcal{G}^1}\left[a;\{\widehat{\phi^1}+\epsilon\widehat{\phi^2}\}\right](k) + \epsilon^2\widehat{\mathcal{G}^2}\left[a;\{\widehat{\phi^1}+\epsilon\widehat{\phi^2}\}\right](k) + O(\epsilon^3)\\ &= G^0(a)\,\delta(k) + \epsilon\widehat{\mathcal{G}^1}\left[a;\{\widehat{\phi^1}\}\right](k)\\ &\quad +\epsilon^2\left\{\widehat{\mathcal{G}^1}\left[a;\{\widehat{\phi^2}\}\right](k) + \widehat{\mathcal{G}^2}\left[a;\{\widehat{\phi^1}\}\right](k)\right\} + O(\epsilon^3).\end{aligned} \tag{3.28}$$

Now the local toughness is [1]

$$\begin{aligned}&G_c\left[x = a + \epsilon\phi^1(a;z) + \epsilon^2\phi^2(a;z) + O(\epsilon^3), z\right]\\ &= \overline{G_c}\left\{1 + \epsilon g_c\left[a + \epsilon\phi^1(a;z) + \epsilon^2\phi^2(a;z) + O(\epsilon^3), z\right]\right\}\\ &= \overline{G_c}\left[1 + \epsilon g_c(a,z) + \epsilon^2\frac{\partial g_c}{\partial x}(a,z)\phi^1(a;z)\right] + O(\epsilon^3).\end{aligned}$$

The Fourier transform of this expression at the point k_1 is

$$\overline{G_c}\left[\delta(k_1) + \epsilon\widehat{g_c}(a,k_1) + \epsilon^2\int_{-\infty}^{+\infty}\frac{\partial\widehat{g_c}}{\partial x}(a,k)\,\widehat{\phi^1}(a;k_1-k)\mathrm{d}k\right] + O(\epsilon^3).$$

Assuming G to be equal to G_c at every point of the crack front and therefore equating the right-hand side of Eq. $(3.28)_2$ (at $k = k_1$) to this expression, one gets the following conditions:

[1] The spatial expansion of G_c here is based on the assumption that the geometrical perturbations of the crack front are small compared to the typical scale over which the local toughness varies in the direction of propagation, that is $|\epsilon\phi| \ll \zeta_x$ where ζ_x is the correlation length of the toughness fluctuations in the direction x; this is verified in the limit of weakly heterogeneous materials.

- At order 0:

$$G^0(a) = \overline{G_c}\,. \tag{3.29}$$

This condition determines the position a of the reference straight front as a function of the loading applied.

- At order 1:

$$\widehat{\mathcal{G}^1}\left[a;\{\widehat{\phi^1}\}\right](k) = \overline{G_c}\,\widehat{g_c}(a,k),$$

which implies, by the expression $(3.23)_1$ of the functional $\widehat{\mathcal{G}^1}\left[a;\{\widehat{\phi^1}\}\right](k)$ and Eq. (3.29), that

$$\widehat{\phi^1}(a;k) = -\frac{\widehat{g_c}(a,k)}{|k| - \frac{\mathrm{d}G^0}{G^0\mathrm{d}a}(a)}. \tag{3.30}$$

- At order 2:

$$\widehat{\mathcal{G}^1}\left[a;\{\widehat{\phi^2}\}\right](k_1) = -\widehat{\mathcal{G}^2}\left[a;\{\widehat{\phi^1}\}\right](k_1) + \overline{G_c}\int_{-\infty}^{+\infty}\frac{\partial\widehat{g_c}}{\partial x}(a,k)\,\widehat{\phi^1}(a;k_1-k)\mathrm{d}k,$$

which implies, by Eqs. (3.23), (3.29) and (3.30), that

$$\begin{aligned}\widehat{\phi^2}(a;k_1) \;=\; & \frac{1}{|k_1| - \frac{\mathrm{d}G^0}{G^0\mathrm{d}a}(a)} \left\{\int_{-\infty}^{+\infty} S(a;k,k_1-k)\,\frac{\widehat{g_c}(a,k)}{|k| - \frac{\mathrm{d}G^0}{G^0\mathrm{d}a}(a)}\,\frac{\widehat{g_c}(a,k_1-k)}{|k_1-k| - \frac{\mathrm{d}G^0}{G^0\mathrm{d}a}(a)}\,\mathrm{d}k \right.\\ & \left. + \int_{-\infty}^{+\infty}\frac{\partial\widehat{g_c}}{\partial x}(a,k)\frac{\widehat{g_c}(a,k_1-k)}{|k_1-k| - \frac{\mathrm{d}G^0}{G^0\mathrm{d}a}(a)}\,\mathrm{d}k\right\}.\end{aligned} \tag{3.31}$$

3.4.3 Some mathematical remarks

It is necessary to discuss here the convergence of the integrals appearing in the expressions of $\widehat{\phi^1}(a;k)$ and $\widehat{\phi^2}(a;k)$ and their inverse Fourier transforms $\phi^1(a;z)$ and $\phi^2(a;z)$. The following hypothesis is introduced on the sign of the first derivative of the unperturbed ERR $G^0(a)$:

$$\frac{\mathrm{d}G^0}{\mathrm{d}a}(a) < 0. \tag{3.32}$$

This condition is necessary for quasi-static propagation to be stable and was fulfilled in all experiments mentioned in the Introduction.

With this condition, the denominator in the expression (3.30) of $\widehat{\phi^1}(a;k)$ can never be zero, so that the integral over k expressing $\phi^1(a;z)$ in terms of $\widehat{\phi^1}(a;k)$ is perfectly convergent. Also, in the integrals appearing in the expression (3.31) of $\widehat{\phi^2}(a;k_1)$, the denominators $|k| - \dfrac{\mathrm{d}G^0}{G^0\mathrm{d}a}(a)$ and $|k_1-k| - \dfrac{\mathrm{d}G^0}{G^0\mathrm{d}a}(a)$ again cannot vanish so they do not raise any problem of convergence either. Finally the integral over k_1 expressing $\phi^2(a;z)$ in terms of $\widehat{\phi^2}(a;k_1)$ involves the denominator $|k_1| - \dfrac{\mathrm{d}G^0}{G^0\mathrm{d}a}(a)$, but again this denominator can never be zero and convergence of the integral is ensured.

Consider now the special but interesting situation where G^0 becomes independent of a. This is in fact a limit-case in which the derivative $\dfrac{\mathrm{d}G^0}{\mathrm{d}a}(a)$ takes very small negative values; in physical terms, this means that the characteristic distance of variation of the unperturbed ERR is much larger than that of fluctuations of the fracture toughness.

When $\dfrac{\mathrm{d}G^0}{\mathrm{d}a}(a) = 0$, the expression (3.30) of $\widehat{\phi^1}(a;k)$ still makes sense, but the integral over k expressing $\phi^1(a;z)$ in terms of $\widehat{\phi^1}(a;k)$ involves the denominator $|k|$ which becomes zero in the interval of integration; hence the integral diverges, except if $\widehat{g_c}(a,0) = 0$. Also, in the expression (3.31) of $\widehat{\phi^2}(a;k_1)$, the integrals are also divergent, except again if $\widehat{g_c}(a,0) = 0$, because they involve the denominators $|k|$ and $|k_1 - k|$. Finally, even if $\widehat{g_c}(a,0) = 0$, the expression of $\widehat{\phi^2}(a;k_1)$ makes sense but that of $\phi^2(a;z)$ is once more a divergent integral over k_1 involving the denominator $|k_1|$.

It may thus be concluded that consideration of this limiting case where $\dfrac{\mathrm{d}G^0}{\mathrm{d}a}(a) = 0$ requires some mathematical precautions. The best way to handle it is to first assume $\dfrac{\mathrm{d}G^0}{\mathrm{d}a}(a) < 0$, perform all calculations with this hypothesis, and only finally examine whether the expressions found make sense in the limit $\dfrac{\mathrm{d}G^0}{\mathrm{d}a}(a) \to 0$, which they may or may not, depending on the quantity of interest.

It remains to check that the functions $\phi^1(a;z)$ and $\phi^2(a;z)$ thus determined uniquely are admissible in the sense that they do not predict any receding of the crack. Now the equations of the crack front at two nearby instants, corresponding to the successive positions $a, a+\delta a$ $(> a)$ of the reference straight front, are given by

$$\left\{\begin{array}{l} x(z) = a + \epsilon\phi^1(a;z) + \epsilon^2\phi^2(a;z) + O(\epsilon^3) \\ (x+\delta x)(z) = a + \delta a + \epsilon\phi^1(a+\delta a;z) + \epsilon^2\phi^2(a+\delta a;z) + O(\epsilon^3) \end{array}\right. \tag{3.33}$$

respectively, so that the difference in the position of the fronts is

$$\begin{array}{rcl} \delta x(z) & = & \delta a + \epsilon\left[\phi^1(a+\delta a;z) - \phi^1(a;z)\right] + \epsilon^2\left[\phi^2(a+\delta a;z) - \phi^2(a;z)\right] + O(\epsilon^3) \\ & = & \delta a\left[1 + \epsilon\dfrac{\partial\phi^1}{\partial a}(a;z) + \epsilon^2\dfrac{\partial\phi^2}{\partial a}(a;z)\right] + O(\epsilon^3). \end{array} \tag{3.34}$$

This quantity is positive since the perturbation procedure used makes sense only in the limit $\epsilon \to 0$. Hence the front does not recede.

The conclusion is that *with condition (3.32), the problem of determination of successive crack front configurations admits a unique solution for which $G = G_c$ at every point of the crack front and every instant.* In other words, crack propagation is possible in the complete absence of dynamic effects and with a continuously advancing front. Note that this conclusion is intimately tied to the hypothesis made of small fluctuations of toughness; for large fluctuations, the crack front may never penetrate certain specially hard obstacles but leave them behind unbroken, and conversely propagate unstably over small distances when suddenly encountering regions of sufficiently low toughness; see Gao and Rice (1989), Schmittbuhl *et al.* (1995) and Bonamy *et al.* (2008).

3.5 Effective apparent fracture properties

In this subsection, we assume that condition (3.32) holds, so that the equality $G = G_c$ may be satisfied all along the crack front and at all instants. We wish to compute the apparent toughness G_{eff} experienced by the crack when propagating along a plane in a randomly inhomogeneous, but statistically homogeneous material. In intuitive terms, this quantity represents the toughness of some 'equivalent homogeneous material'. In more precise terms, it is defined, for every position a of the reference straight crack front, as the *value of the unperturbed ERR for a fictitious straight front having the same average position as the true, curved one*:

$$G_{\text{eff}} \equiv G^0 \left(a + \epsilon \langle \phi^1(a;z) \rangle + \epsilon^2 \langle \phi^2(a;z) \rangle + O(\epsilon^3) \right) \tag{3.35}$$

where $\langle f(a;z) \rangle$ denotes the average value of the function $f(a;z)$ along the front axis z.

To facilitate the calculation of average values, the distribution of toughness is assumed to be periodic in the direction z. The normalized fluctuation $g_c(x,z)$ and its Fourier transform $\widehat{g}_c(x,k)$ are then of the equivalent forms

$$g_c(x,z) \equiv \sum_{m=-\infty}^{+\infty} c_m(x) e^{imk_0 z} \Leftrightarrow \widehat{g}_c(x,k) \equiv \sum_{m=-\infty}^{+\infty} c_m(x) \delta(k - mk_0) \tag{3.36}$$

where k_0 denotes some positive wavenumber and the $c_m(x)$ coefficients. Moreover, the degree of arbitrariness left on the definition of the quantity G_c permits to consider it as identical to the exact average value of the local toughness in the fracture plane Oxz. The toughness fluctuation $g_c(x,z)$ is then zero on average in this plane and even, by the hypothesis of statistical homogeneity, on every straight line parallel to the axis Oz, so that

$$c_0(x) \equiv 0, \ \forall x. \tag{3.37}$$

At order 1, one gets from equations (3.30) and $(3.36)_2$:

$$\widehat{\phi^1}(a;k_1) = - \sum_{m=-\infty}^{+\infty} \frac{c_m(a)}{|m| - \frac{1}{G^0} \frac{\mathrm{d}G^0}{\mathrm{d}a}(a)} \delta(k - mk_0)$$

$$\Rightarrow \phi^1(a;z) = - \sum_{m=-\infty}^{+\infty} \frac{c_m(a)}{|m| - \frac{1}{G^0} \frac{\mathrm{d}G^0}{\mathrm{d}a}(a)} e^{imk_0 z}. \tag{3.38}$$

In this sum, the only term which could a priori give a nonzero contribution in the average value $\langle \phi^1(a;z) \rangle$ has $m = 0$, but this term is zero by Eq. (3.37); hence

$$\langle \phi^1(a;z) \rangle = 0, \forall a. \tag{3.39}$$

At order 2, equations (3.31) and $(3.36)_2$ yield

$$\begin{aligned}
\phi^2(a;z) &= \int_{-\infty}^{+\infty} \frac{1}{|k_1| - \frac{\mathrm{d}G^0}{G^0\mathrm{d}a}(a)} \left\{ \int_{-\infty}^{+\infty} S(a;k,k_1-k)\, \frac{\widehat{g_c}(a,k)}{|k| - \frac{\mathrm{d}G^0}{G^0\mathrm{d}a}(a)}\, \frac{\widehat{g_c}(a,k_1-k)}{|k_1-k| - \frac{\mathrm{d}G^0}{G^0\mathrm{d}a}(a)}\, \mathrm{d}k \right. \\
&\quad \left. + \int_{-\infty}^{+\infty} \frac{\partial \widehat{g_c}}{\partial x}(a,k) \frac{\widehat{g_c}(a,k_1-k)}{|k_1-k| - \frac{\mathrm{d}G^0}{G^0\mathrm{d}a}(a)}\, \mathrm{d}k \right\} e^{ik_1 z} \mathrm{d}k_1 \\
&= \int_{-\infty}^{+\infty} \int_{-\infty}^{+\infty} \left[S(a;k,k')\, \frac{\widehat{g_c}(a,k)}{|k| - \frac{\mathrm{d}G^0}{G^0\mathrm{d}a}(a)}\, \frac{\widehat{g_c}(a,k')}{|k'| - \frac{\mathrm{d}G^0}{G^0\mathrm{d}a}(a)} + \frac{\partial \widehat{g_c}}{\partial x}(a,k) \frac{\widehat{g_c}(a,k')}{|k'| - \frac{\mathrm{d}G^0}{G^0\mathrm{d}a}(a)} \right] \\
&\quad \times \frac{1}{|k+k'| - \frac{\mathrm{d}G^0}{G^0\mathrm{d}a}(a)} e^{i(k'+k)z} \mathrm{d}k \mathrm{d}k' \\
&= \sum_{m=-\infty}^{+\infty} \sum_{n=-\infty}^{+\infty} \left[S(a;mk_0,nk_0)\, \frac{c_m(a)}{|m|k_0 - \frac{\mathrm{d}G^0}{G^0\mathrm{d}a}(a)}\, \frac{c_n(a)}{|n|k_0 - \frac{\mathrm{d}G^0}{G^0\mathrm{d}a}(a)} + c_m'(a) \frac{c_n(a))}{|n|k_0 - \frac{\mathrm{d}G^0}{G^0\mathrm{d}a}(a)} \right] \\
&\quad \times \frac{e^{i(m+n)k_0 z}}{|m+n|k_0 - \frac{\mathrm{d}G^0}{G^0\mathrm{d}a}(a)}.
\end{aligned} \tag{3.40}$$

In this double series, the only terms which do not average out to zero have $m+n=0$; therefore

$$\langle \phi^2(a;z) \rangle = -\frac{G^0(a)}{\frac{\mathrm{d}G^0}{\mathrm{d}a}(a)} \left\{ \sum_{m=-\infty}^{+\infty} \frac{S(a;mk_0,-mk_0) c_m(a) c_{-m}(a)}{\left[|m|k_0 - \frac{\mathrm{d}G^0}{G^0\mathrm{d}a}(a) \right]^2} + \sum_{m=-\infty}^{+\infty} \frac{c_m'(a) c_{-m}(a))}{|m|k_0 - \frac{\mathrm{d}G^0}{G^0\mathrm{d}a}(a)} \right\}. \tag{3.41}$$

Grouping the terms $\dfrac{c_m'(a)c_{-m}(a))}{|m|k_0 - \frac{\mathrm{d}G^0}{G^0\mathrm{d}a}(a)}$ and $\dfrac{c_{-m}'(a)c_m(a))}{|m|k_0 - \frac{\mathrm{d}G^0}{G^0\mathrm{d}a}(a)}$ in the second series and accounting for the fact that the Fourier coefficients of $g_c(x,z)$ satisfy the relation $c_{-m}(a) = \overline{c_m(a)}$ since this function is real, one gets

$$\langle \phi^2(a;z) \rangle = -\frac{G^0(a)}{\frac{\mathrm{d}G^0}{\mathrm{d}a}(a)} \left\{ \sum_{m=-\infty}^{+\infty} \frac{S(a;mk_0,-mk_0) |c_m(a)|^2}{\left[|m|k_0 - \frac{\mathrm{d}G^0}{G^0\mathrm{d}a}(a) \right]^2} + \sum_{m=1}^{+\infty} \frac{(|c_m(a)|^2)'}{mk_0 - \frac{\mathrm{d}G^0}{G^0\mathrm{d}a}(a)} \right\}. \tag{3.42}$$

The right-hand side here fluctuates with a because the coefficients $c_m(a)$ themselves fluctuate. However since the apparent toughness is by nature a macroscopic quantity, it is reasonable when defining it to average $\langle \phi^2(a;z) \rangle$ in the direction x over some distance much larger than the typical distance of fluctuation of the local toughness, though still much smaller than the distance over which $G_0(a)$ varies significantly. The derivatives $(|c_m(a)|^2)'$ then average out to zero so that the expression of $\langle \phi^2(a;z) \rangle$ becomes

$$\begin{aligned}
\langle \phi^2(a;z) \rangle &\simeq -\frac{G^0(a)}{\frac{\mathrm{d}G^0}{\mathrm{d}a}(a)} \sum_{m=-\infty}^{+\infty} \frac{S(a;mk_0,-mk_0) |c_m(a)|^2}{\left[|m|k_0 - \frac{\mathrm{d}G^0}{G^0\mathrm{d}a}(a) \right]^2} \\
&= \frac{1}{2\frac{dG^0}{da}(a)} \sum_{m=-\infty}^{+\infty} \frac{\frac{\mathrm{d}G^0}{\mathrm{d}a}(a) |m|k_0 - \frac{\mathrm{d}^2G^0}{\mathrm{d}a^2}(a)}{\left[|m|k_0 - \frac{\mathrm{d}G^0}{G^0\mathrm{d}a}(a) \right]^2} \langle |c_m(a)|^2 \rangle \\
&= \frac{1}{\frac{\mathrm{d}G^0}{\mathrm{d}a}(a)} \sum_{m=1}^{+\infty} \frac{\frac{\mathrm{d}G^0}{\mathrm{d}a}(a) mk_0 - \frac{\mathrm{d}^2G^0}{\mathrm{d}a^2}(a)}{\left[mk_0 - \frac{\mathrm{d}G^0}{G^0\mathrm{d}a}(a) \right]^2} \langle |c_m(a)|^2 \rangle
\end{aligned} \tag{3.43}$$

where the symbol $\langle |c_m(a)|^2 \rangle$ denotes the average value of $|c_m(a)|^2$ and the expression (3.24) of the function $S(a;k,k')$ has been used.

Combination of Eqs. (3.35), (3.39) and (3.43) then yields,

$$G_{\text{eff}} \simeq \overline{G}_c + \epsilon^2 \sum_{m=1}^{+\infty} \frac{\frac{\mathrm{d}G^0}{\mathrm{d}a}(a) m k_0 - \frac{\mathrm{d}^2 G^0}{\mathrm{d}a^2}(a)}{\left[m k_0 - \frac{\mathrm{d}G^0}{G^0 \mathrm{d}a}(a) \right]^2} \langle |c_m(a)|^2 \rangle + O(\epsilon^3). \tag{3.44}$$

Thus the apparent toughness $G_{\text{eff}}(a)$ depends on the loading through the derivatives $\dfrac{\mathrm{d}G^0}{\mathrm{d}a}$ and $\dfrac{\mathrm{d}^2 G^0}{\mathrm{d}a^2}$. Also, $G_{\text{eff}}(a)$ is slightly lower than the exact average value $\overline{G}_c$ of the local toughness, each term of the series here being negative by inequality (3.32) and the extra hypothesis

$$\frac{\mathrm{d}^2 G^0}{\mathrm{d}a^2} \geq 0 \tag{3.45}$$

which is reasonable since the unpertubed ERR $G^0(a)$ is a positive and decreasing function.

The effect, which disappears in the limit $\dfrac{\mathrm{d}G^0}{\mathrm{d}a} \to 0$, arises from the fact that for a given loading, the real curved crack front in a heterogeneous material is slightly more advanced on average than it would be in a fictitious homogeneous material with the same average toughness ($\langle \phi^2(a;z) \rangle > 0$, see equation (3.43)).

In order to provide an estimate of the effect in practical situations, let us consider a sinusoidal variation of toughness with amplitude ϵg_c and wavelength $\lambda = 2\pi/(m_0 k_0)$. Then the coefficients $c_m(a)$ are zero except $c_{m_0}(a) = c_{m_0}(a) = g_c/2$. Since the denominator in Eq. (3.44) is larger than $(m_0 k_0)^2$, the relative decrease of toughness $(\overline{G}_c - G_{\text{eff}})/\overline{G}_c$ may be bounded by $\dfrac{1}{4}(\epsilon g_c)^2 \left(\dfrac{1}{G^0} \dfrac{\mathrm{d}G^0}{\mathrm{d}a} \dfrac{\lambda}{2\pi} - \dfrac{1}{G^0} \dfrac{\mathrm{d}^2 G^0}{\mathrm{d}a^2} \dfrac{\lambda^2}{4\pi^2} \right)$. For wavelengths much smaller than the typical distance over which $G^0(a)$ varies significantly, the weakening effect is therefore rather limited; but it could play a significant role for wavelengths comparable to this distance.

The result (3.44) must be compared to the predictions of Roux *et al.* (2003) and the observations of Ponson (2009), who actually found an *enhancement* of the apparent toughness due to random heterogeneities. In these studies, higher levels of heterogeneity were considered, so that the front did not propagate smoothly in the disordered landscape of fracture energy, but through sudden jumps from one equilibrium position to another; this intermittency biased the sampling of the local toughness since such instabilities occurred for local values of G actually larger than the local resistance G_c. In contrast, in the present work, the condition $G = G_c$ holds along the whole front and at all times since the limit of weakly disordered materials is considered.

3.6 The shape of crack fronts encountering obstacles

As an application, we shall determine the equilibrium shape of the front of a crack penetrating into a single obstacle of infinite length in the direction of propagation, or a periodic distribution of such obstacles, up to second order in the contrast of toughness. The toughness of the matrix will be denoted G_c^{M}, and the toughness and width of the obstacle(s), G_c^{O} and $2d$, respectively. We shall be particularly interested in the limit-case where $\dfrac{\mathrm{d}G^0}{\mathrm{d}a}(a) \to 0$; this corresponds, in

physical terms, to the situation where the typical distance of variation of the unperturbed ERR is much larger than d (and the period in the periodic case).

3.6.1 Case of a single obstacle

The distribution of toughness in this case is represented in Fig. 3.2. This distribution may be represented by formula (3.25) with

$$\overline{G_c} \equiv G_c^{\mathrm{M}} \quad ; \quad \epsilon \equiv \frac{G_c^{\mathrm{O}} - G_c^{\mathrm{M}}}{G_c^{\mathrm{M}}} \quad ; \quad g_c(x,z) \equiv g_c(z) \equiv \left\{ \begin{array}{lll} 1 & \text{if} & |z| < d \\ 0 & \text{if} & |z| > d. \end{array} \right. \tag{3.46}$$

The Fourier transform of the function $g_c(x,z)$ is given by

$$\widehat{g_c}(x,k) \equiv \widehat{g_c}(k) \equiv \frac{1}{2\pi} \int_{-d}^{d} e^{-ikz}\, \mathrm{d}z = \frac{\sin(kd)}{\pi k}. \tag{3.47}$$

At order 1 in ϵ, one gets from Eqs. (3.30) and (3.47):

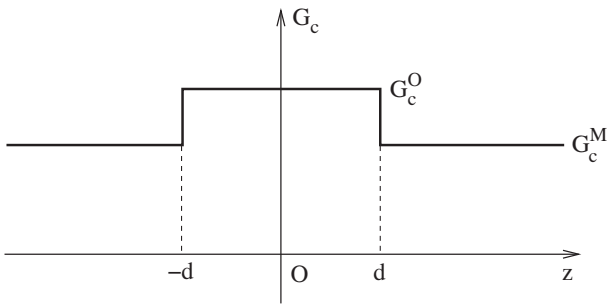

Figure 3.2: The distribution of fracture toughness in an infinite body containing a single infinitely elongated obstacle

$$\widehat{\phi^1}(a;k) = -\frac{\sin(kd)}{\pi k \left[|k| - \frac{\mathrm{d}G^0}{G^0 \mathrm{d}a}(a)\right]}$$

so that

$$\begin{aligned} \phi^1(a;z) &= -\frac{1}{\pi} \int_{-\infty}^{+\infty} \frac{\sin(kd)}{k \left[|k| - \frac{\mathrm{d}G^0}{G^0 \mathrm{d}a}(a)\right]}\, e^{ikz}\, \mathrm{d}k \\ &= -\frac{2}{\pi} \int_{0}^{+\infty} \frac{\sin(kd)}{k \left[k - \frac{\mathrm{d}G^0}{G^0 \mathrm{d}a}(a)\right]}\, \cos(kz)\, \mathrm{d}k. \end{aligned}$$

Now let $\dfrac{\mathrm{d}G^0}{\mathrm{d}a}(a) \to 0$. It is clear that the integral defining $\phi^1(a;z)$ diverges in this limit; this is an illustration of the mathematical difficulties mentioned in Subsection 3.4.3. However we are not really interested in the absolute position of the crack front in the direction x, but only in its deviation from straightness. This deviation is characterized at order 1 by the quantity

$$\widetilde{\phi^1}(a;z) \equiv \phi^1(a;z) - \phi^1(a;0) = \frac{2}{\pi} \int_{0}^{+\infty} \frac{\sin(kd)}{k \left[k - \frac{\mathrm{d}G^0}{G^0 \mathrm{d}a}(a)\right]}\, [1 - \cos(kz)]\, \mathrm{d}k\,. \tag{3.48}$$

This quantity has a well-defined limit $\widetilde{\phi^1}(z)$ for $\dfrac{\mathrm{d}G^0}{\mathrm{d}a}(a) \to 0$ given by

$$\widetilde{\phi^1}(z) \equiv \frac{2}{\pi}\int_0^{+\infty} \frac{\sin(kd)}{k^2}\left[1-\cos(kz)\right]\,\mathrm{d}k\,. \tag{3.49}$$

To calculate this integral explicitly, it suffices, following Chopin (2010), to differentiate it with respect to z, evaluate the derivative using Gradshteyn and Ryzhik (1980)'s formula 3.741.1 and re-integrate. The result is (Chopin, 2010):

$$\widetilde{\phi^1}(z) = \frac{d}{\pi}\left[(1+u)\ln\left(|1+u|\right)+(1-u)\ln\left(|1-u|\right)\right] \quad , \quad u \equiv \frac{z}{d}\,. \tag{3.50}$$

At order 2, Eqs. (3.31) and (3.47) yield, since the function $\widehat{g_c}(x,k)$ is independent of x:

$$\begin{aligned}
\phi^2(a;z) &= \int_{-\infty}^{+\infty}\int_{-\infty}^{+\infty} S(a;k,k')\frac{\widehat{g_c}(k)}{|k|-\frac{\mathrm{d}G^0}{G^0\mathrm{d}a}(a)}\,\frac{\widehat{g_c}(k')}{|k'|-\frac{\mathrm{d}G^0}{G^0\mathrm{d}a}(a)}\,\frac{e^{i(k+k')z}}{|k+k'|-\frac{\mathrm{d}G^0}{G^0\mathrm{d}a}(a)}\,\mathrm{d}k\mathrm{d}k' \\
&= \frac{1}{\pi^2}\int_{-\infty}^{+\infty}\int_{-\infty}^{+\infty} S(a;k,k')\frac{\sin(kd)}{k\left[|k|-\frac{\mathrm{d}G^0}{G^0\mathrm{d}a}(a)\right]}\,\frac{\sin(k'd)}{k'\left[|k'|-\frac{\mathrm{d}G^0}{G^0\mathrm{d}a}(a)\right]} \\
&\qquad \times\frac{e^{i(k+k')z}}{|k+k'|-\frac{\mathrm{d}G^0}{G^0\mathrm{d}a}(a)}\,\mathrm{d}k\mathrm{d}k' \\
&= \frac{2}{\pi^2}\int\int_{k+k'\geq 0} S(a;k,k')\frac{\sin(kd)}{k\left[|k|-\frac{\mathrm{d}G^0}{G^0\mathrm{d}a}(a)\right]}\,\frac{\sin(k'd)}{k'\left[|k'|-\frac{\mathrm{d}G^0}{G^0\mathrm{d}a}(a)\right]} \\
&\qquad \times\frac{\cos[(k+k')z]}{k+k'-\frac{\mathrm{d}G^0}{G^0\mathrm{d}a}(a)}\,\mathrm{d}k\mathrm{d}k'
\end{aligned}$$

where we have grouped the terms (k,k') and $(-k,-k')$ in the double integral and accounted for the fact that $S(a;-k,-k') = S(a;k,k')$, see equation (3.24).

Again, we are interested only in the deviation of the crack front from straightness, characterized at order 2 by the quantity

$$\begin{aligned}
\widetilde{\phi^2}(a;z) \equiv \phi^2(a;z)-\phi^2(a;0) &= \frac{2}{\pi^2}\int\int_{k+k'\geq 0} S(a;k,k')\frac{\sin(kd)}{k\left[|k|-\frac{\mathrm{d}G^0}{G^0\mathrm{d}a}(a)\right]} \\
&\qquad \times\frac{\sin(k'd)}{k'\left[|k'|-\frac{\mathrm{d}G^0}{G^0\mathrm{d}a}(a)\right]}\,\frac{\cos[(k+k')z]-1}{k+k'-\frac{\mathrm{d}G^0}{G^0\mathrm{d}a}(a)}\,\mathrm{d}k\mathrm{d}k'.
\end{aligned} \tag{3.51}$$

This quantity has a well-defined limit $\widetilde{\phi^2}(z)$ for $\dfrac{dG^0}{da}(a) \to 0$ given by

$$\widetilde{\phi^2}(z) \equiv \frac{2}{\pi^2}\int\int_{k+k'\geq 0} S^0(k,k')\,\frac{\sin(kd)}{k|k|}\,\frac{\sin(k'd)}{k'|k'|}\,\frac{\cos[(k+k')z]-1}{k+k'}\,\mathrm{d}k\mathrm{d}k' \tag{3.52}$$

where

$$\begin{aligned}
S^0(k,k') &\equiv \lim_{\mathrm{d}G^0/\mathrm{d}a\to 0} S(a;k,k') \\
&= \frac{1}{8}\left\{\mathrm{sgn}(kk')(k+k')^2+\left[\mathrm{sgn}(k)-\mathrm{sgn}(k')\right]|k+k'|(k-k')-\left(|k|-|k'|\right)^2\right\};
\end{aligned} \tag{3.53}$$

the integral in Eq. (3.52) is convergent because the function $S^0(k,k')$ verifies the properties $S^0(k,0) = S^0(0,k') = 0$.

Quite remarkably, one may calculate the integral in Eq. (3.52) explicitly. To do so, the first step consists in reducing the integration domain $\{(k,k'),\, k+k' \geq 0\}$. This domain consists of two sub-domains, $\{(k,k'),\, k+k' \geq 0,\, k \geq k'\}$ and $\{(k,k'),\, k+k' \geq 0,\, k' \geq k\}$ which yield equal contributions since the integrand is invariant upon interchange of k and k'; hence the integral is equal to twice the integral over the first sub-domain. Also, this sub-domain consists of two sub-sub-domains, $\{(k,k'),\, k \geq 0,\, 0 \leq k' \leq k\}$ and $\{(k,k'),\, k \geq 0,\, -k \leq k' \leq 0\}$, over which the function $S^0(k,k')$ takes the values $kk'/2$ and $-k'(k+k')/2$ respectively; using the change of variable $k'' \equiv -k'$ in the integral over the second sub-sub-domain, then re-using the notation k' instead of k'', one finally gets

$$\begin{aligned}\widetilde{\phi^2}(z) &= \frac{2}{\pi^2}\int_0^{+\infty}\left\{\int_0^k\left(\frac{\sin(kd)}{k}\,\frac{\sin(k'd)}{k'}\,\frac{\cos((k+k')z)-1}{k+k'}\right.\right.\\ &\qquad\left.\left.+\frac{\sin(kd)}{k^2}\,\frac{\sin(k'd)}{k'}\,\left[\cos((k-k')z)-1\right]\right)\mathrm{d}k'\right\}\mathrm{d}k.\end{aligned}$$

In a second step, one may write $k' \equiv \lambda k$, $0 \leq \lambda \leq 1$ and use the variables of integration (k,λ) instead of (k,k'); the preceding equation then becomes

$$\begin{aligned}\widetilde{\phi^2}(z) &= \frac{2}{\pi^2}\int_0^{+\infty}\left\{\int_0^1\left(\frac{\sin(kd)}{k}\,\frac{\sin(\lambda kd)}{\lambda k}\,\frac{\cos((1+\lambda)kz)-1}{(1+\lambda)k}\right.\right.\\ &\qquad\left.\left.+\frac{\sin(kd)}{k^2}\,\frac{\sin(\lambda kd)}{\lambda k}\,\left[\cos((1-\lambda)kz)-1\right]\right)k\mathrm{d}\lambda\right\}\mathrm{d}k\end{aligned}$$

or equivalently, upon change of the order of integration,

$$\widetilde{\phi^2}(z) = \frac{2}{\pi^2}\int_0^1\left\{\frac{J\left[d,\lambda d,(1+\lambda)z\right]-J(d,\lambda d,0)}{\lambda(1+\lambda)}+\frac{J\left[d,\lambda d,(1-\lambda)z\right]-J(d,\lambda d,0)}{\lambda}\right\}\mathrm{d}\lambda \quad (3.54)$$

where

$$J(\alpha,\beta,\gamma) \equiv \int_0^{+\infty}\sin(\alpha x)\sin(\beta x)\cos(\gamma x)\,\frac{\mathrm{d}x}{x^2}\,. \quad (3.55)$$

The third step consists in calculating the integral $J(\alpha,\beta,\gamma)$; this is done in Appendix A.1 and the result is

$$J(\alpha,\beta,\gamma) = \frac{\pi}{8}\left(|\alpha+\beta+\gamma|+|\alpha+\beta-\gamma|-|\alpha-\beta+\gamma|-|\alpha-\beta-\gamma|\right). \quad (3.56)$$

Eq. (3.54) becomes, upon use of this formula, replacement of z by $|z|$ (which is admissible since the function $\widetilde{\phi^2}(z)$ is obviously even) and rearrangement of terms,

$$\widetilde{\phi^2}(z) = \frac{d}{4\pi}\int_0^1\left(\left|1-|u|\right|-2\,\frac{2+\lambda}{1+\lambda}-\frac{1}{\lambda}\left|\frac{1-\lambda}{1+\lambda}-|u|\right|+\frac{1}{\lambda}\left|1+\lambda-(1-\lambda)|u|\right|\right)\mathrm{d}\lambda \quad (3.57)$$

where u has been defined in Eq. $(3.50)_2$. In a fourth and final step, one must evaluate this integral; the calculation is straightforward but somewhat heavy because of the presence of absolute values in the integrand which makes it necessary to distinguish between cases. The final result reads

$$\widetilde{\phi^2}(z) = \begin{cases} -\dfrac{d}{2\pi}\left[(1+u)\ln(1+u)+(1-u)\ln(1-u)\right] & \text{if} \quad |u| \leq 1 \\ -\dfrac{d}{2\pi}\left[(|u|-1)\ln\left(\dfrac{|u|+1}{|u|-1}\right)+2\ln 2\right] & \text{if} \quad |u| \geq 1. \end{cases} \quad (3.58)$$

It is remarkable that by Eqs. (3.50) and $(3.58)_1$, $\widetilde{\phi^2}(z) = -\widetilde{\phi^1}(z)/2$ inside the obstacle ($|u| \leq 1$). Outside the obstacle ($|u| \geq 1$), however, the functions $\widetilde{\phi^1}(z)$ and $\widetilde{\phi^2}(z)$ behave differently; for instance in the limit $|u| \to +\infty$, $\widetilde{\phi^1}(z)$ diverges like $\dfrac{2d}{\pi}\ln(|u|)$ whereas $\widetilde{\phi^2}(z)$ goes to the constant $-\dfrac{d}{\pi}(1+\ln 2)$.

Instead of plotting both $\widetilde{\phi^1}(z)$ and $\widetilde{\phi^2}(z)$, we choose to plot the sole global perturbation of the front defined by

$$\widetilde{\delta a}(z) \equiv \epsilon\phi^1(z) + \epsilon^2\phi^2(z) - \epsilon\phi^1(0) - \epsilon^2\phi^2(0) = \epsilon\widetilde{\phi^1}(z) + \epsilon^2\widetilde{\phi^2}(z) \tag{3.59}$$

deduced from Eqs. (3.50) and (3.58), as a function of the "normalized toughness contrast" ϵ.

Fig. 3.3 shows this quantity for different values of the contrast ϵ. The nonlinear dependence of $\widetilde{\delta a}(z)/d$ upon ϵ is quite conspicuous here: the effect of ϵ seems to "saturate" when this parameter becomes large, that is, the linear theory tends to overestimate the deformation of the crack front for large toughness contrasts. This observation seems to be confirmed by experiments performed by Chopin (2010) for a very large toughness contrast of 50, which have produced relatively modest crack front deformations, thus supporting the idea that the crack front becomes stiffer as its perturbation increases in amplitude for a fixed wavelength. It may be inferred from these

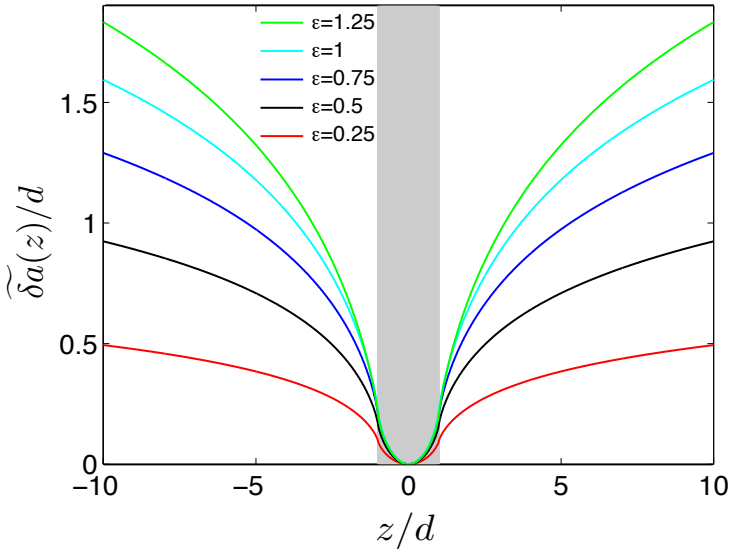

Figure 3.3: Equilibrium shape of a crack front penetrating into a single obstacle (represented by a gray rectangle), for various toughness contrasts

numerical results that the range of values of the normalized toughness contrast ϵ for which the above formulae provide reasonably accurate predictions extends up to about 0.2 if Eq. (3.50) is used alone, and to about 1 if Eqs. (3.50) and (3.58) are used in conjunction.

3.6.2 Case of a periodic distribution of obstacles

The distribution of toughness for a periodic array of infinitely elongated obstacles is represented in Fig. 3.4, where the period is denoted $2L$. This distribution may be represented by formula

(3.25) with

$$\left\{\begin{array}{l} \overline{G_c} \equiv \left(1-\dfrac{d}{L}\right) G_c^{\mathrm{M}} + \dfrac{d}{L}\, G_c^{\mathrm{O}} \quad ; \quad \epsilon \equiv \dfrac{G_c^{\mathrm{O}} - G_c^{\mathrm{M}}}{\overline{G_c}} \quad ; \\ g_c(x,z) \equiv g_c(z) \equiv \left\{\begin{array}{ll} 1-\dfrac{d}{L} & \text{if} \quad |z-2nL| < d \\ -\dfrac{d}{L} & \text{if} \quad |z-2nL| > d \end{array}\right. \qquad ((2n-1)L \le z \le (2n+1)L). \end{array}\right. \tag{3.60}$$

The functions g_c and $\widehat{g_c}$ are then of the equivalent forms

$$g_c(x,z) \equiv \sum_{m=-\infty}^{+\infty} c_m\, e^{imk_0 z} \quad \Leftrightarrow \quad \widehat{g_c}(x,k) \equiv \sum_{m=-\infty}^{+\infty} c_m\, \delta(k-mk_0) \tag{3.61}$$

where

$$k_0 \equiv \frac{\pi}{L} \quad ; \quad c_m \equiv \frac{1}{2L}\int_{-L}^{L} g_c(z) e^{-im\pi z/L}\, \mathrm{d}z = \left\{\begin{array}{ll} 0 & \text{if} \quad m = 0 \\ \dfrac{\sin(m\pi d/L)}{m\pi} & \text{if} \quad m \neq 0. \end{array}\right. \tag{3.62}$$

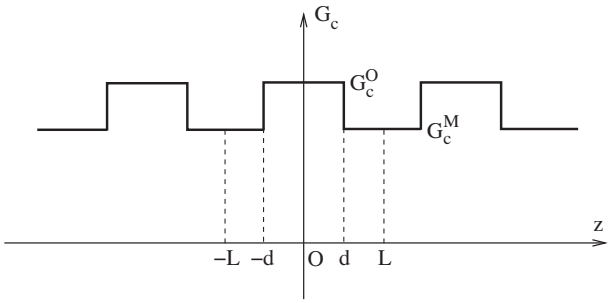

Figure 3.4: The distribution of fracture toughness in an infinite body containing a periodic array of obstacles

At order 1 in ϵ, Eqs. (3.30), $(3.61)_2$ and (3.62) yield

$$\begin{aligned} & \widehat{\phi^1}(a;k) = -\sum_{m=-\infty}^{+\infty} \frac{c_m}{\frac{|m|\pi}{L} - \frac{\mathrm{d}G^0}{G^0 \mathrm{d}a}(a)}\, \delta\left(k - \frac{m\pi}{L}\right) \\ \Rightarrow \quad \phi^1(a;z) &= -\sum_{m=-\infty}^{+\infty} \frac{c_m}{\frac{|m|\pi}{L} - \frac{\mathrm{d}G^0}{G^0 \mathrm{d}a}(a)}\, e^{im\pi z/L} = -\sum_{m\neq 0} \frac{\sin(m\pi d/L)}{m\pi\left[\frac{|m|\pi}{L} - \frac{\mathrm{d}G^0}{G^0 \mathrm{d}a}(a)\right]}\, e^{im\pi z/L} \\ &= -2\sum_{m=1}^{+\infty} \frac{\sin(m\pi d/L)}{m\pi\left[\frac{m\pi}{L} - \frac{\mathrm{d}G^0}{G^0 \mathrm{d}a}(a)\right]}\, \cos(m\pi z/L). \end{aligned}$$

Taking the limit $\dfrac{\mathrm{d}G^0}{\mathrm{d}a}(a) \to 0$ does not raise any particular problem here; $\phi^1(a;z)$ goes to a limit $\phi^1(z)$ given by the following series, which unfortunately can't be expressed in terms of elementary functions:

$$\phi^1(z) \equiv -\frac{2L}{\pi^2}\sum_{m=1}^{+\infty} \frac{\sin(m\pi d/L)}{m^2}\, \cos(m\pi z/L). \tag{3.63}$$

At order 2, one gets from Eqs. (3.31), (3.37), $(3.61)_2$ and (3.62):

$$\begin{aligned}
\phi^2(a;z) &= \int_{-\infty}^{+\infty}\int_{-\infty}^{+\infty} S(a;k,k')\,\frac{\widehat{g_c}(k)}{|k|-\frac{\mathrm{d}G^0}{G^0\mathrm{d}a}(a)}\,\frac{\widehat{g_c}(k')}{|k'|-\frac{\mathrm{d}G^0}{G^0\mathrm{d}a}(a)}\,\frac{e^{i(k+k')z}}{|k+k'|-\frac{\mathrm{d}G^0}{G^0\mathrm{d}a}(a)}\,dkdk' \\
&= \sum_{m=-\infty}^{+\infty}\sum_{n=-\infty}^{+\infty} S\left(a;\frac{m\pi}{L},\frac{n\pi}{L}\right)\frac{c_m}{\frac{|m|\pi}{L}-\frac{\mathrm{d}G^0}{G^0\mathrm{d}a}(a)}\,\frac{c_n}{\frac{|n|\pi}{L}-\frac{\mathrm{d}G^0}{G^0\mathrm{d}a}(a)}\,\frac{e^{i(m+n)\pi z/L}}{\frac{|m+n|\pi}{L}-\frac{\mathrm{d}G^0}{G^0\mathrm{d}a}(a)} \\
&= \sum_{m\neq 0,n\neq 0} S\left(a;\frac{m\pi}{L},\frac{n\pi}{L}\right)\frac{\sin(m\pi d/L)}{m\pi\left[\frac{|m|\pi}{L}-\frac{\mathrm{d}G^0}{G^0\mathrm{d}a}(a)\right]} \\
&\qquad\times\frac{\sin(n\pi d/L)}{n\pi\left[\frac{|n|\pi}{L}-\frac{\mathrm{d}G^0}{G^0\mathrm{d}a}(a)\right]}\,\frac{e^{i(m+n)\pi z/L}}{\frac{|m+n|\pi}{L}-\frac{\mathrm{d}G^0}{G^0\mathrm{d}a}(a)}\,.
\end{aligned}$$

Subtracting the average value $\left\langle\phi^2\right\rangle$ of ϕ^2, corresponding to the terms having $m+n=0$, one gets from there

$$\begin{aligned}
\overline{\phi^2}(a;z)\equiv\phi^2(a;z)-\left\langle\phi^2\right\rangle &= \sum_{m\neq 0,n\neq 0,m+n\neq 0} S\left(a;\frac{m\pi}{L},\frac{n\pi}{L}\right)\frac{\sin(m\pi d/L)}{m\pi\left[\frac{|m|\pi}{L}-\frac{\mathrm{d}G^0}{G^0\mathrm{d}a}(a)\right]} \\
&\qquad\times\frac{\sin(n\pi d/L)}{n\pi\left[\frac{|n|\pi}{L}-\frac{\mathrm{d}G^0}{G^0\mathrm{d}a}(a)\right]}\,\frac{e^{i(m+n)\pi z/L}}{\frac{|m+n|\pi}{L}-\frac{\mathrm{d}G^0}{G^0\mathrm{d}a}(a)} \\
&= \sum_{m\neq 0,n\neq 0,m+n>0} 2S\left(a;\frac{m\pi}{L},\frac{n\pi}{L}\right)\frac{\sin(m\pi d/L)}{m\pi\left[\frac{|m|\pi}{L}-\frac{\mathrm{d}G^0}{G^0\mathrm{d}a}(a)\right]} \\
&\qquad\times\frac{\sin(n\pi d/L)}{n\pi\left[\frac{|n|\pi}{L}-\frac{\mathrm{d}G^0}{G^0\mathrm{d}a}(a)\right]}\,\frac{\cos[(m+n)\pi z/L]}{\frac{(m+n)\pi}{L}-\frac{\mathrm{d}G^0}{G^0\mathrm{d}a}(a)}\,.
\end{aligned}$$

In the limit $\dfrac{\mathrm{d}G^0}{\mathrm{d}a}(a)\to 0$, this expression goes to a limit $\overline{\phi^2}(z)$ given by

$$\begin{aligned}
\overline{\phi^2}(z) &\equiv \frac{2L^3}{\pi^5}\sum_{m\neq 0,n\neq 0,m+n>0} S^0\left(\frac{m\pi}{L},\frac{n\pi}{L}\right)\frac{\sin(m\pi d/L)}{m|m|} \\
&\qquad\times\frac{\sin(n\pi d/L)}{n|n|}\,\frac{\cos[(m+n)\pi z/L]}{m+n}\,.
\end{aligned}$$

Accounting finally for the expression (3.53) of the function $S^0(k,k')$, one gets from there, after a few transformations:

$$\begin{aligned}
\overline{\phi^2}(z) &= \frac{L}{\pi^3}\sum_{m=1}^{+\infty}\sum_{n=1}^{+\infty}\frac{\sin(m\pi d/L)}{m(m+n)}\left[\frac{\sin(n\pi d/L)}{n}\cos[(m+n)\pi z/L]\right. \\
&\qquad\left.+2\frac{\sin[(m+n)\pi d/L]}{m+n}\cos(n\pi z/L)\right]\,.
\end{aligned}\tag{3.64}$$

Eqs. (3.63) and (3.64) permit to calculate the normalized perturbation of the front

$$\overline{\delta a}(z)\equiv\epsilon\phi^1(z)+\epsilon^2\phi^2(z)-\epsilon\phi^1(0)-\epsilon^2\phi^2(0)=\epsilon\phi^1(z)+\epsilon^2\overline{\phi^2}(z)-\epsilon\phi^1(0)-\epsilon^2\overline{\phi^2}(0)\tag{3.65}$$

numerically, as a function of the normalized toughness contrast ϵ and the dimensionless parameter L/d comparing the respective sizes of the period and the obstacle. Figs. 3.5 and 3.6 show the results obtained; Figure 3.5 is for $\epsilon=1$ and various values of L/d, and Figure 3.6 for $L/d=3$ and various values of ϵ. One sees in Fig. 3.5 that the influence of the finiteness

of the period is maximum half-way between the obstacles, where the slope of the front is zero for symmetry reasons. One also sees in Fig. 3.6 that in the periodic case, the nonlinear effect of the toughness contrast is weak, except near the boundary of the obstacles (observe that at $z/d = \pm 1$, the gap between the red and green curves, corresponding to values of ϵ differing by a factor of 5, is lower than what the linear theory would predict).

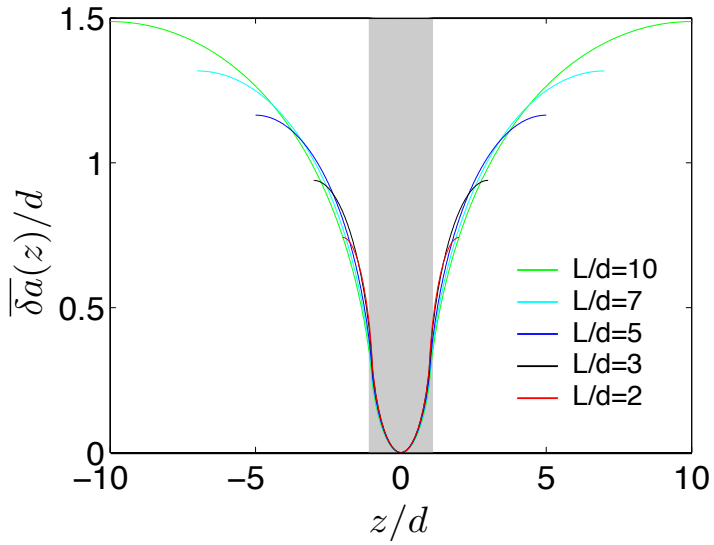

Figure 3.5: Equilibrium shape of a crack front penetrating into a periodic array of obstacles - Influence of the relative sizes of the period and the obstacle for a fixed toughness contrast ($\epsilon = 1$)

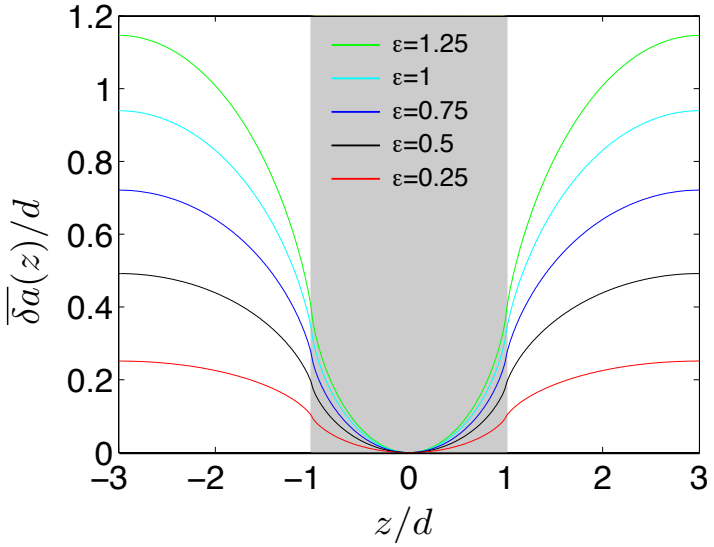

Figure 3.6: Equilibrium shape of a crack front penetrating into a periodic array of obstacles - Influence of the toughness contrast for fixed relative sizes of the matrix and the obstacle ($L/d = 3$)

Finally, it is worth noting that in the limit of a very large period, the results for a periodic array of obstacles converge toward those for a single one; this is illustrated in Fig. 3.7 which compares crack front shapes obtained for a single obstacle and a periodic array having $L/d =$

640, for a normalized toughness contrast ϵ of unity.

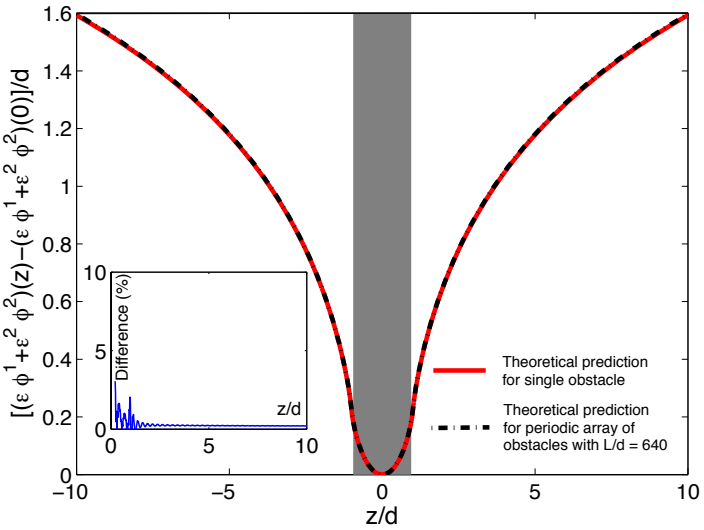

Figure 3.7: Comparison of equilibrium shapes of crack fronts penetrating into a single obstacle and a periodic array of obstacles with a large period ($L/d = 640$), for a normalized toughness contrast $\epsilon = 1$

The theoretical predictions of Eqs. (3.50) and (3.58) for an isolated pinning obstacle on the one hand, and (3.63) and (3.64) for a periodic array of obstacles on the other hand, provide a basis to interpret crack front patterns observed in heterogeneous interfaces (see e.g. Dalmas *et al.* (2009), Chopin *et al.* (2011), Xia *et al.* (2012)). In particular, it provides an efficient means of measuring the toughness of defects or impurities in these systems, using the toughness contrast as an adjustable parameter in the fit of experimental data.

3.6.3 Case of a sinusoidal distribution of obstacles

The toughness field corresponding to a sinusoidal distribution of infinitely elongated obstacles is represented in Figure 3.8, where the wavenumber of the distribution is denoted k_0. This distribution may be represented by formula (3.25) with,

$$\epsilon \equiv \frac{G_c^{\max} - G_c^{\min}}{\overline{G_c}} \quad ; \quad g_c(x,z) \equiv g_c(z) \equiv \frac{1}{2}\cos(k_0 z) \tag{3.66}$$

where $k_0 = 2\pi/\lambda_0$ is the wavenumber and λ_0 is the wavelength of the sinusoidal distribution. The Fourier transform of the functions g_c is given by

$$\widehat{g_c}(x,k) \equiv \widehat{g_c}(k) = \frac{1}{4}\left[\delta(k+k_0) + \delta(k-k_0)\right]. \tag{3.67}$$

Using this equation in the Eq. (3.30) one gets:

$$\widehat{\phi^1}(a;k) = -\frac{\delta(k+k_0) + \delta(k-k_0)}{4\left[|k| - \frac{\mathrm{d}G^0}{G^0 \mathrm{d}a}(a)\right]}$$

so that

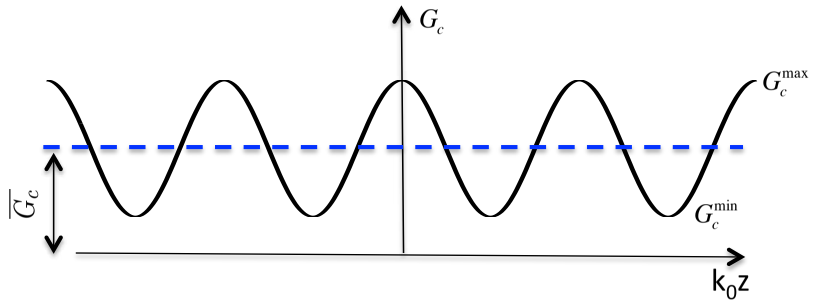

Figure 3.8: Sinusoidal distribution of fracture toughness perpendicular to the crack propagation direction.

$$\begin{aligned}\phi^1(a;z) &= -\frac{1}{4}\int_{-\infty}^{+\infty}\frac{\delta(k+k_0)+\delta(k-k_0)}{\left[|k|-\frac{\mathrm{d}G^0}{G^0\mathrm{d}a}(a)\right]}\,e^{ikz}\,\mathrm{d}k\\ &= -\frac{1}{4}\int_{-\infty}^{+\infty}\frac{\delta(k+k_0)+\delta(k-k_0)}{\left[|k|-\frac{\mathrm{d}G^0}{G^0\mathrm{d}a}(a)\right]}\,\cos(kz)\,\mathrm{d}k.\end{aligned}$$

Again, we are interested only in the deviation of the crack front from straightness, that is

$$\widetilde{\phi^1}(a;z)\equiv\phi^1(a;z)-\phi^1(a;0)=\frac{1}{4}\int_{-\infty}^{+\infty}\frac{\delta(k+k_0)+\delta(k-k_0)}{\left[|k|-\frac{\mathrm{d}G^0}{G^0\mathrm{d}a}(a)\right]}\,[1-\cos(kz)]\,\mathrm{d}k\,. \tag{3.68}$$

This quantity has a well-defined limit $\widetilde{\phi^1}(z)$ for $\dfrac{\mathrm{d}G^0}{\mathrm{d}a}(a)\to 0$ given by

$$\widetilde{\phi^1}(z)\equiv\frac{1}{4}\int_{-\infty}^{+\infty}[\delta(k+k_0)+\delta(k-k_0)]\,\frac{1-\cos(kz)}{|k|}\,\mathrm{d}k\,. \tag{3.69}$$

Using the properties of Dirac distribution function δ, one obtains,

$$\widetilde{\phi^1}(z)\equiv\frac{1}{2k_0}\,[1-\cos(k_0 z)]\,. \tag{3.70}$$

At second-order, Eqs. (3.31) and (3.67) yield to

$$\begin{aligned}\phi^2(a;z) &= \frac{1}{16}\int_{-\infty}^{+\infty}\int_{-\infty}^{+\infty}S(a;k,k')\frac{\delta(k+k_0)+\delta(k-k_0)}{|k|-\frac{\mathrm{d}G^0}{G^0\mathrm{d}a}(a)}\,\frac{\delta(k'+k_0)+\delta(k'-k_0)}{|k'|-\frac{\mathrm{d}G^0}{G^0\mathrm{d}a}(a)}\,\frac{e^{i(k+k')z}}{|k+k'|-\frac{\mathrm{d}G^0}{G^0\mathrm{d}a}(a)}\,\mathrm{d}k\mathrm{d}k'\\ &= \frac{1}{16}\int_{-\infty}^{+\infty}\int_{-\infty}^{+\infty}S(a;k,k')\frac{\delta(k+k_0)+\delta(k-k_0)}{|k|-\frac{\mathrm{d}G^0}{G^0\mathrm{d}a}(a)}\,\frac{\delta(k'+k_0)+\delta(k'-k_0)}{|k'|-\frac{\mathrm{d}G^0}{G^0\mathrm{d}a}(a)}\,\frac{\cos[(k+k')z]}{|k+k'|-\frac{\mathrm{d}G^0}{G^0\mathrm{d}a}(a)}\,\mathrm{d}k\mathrm{d}k'\end{aligned}$$

where we have used the parity of the function $S(a;k,k')$. Again, we are interested by deviation to straightness that follows

$$\begin{aligned}\widetilde{\phi^2}(a;z)\equiv\phi^2(a;z)-\phi^2(a;0) &= \frac{1}{16}\int_{-\infty}^{+\infty}\int_{-\infty}^{+\infty}S(a;k,k')\frac{\delta(k+k_0)+\delta(k-k_0)}{|k|-\frac{\mathrm{d}G^0}{G^0\mathrm{d}a}(a)}\\ &\quad\times\frac{\delta(k'+k_0)+\delta(k'-k_0)}{|k'|-\frac{\mathrm{d}G^0}{G^0\mathrm{d}a}(a)}\,\frac{\cos[(k+k')z]-1}{|k+k'|-\frac{\mathrm{d}G^0}{G^0\mathrm{d}a}(a)}\,\mathrm{d}k\mathrm{d}k'.\end{aligned} \tag{3.71}$$

This expression has a well defined limit $\widetilde{\phi^2}(z)$ for $\dfrac{\mathrm{d}G^0}{\mathrm{d}a}(a)\to 0$ given by

$$\begin{aligned}\widetilde{\phi^2}(z) &\equiv \frac{1}{16}\int_{-\infty}^{+\infty}\int_{-\infty}^{+\infty} S^0(k,k')\frac{\delta(k+k_0)+\delta(k-k_0)}{|k|}\frac{\delta(k'+k_0)+\delta(k'-k_0)}{|k'|} \\ &\quad\times\frac{\cos[(k+k')z]-1}{|k+k'|}\,\mathrm{d}k\mathrm{d}k'.\end{aligned} \tag{3.72}$$

Using again the properties of Dirac distribution function δ, first on variable k' and then on k, one obtains

$$\widetilde{\phi^2}(z) \equiv \frac{1}{16k_0^3}S^0(k_0,k_0)\left[\cos(2k_0z)-1\right] \tag{3.73}$$

where the property $S^0(-k,-k') = S^0(k,k')$ has been used. From Eq. (3.53), we finally plug the value of $S^0(k_0,k_0) = k_0^2/2$ into the former expression to obtain

$$\widetilde{\phi^2}(z) \equiv \frac{1}{32k_0}\left[\cos(2k_0z)-1\right]. \tag{3.74}$$

Thus total front perturbation is given by

$$\begin{aligned}\widetilde{\delta a}(z) &\equiv \epsilon\phi^1(z)+\epsilon^2\phi^2(z)-\epsilon\phi^1(0)-\epsilon^2\phi^2(0) = \epsilon\widetilde{\phi^1}(z)+\epsilon^2\widetilde{\phi^2}(z) \\ &\equiv \frac{\epsilon}{2k_0}\left[1-\cos(k_0z)\right]+\frac{\epsilon^2}{32k_0}\left[\cos(2k_0z)-1\right].\end{aligned} \tag{3.75}$$

Fig. 3.9 (a) shows the calculated front deformations for different contrast values $\epsilon = 0.4$ and $\epsilon = 0.8$. Note that the results are normalized by the wavelength λ_0 of the toughness field. It can be noticed that for a given value of contrast ϵ, the amplitude of the deformations remains the same for first - and second-order developments. However, the shape of the front is different. That means that the first-order term only contributes to the total amplitude:

$$|\widetilde{\delta a}(z)| \equiv \Delta a = \frac{\epsilon}{k_0} = \frac{\lambda_0\epsilon}{2\pi}. \tag{3.76}$$

As a result, the perturbation amplitude is linear in toughness contrast ϵ as shown on Fig. 3.9 (b) that represents the amplitude normalized by the wavelength as a function of toughness contrast ϵ. In order to highlight the effect of the second-order correction on the front shape, we normalise now $\widetilde{\delta a}(z)$ by the amplitude, and not the wavelength (see Fig. 3.9 (c)). The results correspond here to the contrast ϵ equal to 0.4 and 0.8. As expected, the normalized curves have the same amplitude. But we observe that the front deformation gets flatter as contrast increases, large and large parts of the crack front remain pinned in tougher zone of the sinusoidal toughness field.

We now would like to discuss why the second order approximation doesn't contribute to the amplitude of the front perturbations. It can be rationalised by considering the symmetry of the field of the fracture energy (3.66): As we change the contrast form ϵ to $-\epsilon$, the sinusoidal toughness field given by Eqs. (3.25) and (3.66) remains identical after translated by half of a wavelength along the $z-$axis, as illustrated on Fig. 3.10

$$G_c^{(-\epsilon)}(k_0z) = G_c^{(\epsilon)}(k_0z+\pi) \tag{3.77}$$

where $G_c^{(-\epsilon)}$ is the toughness field corresponding to negative contrast and $G_c^{(\epsilon)}$ to positive contrast. This implies that the front perturbation has also same property, *i.e :*

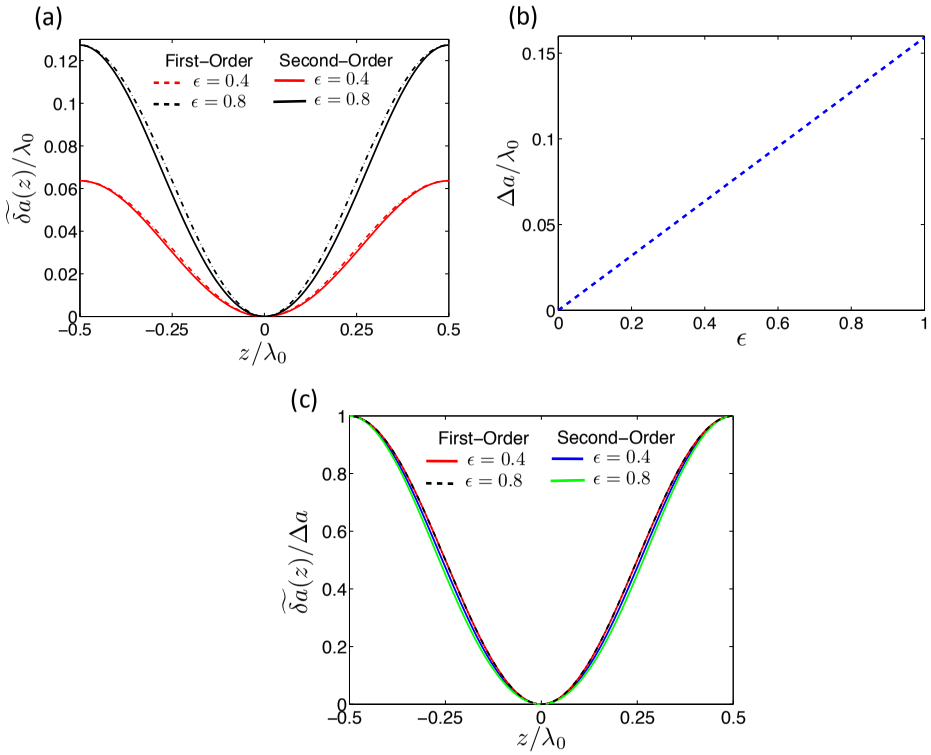

Figure 3.9: Crack front perturbations (a) normalized by its wavelength $k_0 = 2\pi/\lambda_0$; (b) normalized amplitude versus contrast; (c) normalized by its amplitude Δa.

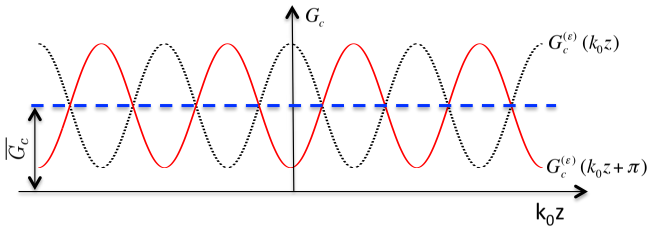

Figure 3.10: Schematic representation of the symmetry property of the sinusoidal distribution of fracture toughness in an infinite body

$$\widetilde{\delta a}^{(\epsilon)}(k_0 z) = \widetilde{\delta a}^{(-\epsilon)}(k_0 z + \pi).$$

This means that

$$\epsilon\widetilde{\phi^1}^{(\epsilon)}(k_0 z) + \epsilon^2\widetilde{\phi^2}^{(\epsilon)}(k_0 z) = -\epsilon\widetilde{\phi^1}^{(-\epsilon)}(k_0 z + \pi) + \epsilon^2\widetilde{\phi^2}^{(-\epsilon)}(k_0 z + \pi). \tag{3.78}$$

which gives the following properties:

$$\begin{cases} \widetilde{\phi^1}^{(\epsilon)}(k_0 z) = -\widetilde{\phi^1}^{(-\epsilon)}(k_0 z + \pi) \\ \widetilde{\phi^2}^{(\epsilon)}(k_0 z) = \widetilde{\phi^2}^{(-\epsilon)}(k_0 z + \pi). \end{cases} \tag{3.79}$$

The Eq. $(3.79)_1$ that shows anti-symmetry of $\widetilde{\phi^1}$ of period $\lambda_0/2$ is consisted with the behaviour of $\widetilde{\phi^1}$ that is periodic of period λ_0. More interestingly, Eq. $(3.79)_2$ shows that the second-order

contribution is necessarily of period $\lambda_0/2$, consisted with the calculated expression of $\widetilde{\phi^1}$ given in Eq. (3.74). Since the deformation amplitude follows

$$\Delta a \equiv \widetilde{\delta a}(\lambda_0/2) - \widetilde{\delta a}(0) = \epsilon \left[\widetilde{\phi^1}(\lambda_0/2) - \widetilde{\phi^1}(0)\right] + \epsilon^2 \left[\widetilde{\phi^2}(\lambda_0/2) - \widetilde{\phi^2}(0)\right] \tag{3.80}$$

the periodicity of $\widetilde{\phi^2}$ with period $\lambda_0/2$ also implies that the second-order (but also all the terms of even-order) *does not* contribute to the overall amplitude. This property does also hold for the periodic array of obstacles with width equal to the their spacing (*i.e.* $L = 2d$ in Eq. 3.62), that also displays a toughness invariant by the transformation $\epsilon \to -\epsilon$. This means that in such cases of toughness fields, second-order approximation is not enough to determine to which value of contrast the first-order can work with better prediction. One needs higher order approximation to distinguish the range of first-order approximations. However, it is possible to calculate this range of contrast by looking at the change in front shape due to second order as presented in Fig. 3.9 (c). One may define the error to quantify the change in front shape due to second order like ratio between second-order term and first-order term at $z = \lambda_0/4$:

$$\text{Err} \sim \frac{|\widetilde{\phi^2}(\lambda_0/4)|}{|\widetilde{\phi^1}(\lambda_0/4)|} = \frac{\epsilon}{4}. \tag{3.81}$$

This results that for an acceptable error level of 0.1, the first order approximation can be used as long as the contrast is lower than 0.4.

3.6.4 Effect of the toughness contrast on the front deformation amplitude

Before going to the final conclusive remarks, let us look at the effect of toughness contrast on the front perturbation amplitude for the threes examples of toughness field explored in this chapter.

In order to do that, let us first define the amplitude of the crack front deformations in these different cases. For example, in the case of a sinusoidal distribution it has been given by Eq. (3.80), *i.e.* that the amplitude corresponds to the difference in front deformations at points $z = 0$ and $z = \lambda_0/2$. The same definition holds in the case of a periodic array of obstacles with wavelength of $2L$, *i.e.* $\Delta a \equiv \overline{\delta a}(z = L) - \overline{\delta a}(z = 0)$. In the case of a single obstacle, we choose to define the amplitude as the difference of deformation between the front position at the defect edge $z = d$ and at the defect center $z = 0$:

$$\Delta a \equiv \widetilde{\delta a}(z = d) - \widetilde{\delta a}(z = 0) = \frac{d}{\pi}\epsilon\,(2 - \epsilon)\ln 2. \tag{3.82}$$

Fig. 3.11 plots the toughness contrast $\epsilon = \Delta G_c/\overline{G}_c$ versus amplitude normalized by either the defect size (in the case of single obstacle) or the wavelength (in periodic array and sinusoidal distribution). At first in the vicinity of contrast $\Delta G_c/\overline{G}_c = 0$, it can be noticed that all curves corresponding to different examples, are linear in ϵ and symmetric under the $\epsilon \to -\epsilon$ transformation up to some range of the contrast values. This is the range of contrast in which first-order approximation works with better precision. After this range of contrast value, the curves start to deviate due to the effect of the second-order term.

One shall notice that the range of contrast values where the first-order approximation is valid is not same in all examples represented here. For example, in the case of single obstacle, this range goes up to $\Delta G_c/\overline{G}_c = 0.2$, while in the case of periodic array of obstacles with

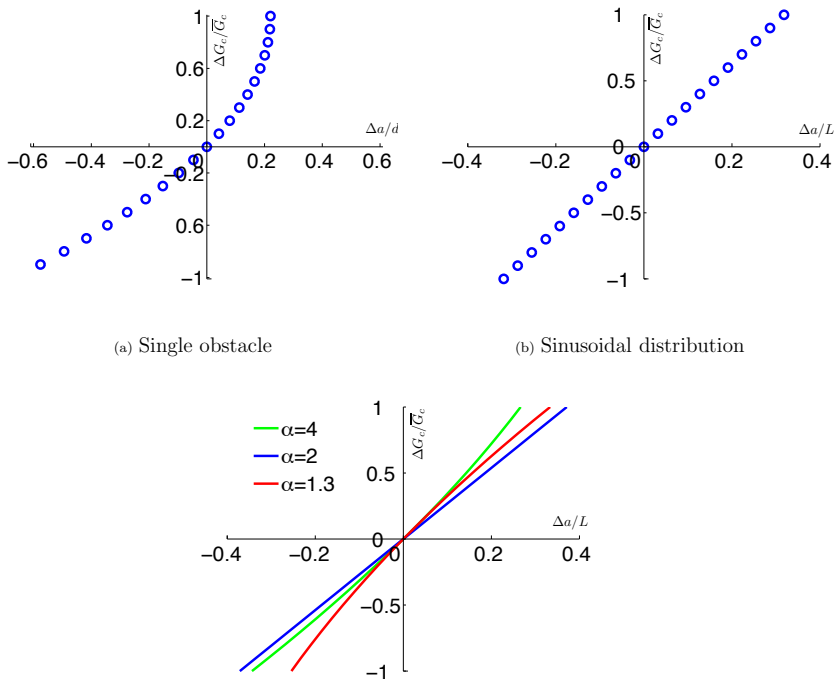

(a) Single obstacle

(b) Sinusoidal distribution

(c) Periodic array of obstacles

Figure 3.11: Different solutions for the amplitude Δa as a function of contrast $\epsilon = \Delta G_c/\overline{G}_c$ when half-plane crack interact with (a) single obstacle: the intrinsic length of toughness field is given by half-width of obstacle d, (b) Sinusoidal distribution of obstacles: the intrinsic length of toughness field is given by wavelength $\lambda_0 = 2L = 2\pi/k_0$, (b) periodic array of obstacles: the intrinsic length of toughness field is given by half-wavelength of the periodic array $L = \alpha d$.

$\alpha = 4$ and $\alpha = 1.3$ as presented on the Fig. 3.11 (c) (*green* and *red* curves), it goes up to $\Delta G_c/\overline{G}_c = 0.4$. This means there are effects not only due to the toughness contrast but also due to the geometry of the heterogeneities and their size (defined by the obstacle size (single obstacle) or by the wavelength of distribution of such obstacles (periodic)).

In the case of sinusoidal distribution of the toughness field as presented on the Fig. 3.11 (b) and in the case of periodic array of obstacles with $\alpha = 2$ as presented on the Fig. 3.11 (c) (*blue* curve), the toughness field holds symmetry property as discussed previously. As a result, the second-order doesn't contribute to the total front deformation amplitude and therefore, corresponding curves of the amplitude Δa is linear and symmetric under the $\epsilon \to -\epsilon$ transformation for any value of the contrast. As discussed previously, this means that in such cases, second-order approximation is not enough to determine up to which value of contrast the first-order can work with a good precision.

We finally see that, as we have assumed Griffith's equilibrium, for any value of the toughness contrast one always finds the solution for the crack deformation amplitude. However, this might not be always true: In particular in the part devoted to numerical simulations, we will see that beyond some contrast value this hypothesis of Griffith's equilibrium does not exist. As a result, larger toughness contrast doesn't admit any solution in terms of amplitude of the front deformations.

3.7 Concluding remarks

The aim of this chapter was to investigate geometrically nonlinear effects in the quasi static, coplanar propagation of cracks in heterogenous materials. The simplest case of a semi-infinite crack in an infinite body was considered.

In a first step, this required an extension of Leblond *et al.* (2012)'s treatment of second-order in-plane perturbation of a crack to the case where the unperturbed SIF $K^0(a)$, for the straight configuration of the front, depends on its position a within the crack plane. Indeed when $dK^0/da = 0$, mathematical difficulties arise in the form of divergent integrals appearing in the expression of the equilibrium shape of the crack front resulting from a given distribution of fracture toughness. Consideration of this interesting limiting case therefore requires to first perform all calculations with $\mathrm{d}K^0/\mathrm{d}a \neq 0$, before finally (and carefully) taking the limit $\mathrm{d}K^0/\mathrm{d}a \to 0$. In addition, the more general new formula not making any assumption on the value of $\mathrm{d}K^0/\mathrm{d}a$ extends the second-order expression of the stress intensity factor of a perturbed crack front to more realistic fracture test geometries.

In a second step, the formulae obtained for the first- and second-order variations of the SIF resulting from a given perturbation of the front were applied to the explicit calculation of the equilibrium shape of the front of a semi-infinite crack propagating in an infinite heterogeneous medium according to Griffith's criterion, up to second order in the fluctuations of fracture toughness.

As a first application, we determined the apparent fracture toughness experienced by a crack propagating in a randomly heterogeneous, but statistically homogeneous material. This apparent toughness was found to depend on the loading and be slightly less than the exact average value of the local toughness, the effect being tied to the necessary decrease of the unperturbed ERR with the distance of propagation, and disappearing in the limit of negligibly small rates of decrease.

As a second application, we calculated the equilibrium shape of a crack front penetrating into a single obstacle of infinite length in the direction of propagation, or a periodic array or sinusoidal distribution of such obstacles, up to second order in the contrast of toughness between the matrix and the obstacle(s). The second-order perturbation of the front was expressed in a very simple analytical form for a single obstacle and for a sinusoidal distribution, and as an infinite double series for an array of obstacles. One major outcome of the work is that in the case of single obstacle, or some cases of periodic array of such obstacles, the second-order correction relevant for large toughness contrasts shows that the crack front *stiffens* under the action of strong obstacles; in other words, the first-order approximation *overestimates* the deformation of the crack pinned by such obstacles. However, in the case of sinusoidal toughness field, second-order is only relevant in front shape changes while it is irrelevant in contributing to the front deformation amplitude.

The next step will be to introduce the finite size of specimen in the formulation. This will be done in the next chapter.

Chapter 4

Second-order perturbation of a semi-infinite mode I crack lying on the mid-plane of an infinite plate

The aim of this chapter[1] is to study the effect of geometrical nonlinearities along with that of the finite size of samples on crack propagation in heterogeneous media. We shall consider the typical configuration, often used in actual experiments, of a crack lying on the mid-plane of a plate of finite thickness.

The chapter is organized as follows:

- Section 4.1 recalls, as a prerequisite, some established results for planar cracks with slightly perturbed fronts located on the mid-plane of a plate (Legrand *et al.*, 2011).

- Section 4.2 presents an extension of Legrand *et al.* (2011)'s first-order results for a cracked plate to the second order, using Rice (1989)'s general results.

- Section 4.3 applies the results found to the case of a semi-infinite crack propagating quasi-statically along the mid-plane of an infinite plate having some heterogeneous distribution of toughness. Assuming the stress intensity factor to be equal to the toughness at every point of the crack front, we determine the resulting shape of this front up to second order in the toughness fluctuations.

- As an application, Section 4.4 considers the case of a crack penetrating into a single obstacle of infinite length in the direction of propagation. The equilibrium shape of the front is calculated up to second order in the contrast of toughness between the matrix and the obstacle.

- Section 4.5 finally provides a summary of, and some comments on, the results obtained.

[1] The results presented in this chapter constitute the bulk of the material published in Vasoya *et al.* (2014).

4.1 Legrand *et al.* (2011)'s first-order solution for a crack lying on the mid-plane of a plate

Let us consider (Figure 4.1(a)) a semi-infinite plate of thickness $2h$. Choose the coordinate axes in such a way that this plate occupies the domain $0 \leq x < +\infty, -h \leq y \leq h, -\infty < z < +\infty$ in 3D space. Assume that there is an emerging crack on the mid-plane of the plate, occupying the region $0 \leq x \leq A, y = 0, -\infty < z < +\infty$, where A denotes the distance from the plate boundary to the crack front. Finally assume that the upper and lower parts of the boundary are subjected to opposite prescribed displacements perpendicular to the crack plane, generating a state of pure mode I at every point of the crack front.

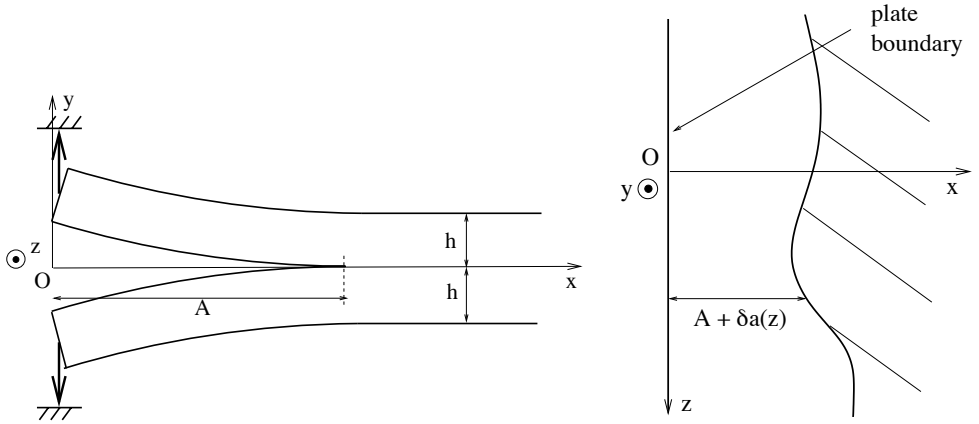

(a) View of the original crack in the Oxy plane.

(b) View of the perturbed crack in the Ozx plane.

Figure 4.1: A slightly perturbed emerging crack lying on the mid-plane of a semi-infinite plate.

Assume now that the crack front is perturbed by a small distance $\delta a(z)$ within the crack plane (Figure 4.1(b)). Under such conditions, Legrand *et al.* (2011) expressed the infinitesimal variation of the local SIF in the following form:

$$\frac{\delta K(z_1)}{K^0(A)} = -2\frac{\delta a(z_1)}{A} + PV\int_{-\infty}^{+\infty} \frac{f(\frac{A}{h};\frac{z-z_1}{h})}{(z-z_1)^2}[\delta a(z) - \delta a(z_1)]\,\mathrm{d}z \tag{4.1}$$

where $K^0(A)$ denotes the unperturbed SIF, depending on the location A of the unperturbed front, and *the function* $f(\frac{A}{h};\frac{z-z_1}{h})/(z_1-z)^2$ *represents the FK for the semi-infinite cracked plate considered, subjected to displacements prescribed on its boundary.* A fully explicit formula was provided for this specific FK.

An interesting limit-case is that of a semi-infinite crack in an infinite plate ($A \to +\infty$). The conditions of prescribed displacements on the boundary then become equivalent to conditions of prescribed bending moments far from the crack front[1]. In such a limit-case, Eq. (4.1) becomes

$$\frac{\delta K(z_1)}{K^0} = PV\int_{-\infty}^{+\infty} \frac{f(\frac{z-z_1}{h})}{(z-z_1)^2}[\delta a(z) - \delta a(z_1)]\,\mathrm{d}z \tag{4.2}$$

[1]In the limit $A \to \infty$, no matter the boundary conditions on the boundary of the plate, the loading becomes equivalent to a prescribed bending moment. This is illustrated in Appendix B.1 by considering for instance the case of a prescribed force on this boundary before taking the limit $A \to \infty$.

where the function $f(\frac{z-z_1}{h})/(z-z_1)^2 \equiv f(+\infty;\frac{z-z_1}{h})/(z-z_1)^2$ now represents *the FK for an infinite cracked plate subjected to prescribed forces only.* Attention will be focused on this sole special case in the sequel.

The Fourier transform of $\delta K(z_1)$ is readily found by expressing the function δa in Eq. (4.2) in terms of its Fourier transform $\widehat{\delta a}$: one thus obtains

$$\frac{\delta K(z_1)}{K^0} = \int_{-\infty}^{+\infty} \widehat{\delta a}(k) \left[PV \int_{-\infty}^{+\infty} \frac{f(\frac{z-z_1}{h})}{(z-z_1)^2} \left(e^{ikz} - e^{ikz_1} \right) \mathrm{d}z \right] \mathrm{d}k.$$

Writing now $e^{ikz} - e^{ikz_1}$ as $e^{ikz_1}(e^{ik(z-z_1)} - 1)$, one gets from there, with a few transformations,

$$\frac{\widehat{\delta K}(k)}{K^0} = -|k| X(kh) \widehat{\delta a}(k) \tag{4.3}$$

where

$$X(p) \equiv \frac{1}{|p|} PV \int_{-\infty}^{+\infty} \frac{f(u)}{u^2} \left(1 - e^{ipu} \right) \mathrm{d}u \quad \Leftrightarrow \quad f(u) \equiv \frac{1}{2\pi} \int_{-\infty}^{+\infty} \left[|p| X(p) \right]'' e^{-ipu} \, \mathrm{d}p. \tag{4.4}$$

Eq.$(4.4)_1$ here is obtained directly, and Eq.$(4.4)_2$ is then easily established by calculating $[|p|X(p)]''$ (Note that this second-derivative must be understood in the sense of distributions).

In the work of Legrand *et al.* (2011), Eq. (4.2) was not obtained directly but through Fourier inversion of Eq. (4.3). This equation was itself established by solving the elasticity problem of a plate the mid-plane of which contained a crack with a sinusoidal front, both analytically in the case of an infinitesimal plate thickness, and by the finite element method in the case of a finite one. The procedure yielded the following explicit expression of the function $X(p)$:

$$X(p) \simeq \frac{1}{2} \left[1 + \frac{3}{1 + \frac{1}{3}|p|^{4/3}} \right]. \tag{4.5}$$

This expression is (slightly) approximate in general because of the numerical method used to determine it, but exact in the two limits $p \to 0$ and $p \to \pm\infty$.

It is finally instructive to consider a sinusoidal perturbation of the front of wavelength λ. For such a perturbation the only values of the wavenumber k to be considered are $k = \pm 2\pi/\lambda$. Then:

- if $h \gg \lambda, |kh| \gg 1$ so that, by Eq. (4.5), $X(kh) \to \dfrac{1}{2}$ and Eq. (4.3) becomes identical to a formula of Rice (1985) for a semi-infinite crack in an infinite body;

- if $h \ll \lambda, |kh| \ll 1$, so that $X(kh) \to 2$ and Eq. (4.3) becomes identical to the formula established analytically by Legrand *et al.* (2011) for a semi-infinite crack lying on the mid-plane of a plate of infinitesimal thickness.

The value of $\delta K(z)$ is thus 4 times larger, for a given crack front perturbation $\delta a(z)$, in a very thin plate than in an infinite body.

4.2 Coplanar perturbation of a semi-infinite crack lying on the mid-plane of an infinite plate

4.2.1 Notations

For now on, we consider (Figure 4.2) the case of a semi-infinite crack located on the mid-plane of an infinite plate of thickness $2h$, loaded in pure mode I through prescribed forces only.

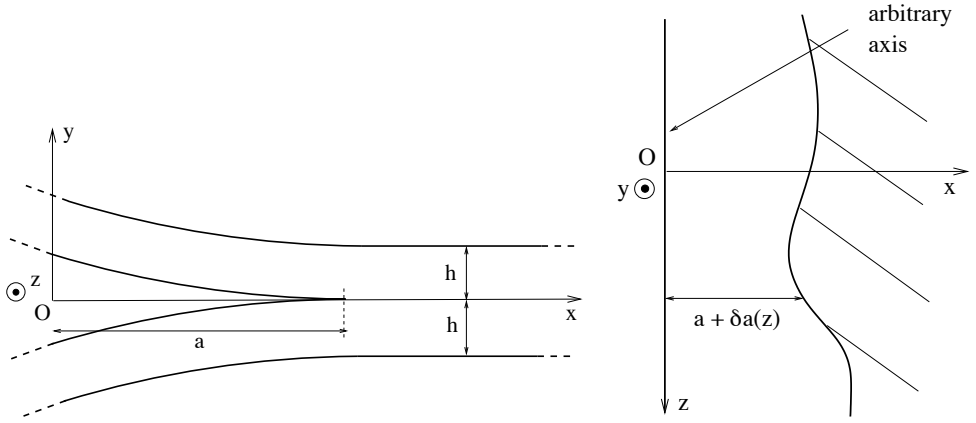

(a) View of the original crack in the Oxy plane.

(b) View of the perturbed crack in the Ozx plane.

Figure 4.2: A slightly perturbed semi-infinite crack lying on the mid-plane of an infinite plate.

We assume that the crack front perturbation $\delta a(z)$ is of a form similar to that in previous chapter, that is,

$$x(z) = a + \delta a(z) = a + \epsilon\phi(z) \tag{4.6}$$

where a denotes the distance front the arbitrary Oz axis to the reference straight crack front. The expansions of the SIF and FK in ϵ are then similar to those given by Eq. (3.2) with the same assumption that the loading has a translatory invariance in the direction z of the crack front, so that the unperturbed SIF $K^0(a)$ depends on the location a of the (straight) front but not on the position of the point of observation along it. With this background our interest here again lies in the second-order expression of the SIF $K(a, \epsilon; z)$ and the first-order expression of the FK $Z(\epsilon; z_1, z_2)$. The only difference is that now both the SIF and the FK involve the finite thickness h of the plate as an extra argument.

4.2.2 First-order expansion of the fundamental kernel

Since both the special loading considered by Legrand *et al.* (2011) when deriving Eqs. (4.2), (4.4) and (4.5), and the more general one considered here, involve prescribed forces only, the FK $Z^0(z_1, z_2)$ for the unperturbed configuration of the crack is the same as in Eq. (4.2),

$$Z^0(z_1, z_2) \equiv \frac{f(\frac{z_1 - z_2}{h})}{(z_1 - z_2)^2} \tag{4.7}$$

where the function f is given by Eqs. (4.4) and (4.5).

In the specific case considered, the ancillary perturbation $\delta_* a(z) \equiv \epsilon\phi_*(z)$ of Rice (1989)'s second formula (2.12) may again be taken as a suitable combination of a translatory motion and a rotation as defined in Eq. (3.5). The lack of a homothetical transformation of the crack front here (which basically arises from its initial straightness) implies that it undergoes a mere rigid-body motion. *Under such a motion the thickness of the plate, and therefore the overall geometry, remain unchanged*[1] *so that* $\delta_* Z$ *is zero.* Eq. (2.12) therefore applies and gives

$$Z^1(z_1, z_2) = PV \int_{-\infty}^{+\infty} \frac{f(\frac{z_1-z}{h}) f(\frac{z-z_2}{h})}{(z_1-z)^2(z-z_2)^2} [\phi(z) - \phi_*(z)] \, \mathrm{d}z \tag{4.8}$$

where use has been made of Eq. (4.7).

4.2.3 Second-order expansion of the stress intensity factor

At order 1 in ϵ, the expression of $K^1(a; z)$ is obtained through direct application of Rice (1989)'s first formula (2.10) for the variation of the SIF to the straight configuration of the front:

$$K^1(a; z_1) = \frac{dK^0}{da}(a)\, \phi(z_1) + K^0(a)\, PV \int_{-\infty}^{+\infty} \frac{f(\frac{z-z_1}{h})}{(z-z_1)^2} [\phi(z) - \phi(z_1)] \, \mathrm{d}z. \tag{4.9}$$

This equation is identical to Eq. (4.2) of Legrand *et al.* (2011) except for the additional first term in the right-hand side. This term was zero for the special loading envisaged by Legrand *et al.* (2011) because the unperturbed SIF was independent of the location of the (straight) crack front within the crack plane, but this does not remain true for the more general loading considered here.

In the same way, at order 2, $K^2(a; z)$ may be obtained by again applying Rice (1989)'s first formula (2.10), considering some pre-perturbed configuration of the front upon which is superimposed a secondary, infinitesimal *proportional* perturbation. When doing so, one must use formulae for the SIF and the FK on the pre-perturbed configuration accurate to first order in the primary perturbation; the first of these formulae is provided by Eq. (4.9) and the second by Rice (1989)'s second formula (2.12), which takes the form (4.8) in the present case. The output is an expression of $\partial K(a, \epsilon; z)/\partial\epsilon$ accurate to first order in ϵ, which immediately yields the second-order expression of $K(a, \epsilon; z)$ upon integration. This was the procedure followed by Leblond *et al.* (2012) and described in the previous chapter in the case of an infinite body. The reasoning for a plate is analogous and therefore will not be repeated. The final result reads :

$$\begin{aligned} K^2(a; z_1) \;=\; & \frac{1}{2}\frac{\mathrm{d}^2 K^0}{\mathrm{d}a^2}(a)\, [\phi(z_1)]^2 + \frac{1}{2}\frac{\mathrm{d}K^0}{\mathrm{d}a}(a)\, PV \int_{-\infty}^{+\infty} \frac{f(\frac{z-z_1}{h})}{(z-z_1)^2} [\phi^2(z) - \phi^2(z_1)] \, dz \\ & + \frac{K^0(a)}{2} \Bigg\{ PV \int_{-\infty}^{+\infty} \int_{-\infty}^{+\infty} \frac{f(\frac{z-z_1}{h}) f(\frac{z'-z}{h})}{(z-z_1)^2(z'-z)^2} [\phi(z) - \phi(z_1)][\phi(z') - \phi(z)] \, \mathrm{d}z\mathrm{d}z' \\ & + PV \int_{-\infty}^{+\infty} \int_{-\infty}^{+\infty} \frac{f(\frac{z'-z_1}{h}) f(\frac{z'-z}{h})}{(z'-z_1)^2(z'-z)^2} \left[\phi(z') - \phi(z_1) - \frac{\phi(z) - \phi(z_1)}{z - z_1}(z' - z_1) \right] \\ & \qquad \times [\phi(z) - \phi(z_1)] \, \mathrm{d}z\mathrm{d}z' \Bigg\}. \end{aligned} \tag{4.10}$$

[1] Note that the hypothesis of infiniteness of the plate plays a central role here; if it were semi-infinite, like at the beginning of Section 4.1, the rotation of the crack front would not leave the geometry unchanged since this front would not remain parallel to the plate boundary.

4.2.4 Formulae in Fourier's space

Stress intensity factor:

With regard to the SIF, at order 1 in ϵ, the expression of the Fourier transform of $K^1(a;z_1)$ is easily established by expressing the function ϕ in Eq. (4.9) in terms of its Fourier transform $\widehat{\phi}$ and using Eq. $(4.4)_1$; one thus gets

$$\widehat{K^1}(a;k) = \left[\frac{\mathrm{d}K^0}{\mathrm{d}a}(a) - K^0(a)|k|X(kh)\right]\widehat{\phi}(k). \tag{4.11}$$

This expression extends Eq. (4.3), due to Legrand *et al.* (2011), by including the term $\dfrac{\mathrm{d}K^0}{\mathrm{d}a}(a)\widehat{\phi}(k)$, which was absent in this equation since for the loading considered by these authors, the unperturbed K^0 was independent of the location of the crack front within the crack plane.

In the same way, at order 2, the expression of the Fourier transform of $K^2(a;z_1)$ can be established by expressing the function ϕ in Eq. (4.10) in terms of its Fourier transform $\widehat{\phi}$; one thus gets

$$\begin{aligned}
K^2(a;z_1) \;=\; & \int_{-\infty}^{+\infty}\int_{-\infty}^{+\infty}\widehat{\phi}(k)\widehat{\phi}(k')\left\{\frac{1}{2}\frac{\mathrm{d}^2K^0}{\mathrm{d}a^2}(a)e^{i(k+k')z_1}\right.\\
& +\frac{1}{2}\frac{\mathrm{d}K^0}{\mathrm{d}a}(a)PV\int_{-\infty}^{+\infty}\frac{f(\frac{z-z_1}{h})}{(z-z_1)^2}\left(e^{i(k+k')z}-e^{i(k+k')z_1}\right)\mathrm{d}z\\
& +\frac{K^0(a)}{2}\left[PV\int_{-\infty}^{+\infty}\int_{-\infty}^{+\infty}\frac{f(\frac{z-z_1}{h})f(\frac{z'-z}{h})}{(z-z_1)^2(z'-z)^2}\left(e^{ikz}-e^{ikz_1}\right)\left(e^{ik'z'}-e^{ik'z}\right)\mathrm{d}z\mathrm{d}z'\right.\\
& +PV\int_{-\infty}^{+\infty}\int_{-\infty}^{+\infty}\frac{f(\frac{z'-z_1}{h})f(\frac{z'-z}{h})}{(z'-z_1)^2(z'-z)^2}\left(e^{ikz'}-e^{ikz_1}-\frac{e^{ikz}-e^{ikz_1}}{z-z_1}(z'-z_1)\right)\\
& \left.\left.\times\left(e^{ik'z}-e^{ik'z_1}\right)dzdz'\right]\right\}\mathrm{d}k\mathrm{d}k'.
\end{aligned} \tag{4.12}$$

Now, taking $e^{i(k+k')z_1}$ as a common factor in the integrands and using Eq. $(4.4)_1$, one gets

$$\begin{aligned}
K^2(a;z_1) \;=\; & \int_{-\infty}^{+\infty}\int_{-\infty}^{+\infty}\widehat{\phi}(k)\widehat{\phi}(k')\left\{\frac{1}{2}\frac{\mathrm{d}^2K^0}{\mathrm{d}a^2}(a)-\frac{1}{2}\frac{\mathrm{d}K^0}{\mathrm{d}a}(a)|k+k'|X((k+k')h)\right.\\
& \left.+\frac{K^0(a)}{2}\left[I_1(h;k,k';z_1)+I_2(h;k,k';z_1)\right]\right\}e^{i(k+k')z_1}\mathrm{d}k\mathrm{d}k',
\end{aligned} \tag{4.13}$$

where $I_1(h;k,k';z_1)$ and $I_2(h;k,k';z_1)$ are double integrals, the expression and calculation of which is presented in Appendix B.2, with the conclusion that they are in fact independent of z_1, and given by

$$\left\{\begin{array}{rcll}
I_1(h;k,k';z_1) & \equiv & I_1(h;k,k') & = |k'|X(k'h)\left[|k+k'|X((k+k')h)-|k'|X(k'h)\right]\\
I_2(h;k,k';z_1) & \equiv & I_2(h;k,k') & = \dfrac{1}{2}\left[k^2X^2(kh)-(k+k')^2X^2((k+k')h)-k'^2X^2(k'h)\right.\\
 & & & \left.+2|k+k'||k'|X((k+k')h)X(k'h)\right].
\end{array}\right. \tag{4.14}$$

Equation (4.13) becomes, upon use of these formulae and "symmetrization" of the integrand with respect to k and k',

$$K^2(a;z_1) = K^0(a)\int_{-\infty}^{+\infty}\int_{-\infty}^{+\infty} R(a;h;k,k')\widehat{\phi}(k)\widehat{\phi}(k')e^{i(k+k')z_1}\mathrm{d}k\mathrm{d}k' \tag{4.15}$$

where

$$\begin{aligned} R(a;h;k,k') \equiv\ & \frac{1}{2}\frac{\mathrm{d}^2K^0}{K^0\mathrm{d}a^2}(a) - \frac{1}{2}\frac{\mathrm{d}K^0}{K^0\mathrm{d}a}(a)|k+k'|X((k+k')h) \\ & + \frac{|k+k'|}{2}X((k+k')h)\left[|k|X(kh)+|k'|X(k'h)\right] \\ & - \frac{1}{4}\left[(k+k')^2X^2((k+k')h) + k^2X^2(kh) + k'^2X^2(k'h)\right]. \end{aligned} \tag{4.16}$$

Using the change of variable $k_1 = k+k'$, the preceding expression of $K^2(a;z_1)$ may be rewritten in the form

$$K^2(a;z_1) = K^0(a)\int_{-\infty}^{+\infty}\left[\int_{-\infty}^{+\infty} R(a;h;k,k_1-k)\widehat{\phi}(k)\widehat{\phi}(k_1-k)\mathrm{d}k\right]e^{ik_1z_1}dk_1$$

which implies, upon comparison with the definition (3.16) of the Fourier transform, that

$$\widehat{K^2}(a;k_1) = K^0(a)\int_{-\infty}^{+\infty} R(a;h;k,k_1-k)\widehat{\phi}(k)\widehat{\phi}(k_1-k)\mathrm{d}k. \tag{4.17}$$

Note the remarkable property that $\widehat{K^2}(a;k_1)$, just like $\widehat{K^1}(a;k_1)$, depends upon the FK of the cracked geometry considered through the sole function X defined by Eq. (4.4) (since the expression (4.16) of $R(a;h;k,k')$ involves only X).

A comparison with the results of Vasoya *et al.* (2013) for an infinite body expounded in the previous chapter is in order here, by letting h go to infinity. The function R becomes in this limit, since $X(kh) \to \dfrac{1}{2}$ then (see Eq. (4.5)):

$$\begin{aligned} \lim_{h\to+\infty} R(a;h;k,k') = & \frac{1}{2}\frac{\mathrm{d}^2K^0}{K^0\mathrm{d}a^2}(a) - \frac{1}{4}\frac{\mathrm{d}K^0}{K^0\mathrm{d}a}(a)|k+k'| \\ & + \frac{1}{16}\left[2|k+k'|\left(|k|+|k'|\right) - (k+k')^2 - k^2 - k'^2\right] \end{aligned} \tag{4.18}$$

which is another form of the function R found by Vasoya *et al.* (2013), recalled in Eq. (3.21) of the previous chapter. This establishes the equivalence of the results found in the case of an infinite body.

Energy-release rate:

The expansion of the Fourier transform $\widehat{G}(a,\epsilon;k)$ of the elastic energy-release-rate $G(a,\epsilon;z)$ follows from Irwin's formula and the expressions (4.11) and (4.17) of $\widehat{K^1}(a;k)$ and $\widehat{K^2}(a;k)$. It is given by Eq. (3.22) of chapter 3 where

$$\left\{\begin{array}{lll} \widehat{G^1}(a;k) & = & G^0(a)\left[\dfrac{1}{G^0}\dfrac{\mathrm{d}G^0}{\mathrm{d}a}(a) - 2|k|X(kh)\right]\widehat{\phi}(k) \\ \widehat{G^2}(a;k_1) & = & G^0(a)\displaystyle\int_{-\infty}^{+\infty} S(a;h;k,k_1-k)\,\widehat{\phi}(k)\,\widehat{\phi}(k_1-k)\,\mathrm{d}k \end{array}\right. \tag{4.19}$$

where

$$\begin{aligned} S(a;h;k,k') \equiv\ & \frac{1}{2}\frac{\mathrm{d}^2G^0}{G^0\mathrm{d}a^2}(a) - \frac{1}{2}\frac{\mathrm{d}G^0}{G^0\mathrm{d}a}(a)\big[|k+k'|X((k+k')h) + |k|X(kh) + |k'|X(k'h)\big] \\ & -\frac{1}{2}\big[|k+k'|X((k+k')h) - |k|X(kh) - |k'|X(k'h)\big]^2 \\ & +2|k||k'|X(kh)X(k'h). \end{aligned} \tag{4.20}$$

4.3 The equilibrium shape of the front of a crack propagating in a heterogeneous plate

In the same way as we have examined, in the previous chapter, the shape of the front of a crack propagating in an infinite body, we shall now apply the preceeding results to calculate the equilibrium front geometry of a crack propagating along the mid-plane of an infinite plate subjected to some mode I loading, propagation being governed by Griffith's criterion with a heterogeneous fracture toughness $G_c(x,z)$ given by Eq. (3.25). Following the same procedure as in § 3.4 to calculate the parameter a (unperturbed crack position) and the functions $\phi^1(a;z)$ and $\phi^2(a;z)$ defining the crack front perturbation, one gets the following conditions:

- At order 0:
$$G^0(a) = \overline{G_c}\,. \tag{4.21}$$
This condition again determines the mean location a of the crack front.

- At order 1:
$$\widehat{\mathcal{G}^1}\left[a;\{\widehat{\phi^1}\}\right](k) = \overline{G_c}\,\widehat{g_c}(a,k)$$
which implies, by the expression $(4.19)_1$ of the functional $\widehat{\mathcal{G}^1}$ and equation (4.21), that
$$\widehat{\phi^1}(a;k) = -\frac{\widehat{g_c}(a,k)}{2|k|X(kh) - \frac{\mathrm{d}G^0}{G^0\mathrm{d}a}(a)}. \tag{4.22}$$

- At order 2:
$$\widehat{\mathcal{G}^1}\left[a;\{\widehat{\phi^2}\}\right](k_1) = -\widehat{\mathcal{G}^2}\left[a;\{\widehat{\phi^1}\}\right](k_1) + \overline{G_c}\int_{-\infty}^{+\infty}\frac{\partial\widehat{g_c}}{\partial x}(a,k)\,\widehat{\phi^1}(a;k_1-k)\mathrm{d}k$$
which implies, by expressions (4.19) of $\widehat{\mathcal{G}^1}$ and $\widehat{\mathcal{G}^2}$ and Eqs. (4.21) and (4.22), that
$$\begin{aligned} \widehat{\phi^2}(a;k_1) =\ & \frac{1}{2|k_1|X(k_1h) - \frac{\mathrm{d}G^0}{G^0\mathrm{d}a}(a)}\Big\{\int_{-\infty}^{+\infty} S(a;h;k,k_1-k) \\ & \times\frac{\widehat{g_c}(a,k)}{2|k|X(kh) - \frac{\mathrm{d}G^0}{G^0\mathrm{d}a}(a)}\,\frac{\widehat{g_c}(a,k_1-k)}{2|k_1-k|X((k_1-k)h) - \frac{\mathrm{d}G^0}{G^0\mathrm{d}a}(a)}\,\mathrm{d}k \\ & +\int_{-\infty}^{+\infty}\frac{\partial\widehat{g_c}}{\partial x}(a,k)\frac{\widehat{g_c}(a,k_1-k)}{2|k_1-k|X((k_1-k)h) - \frac{\mathrm{d}G^0}{G^0\mathrm{d}a}(a)}\,\mathrm{d}k\Big\}. \end{aligned} \tag{4.23}$$

Again, in order to warrant convergence of the integrals appearing in these expressions of $\widehat{\phi^1}(a;k)$ and $\widehat{\phi^2}(a;k)$ and their inverse Fourier transforms $\phi^1(a;z)$ and $\phi^2(a;z)$, it is necessary to make the hypothesis defined by Eq.(3.32) on the sign of the derivative of the unperturbed ERR G^0 with respect to the unperturbed crack position, ensuring that the denominators of the various fractions never vanish.

4.4 The shape of a crack front encountering a single obstacle

As an application, we shall again determine the equilibrium shape of the front of a crack lying on the mid-plane of an infinite plate and penetrating into a single obstacle of infinite length in the direction of propagation, up to second order in the contrast of toughness. The distribution of toughness is again represented by Eq. (3.46). At order 1, one gets from equations (4.22) and (3.47):

$$\widehat{\phi^1}(a;k) = -\frac{\sin(kd)}{\pi k\left[2|k|X(kh) - \frac{dG^0}{G^0 da}(a)\right]}$$

so that

$$\begin{aligned}\phi^1(a;z) &= -\frac{1}{\pi}\int_{-\infty}^{+\infty} \frac{\sin(kd)}{k\left[2|k|X(kh) - \frac{\mathrm{d}G^0}{G^0\mathrm{d}a}(a)\right]} e^{ikz}\,\mathrm{d}k \\ &= -\frac{2}{\pi}\int_{0}^{+\infty} \frac{\sin(kd)}{k\left[2kX(kh) - \frac{\mathrm{d}G^0}{G^0\mathrm{d}a}(a)\right]} \cos(kz)\,\mathrm{d}k.\end{aligned}$$

In the limit $\dfrac{\mathrm{d}G^0}{\mathrm{d}a}(a) \to 0^-$, the integral defining $\phi^1(a;z)$ here diverges. However we are interested only in the deviation of the crack front from straightness, characterized again at order 1 by the quantity

$$\widetilde{\phi^1}(a;z) \equiv \phi^1(a;z) - \phi^1(a;0) = \frac{2}{\pi}\int_0^{+\infty} \frac{\sin(kd)}{k\left[2kX(kh) - \frac{\mathrm{d}G^0}{G^0\mathrm{d}a}(a)\right]} \left[1-\cos(kz)\right]\,\mathrm{d}k\,. \qquad (4.24)$$

This quantity has a well-defined limit $\widetilde{\phi^1}(z)$ for $\dfrac{\mathrm{d}G^0}{\mathrm{d}a}(a) \to 0^-$ given by

$$\widetilde{\phi^1}(z) \equiv \frac{1}{\pi}\int_0^{+\infty} \frac{\sin(kd)}{k^2X(kh)} \left[1-\cos(kz)\right]\,\mathrm{d}k\,. \qquad (4.25)$$

At order 2, equations (4.23) and (3.47) yield, since the function $\widehat{g_c}(x,k)$ is independent of x:

$$\begin{aligned}\phi^2(a;z) &= \frac{1}{\pi^2}\int_{-\infty}^{+\infty}\int_{-\infty}^{+\infty} S(a;h;k,k') \frac{\sin(kd)}{k\left[2|k|X(kh) - \frac{\mathrm{d}G^0}{G^0\mathrm{d}a}(a)\right]} \frac{\sin(k'd)}{k'\left[2|k'|X(k'h) - \frac{\mathrm{d}G^0}{G^0\mathrm{d}a}(a)\right]} \\ &\qquad \times \frac{e^{i(k+k')z}}{2|k+k'|X((k+k')h) - \frac{\mathrm{d}G^0}{G^0\mathrm{d}a}(a)}\,\mathrm{d}k\mathrm{d}k' \\ &= \frac{2}{\pi^2}\int\int_{k+k'\geq 0} S(a;h;k,k') \frac{\sin(kd)}{k\left[2|k|X(kh) - \frac{\mathrm{d}G^0}{G^0\mathrm{d}a}(a)\right]} \frac{\sin(k'd)}{k'\left[2|k'|X(k'h) - \frac{\mathrm{d}G^0}{G^0\mathrm{d}a}(a)\right]} \\ &\qquad \times \frac{\cos[(k+k')z]}{2(k+k')X((k+k')h) - \frac{\mathrm{d}G^0}{G^0\mathrm{d}a}(a)}\,\mathrm{d}k\mathrm{d}k'\end{aligned}$$

where we have grouped the terms (k,k') and $(-k,-k')$ in the double integral and accounted for the fact that $S(a;h;-k,-k')=S(a;h;k,k')$, see equation (4.20).

Again, we are interested only in the deviation of the crack front from straightness, characterized at order 2 by the quantity

$$\begin{aligned}\widetilde{\phi^2}(a;z)\equiv\phi^2(a;z)-\phi^2(a;0) &= \frac{2}{\pi^2}\int\!\!\int_{k+k'\geq 0} S(a;h;k,k')\frac{\sin(kd)}{k\left[2|k|X(kh)-\frac{\mathrm{d}G^0}{G^0\mathrm{d}a}(a)\right]}\\ &\times\frac{\sin(k'd)}{k'\left[2|k'|X(k'h)-\frac{\mathrm{d}G^0}{G^0\mathrm{d}a}(a)\right]}\,\frac{\cos[(k+k')z]-1}{2(k+k')X((k+k')h)-\frac{\mathrm{d}G^0}{G^0\mathrm{d}a}(a)}\,\mathrm{d}k\mathrm{d}k'.\end{aligned} \tag{4.26}$$

This quantity has a well-defined limit $\widetilde{\phi^2}(z)$ for $\dfrac{\mathrm{d}G^0}{\mathrm{d}a}(a)\to 0^-$ given by

$$\widetilde{\phi^2}(z)\equiv\frac{1}{4\pi^2}\int\!\!\int_{k+k'\geq 0} S^0(h;k,k')\,\frac{\sin(kd)}{k|k|X(kh)}\,\frac{\sin(k'd)}{k'|k'|X(k'h)}\,\frac{\cos[(k+k')z]-1}{(k+k')X((k+k')h)}\,\mathrm{d}k\mathrm{d}k' \tag{4.27}$$

where

$$\begin{aligned}S^0(h;k,k') &\equiv \lim_{\mathrm{d}G^0/\mathrm{d}a\to 0^-} S(a;h;k,k')\\ &= -\frac{1}{2}\left[|k+k'|X((k+k')h)-|k|X(kh)-|k'|X(k'h)\right]^2+2|k||k'|X(kh)X(k'h).\end{aligned} \tag{4.28}$$

The integral in equation (4.27) is convergent because the function $S^0(h;k,k')$ verifies the properties $S^0(h;k,0)=S^0(h;0,k')=0$.

Since the function S^0 is obviously invariant upon interchange of k and k', the integral in Eq. (4.27) can be simplified by reducing the integration domain $\{(k,k'),\,k+k'\geq 0\}$ in the same way as for integral (3.52); one thus gets

$$\begin{aligned}\widetilde{\phi^2}(z) &= \frac{1}{2\pi^2}\int_0^{+\infty}\left\{\int_0^k\left[S^0(h;k,k')\frac{\cos((k+k')z)-1}{(k+k')X((k+k')h)}\right.\right.\\ &\left.\left.+S^0(h;k,-k')\frac{\cos((k-k')z)-1}{(k-k')X((k-k')h)}\right]\frac{\sin(kd)}{k^2X(kh)}\,\frac{\sin(k'd)}{k'^2X(k'h)}\mathrm{d}k'\right\}\mathrm{d}k.\end{aligned}$$

One may now write $k'\equiv\lambda k$, $0\leq\lambda\leq 1$ and use the variables of integration (k,λ) instead of (k,k'); the preceding equation then becomes

$$\begin{aligned}\widetilde{\phi^2}(z) &= \frac{1}{2\pi^2}\int_0^{+\infty}\left\{\int_0^1\left[S^0(h;k,\lambda k)\frac{\cos((1+\lambda)kz)-1}{(1+\lambda)X((1+\lambda)kh)}\right.\right.\\ &\left.\left.+S^0(h;k,-\lambda k)\frac{\cos((1-\lambda)kz)-1}{(1-\lambda)X((1-\lambda)kh)}\right]\frac{\sin(kd)}{X(kh)}\,\frac{\sin(\lambda kd)}{\lambda^2X(\lambda kh)}\mathrm{d}\lambda\right\}\frac{\mathrm{d}k}{k^4}.\end{aligned}$$

Introducing the notation

$$\frac{S^0(h;k,\lambda k)}{k^2X(kh)X(\lambda kh)X((1+\lambda)kh)}\equiv T^0(kh,\lambda) \tag{4.29}$$

in the preceding integral and changing the order of integration, one gets the final expression of $\widetilde{\phi^2}(z)$:

$$\begin{aligned}\widetilde{\phi^2}(z) &= \frac{1}{2\pi^2}\int_0^1\left\{\frac{J\left[h;\lambda;d,\lambda d,(1+\lambda)z\right]-J(h;\lambda;d,\lambda d,0)}{1+\lambda}\right.\\ &\left.+\frac{J\left[h;-\lambda;d,\lambda d,(1-\lambda)z\right]-J(h;-\lambda;d,\lambda d,0)}{1-\lambda}\right\}\frac{\mathrm{d}\lambda}{\lambda^2}\end{aligned} \tag{4.30}$$

where

$$J(h;\lambda;\alpha,\beta,\gamma) \equiv \int_0^{+\infty} T^0(kh,\lambda)\sin(\alpha k)\sin(\beta k)\cos(\gamma k)\,\frac{\mathrm{d}k}{k^2}. \tag{4.31}$$

4.4.1 Limiting cases of infinite and infinitesimal thicknesses

In the limit of an infinite body ($h \to +\infty$), for which $X(kh) \to \dfrac{1}{2}$, the integrals in Eqs. (4.25), (4.30) and (4.31) may be calculated analytically, and the final results for $\widetilde{\phi^1}$ and $\widetilde{\phi^2}$ read (Chopin *et al.*, 2011; Vasoya *et al.*, 2013)

$$\left\{\begin{array}{rcl} \displaystyle\lim_{h\to+\infty}\widetilde{\phi^1}(z) & = & \dfrac{d}{\pi}\big[\,(1+u)\ln(|1+u|)+(1-u)\ln(|1-u|)\,\big] \\ \displaystyle\lim_{h\to+\infty}\widetilde{\phi^2}(z) & = & \left\{\begin{array}{ll} -\dfrac{d}{2\pi}\big[(1+u)\ln(1+u)+(1-u)\ln(1-u)\big] & \text{if} \quad |u|\le 1 \\ -\dfrac{d}{2\pi}\left[(|u|-1)\ln\left(\dfrac{|u|+1}{|u|-1}\right)+2\ln 2\right] & \text{if} \quad |u|\ge 1. \end{array}\right. \end{array}\right. \tag{4.32}$$

On the other hand, for an infinitely thin plate ($h \to 0$), X is multiplied by a factor of 4 with respect to the case $h \to +\infty$, so that by Eqs. (4.25), (4.28), (4.29), (4.30) and (4.31), $\widetilde{\phi^1}$ and $\widetilde{\phi^2}$ are simply divided by a factor of 4; that is,

$$\left\{\begin{array}{rcl} \displaystyle\lim_{h\to0}\widetilde{\phi^1}(z) & = & \dfrac{d}{4\pi}\big[\,(1+u)\ln(|1+u|)+(1-u)\ln(|1-u|)\,\big] \\ \displaystyle\lim_{h\to0}\widetilde{\phi^2}(z) & = & \left\{\begin{array}{ll} -\dfrac{d}{8\pi}\big[(1+u)\ln(1+u)+(1-u)\ln(1-u)\big] & \text{if} \quad |u|\le 1 \\ -\dfrac{d}{8\pi}\left[(|u|-1)\ln\left(\dfrac{|u|+1}{|u|-1}\right)+2\ln 2\right] & \text{if} \quad |u|\ge 1. \end{array}\right. \end{array}\right. \tag{4.33}$$

4.4.2 Numerical solutions for arbitrary values of the thickness

For arbitrary values of h, the integrals appearing in Eqs. (4.25), (4.30) and (4.31) may be calculated numerically. Instead of plotting both $\widetilde{\phi^1}(z)$ and $\widetilde{\phi^2}(z)$, we again choose to plot the total perturbation of the front defined by Eq. (3.59). In the following figures, the value the normalized toughness contrast is chosen.

Fig. 4.3 first compares, in the two limiting cases $h \to +\infty$ and $h \to 0$, and for a normalized toughness contrast ϵ of unity, the value of $\widetilde{\delta a}(z)/d$ obtained numerically (full lines) and analytically (dotted lines). The agreement is excellent in both cases, which shows that the numerical calculation of the integrals is correct and accurate.

Fig. 4.4 now shows the same quantity as a function of the normalized plate thickness h/d, for the same normalized toughness contrast ϵ of unity. The dependence of $\delta a(z)/d$ upon h/d is quite clear here: when the plate becomes thinner, the deformation of the crack front decreases, that is, this front becomes "stiffer". Note that although the value $\epsilon = 1$ here is admittedly high, the perturbation of the front remains reasonably small, at least for thin plates.

It is worth noting that the effect of the finite thickness of the plate on the crack front geometry is more pronounced in the thick plate regime, $h \gg d$, than in the thin plate regime, $h \ll d$. Indeed the solution for an infinitely thick plate provides an acceptable approximation (within 10% in the domain $|z/d| \le 6$) only for values of h/d exceeding 100, whereas that for an infinitely thin plate remains acceptable (with the same error on the same domain) up to values of h/d of the order of 0.4. This observation suggests that the finite thickness of the specimen

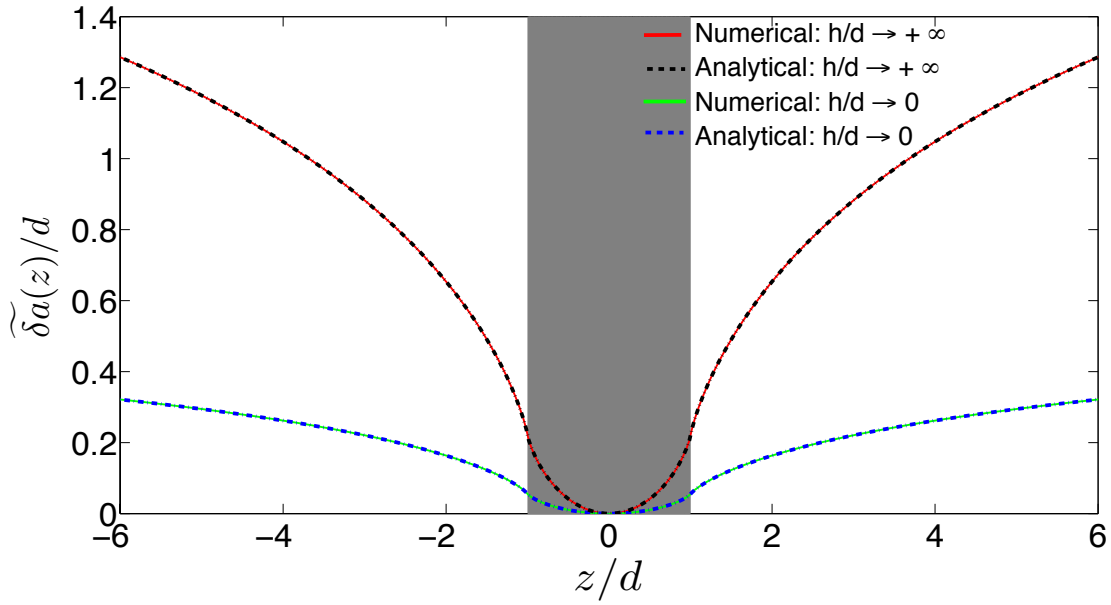

Figure 4.3: Equilibrium shape of a crack front penetrating into a single obstacle of normalized toughness contrast $\epsilon = 1$, in plates of infinite and infinitesimal thicknesses.

may have had a significant impact on the experimental front geometries reported in the works of Delaplace *et al.* (1999) and Dalmas *et al.* (2008).

Another interesting feature is that the range of validity of the first-order approximation is independent of the specimen thickness, and extends (within 10% for all values of z) up to contrasts $\epsilon \simeq 0.2$. Indeed, in both limiting cases of infinitely thin and thick plates, the first-*and* second-order contributions are proportional to each other by a factor of 4 (see Eqs. (4.32) and (4.33)).

4.5 Concluding remarks

The primary objective of this work was to provide a quantitative description of the process of crack pinning by moderately strong heterogeneities in specimens of finite size, and especially in plates of arbitrary thickness.

This problem was addressed theoretically by calculating the second-order expansion of the stress intensity factor resulting from some small, but otherwise arbitrary coplanar perturbation of the front of a semi-infinite crack lying on the mid-plane of an infinite plate of finite thickness and subjected to general mode I loading conditions. The results obtained were used to predict the equilibrium geometry of the crack for a given heterogeneous distribution of fracture toughness within its plane, assuming the stress intensity factor for an unperturbed crack front to be a decreasing function of the crack extent. Specializing to the case where this decrease becomes negligibly small and the crack is pinned by a single infinitely elongated obstacle, we found a formula for the shape of the crack front accurate to second order in the toughness contrast. This formula was fully explicit in all cases, and entirely analytic (i.e. did not require the numerical evaluation of any integrals) in the two extreme limits of infinitely thick and infinitely thin plates.

This work highlights the following generic features of crack pinning in samples of finite size:

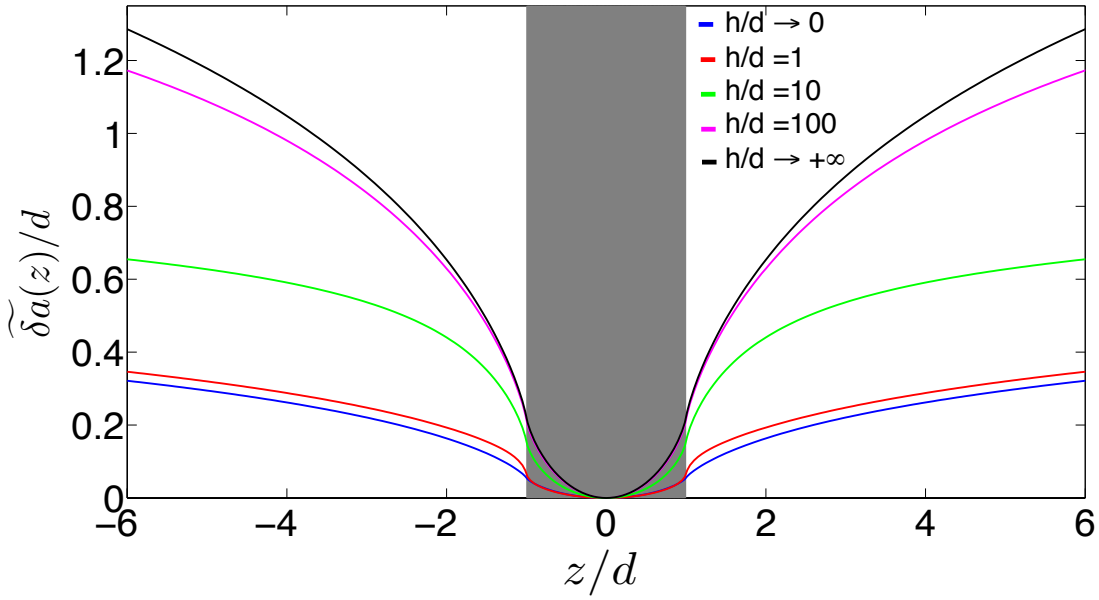

Figure 4.4: Equilibrium shape of a crack front penetrating into a single obstacle of normalized toughness contrast $\epsilon = 1$, in plates of various thicknesses.

- For a given distribution of obstacles, the thinner the sample, the smaller the deformation of the front. In the limit of a very thin specimen, this deformation is exactly 4 times smaller than in the limit of an infinitely thick one.
- Again, as has been shown in the previous chapter, the second-order correction relevant for larger toughness contrasts shows that the crack front *stiffens* under the action of stronger obstacles.
- Although the effect of the specimen thickness may now be taken into account quantitatively, the finite width of the specimen might also play a significant role and deserves further investigations.

In the next chapter, the results obtained here will be used to interpret peeling experiments.

Chapter 5

Experimental investigation of crack pinning by strong heterogeneities

The aim of this chapter[1] is to study experimentally the problem of crack pinning by strong heterogeneities. Since the pioneering work of Rice (1985) a large amount of theoretical works have been devoted to the study of the SIF along a perturbed planar crack under different loading and geometrical conditions (Gao and Rice, 1986; Leblond *et al.*, 1996; Lazarus and Leblond, 1998, 2002; Favier *et al.*, 2006). These models have led to the development of a powerful theoretical tools to address these problems, that can be used to predict the crack geometry and its behaviour as it encounters heterogeneities. Surprisingly, experimental studies of these questions are rather scarce, despite their relevance to test these theoretical models and determine their range of validity. The exploration of front deformation by toughness heterogeneities on experimental examples will be the main purpose of this chapter.

The small number of experimental study in the field can be explained (i) by the difficulty to make direct observations of the crack front geometry, and (ii) by the difficulty to design material with controlled and known toughness field. Daguier *et al.* (1995) have proposed an experimental method injecting ink into the crack after propagation, hence allows one to study crack geometry at some given time in an *opaque* material (here, a metallic alloy). Mower and Argon (1995) were first able to capture directly the propagation of a crack in a transparent epoxy containing defaults as nylon rods. Their main aim was to study, at large toughness contrast, the crack trapping by *unbroken* nylon rods at the wake of the crack. Schmittbuhl and Maloy (1997) explored the propagation of a crack within a plane containing a *random* distribution of defects using two transparent Plexiglas blocks. In their experiment, a disorder toughness pattern is obtained by sandblasting the surface of one of the Plexiglass block before merging them together by heat-treatment to create a weak heterogenous interface. This setup has widely been used to obtain statistical properties of crack front roughness in disordered materials (Delaplace *et al.*, 1999; Santucci *et al.*, 2010). However, quantitative comparisons with models beyond the scaling properties of the roughness seem out of reach, because of the uncontrolled nature of the heterogeneities resulting from the sandblasting technique. To explore pinning by individual obstacles, Dalmas *et al.* (2009), followed by Patinet *et al.* (2013), have studied the problem of crack propagating along a patterned interface using classical Double Cantilever Beam (DGB) geometry and they analyzed the crack front morphology in the framework of the

[1]The results presented in this chapter constitute the bulk of the material published in Vasoya *et al.* (2014).

crack perturbation *linear* theory. The main advantages of their experimental setup is that (i) the crack is loaded in pure tensile mode, and (ii) the crack propagation is purely in-plane. They infer the toughness contrast from the front geometry obtained in experiments: After recording the experimental front geometry, they indeed fit it using first-order perturbation approximation by adjusting the toughness contrast used here as a free parameter. They have compared finally the obtained values of the toughness contrast with the one obtained using FE calculations. By taking the geometrical dimensions of the experimental sample, morphology of the crack front and the associated opening displacement, they have solved the static elasticity problem by FE. The 3D displacement fields obtained from FE calculations then have been used to obtain the local ERR along the front with the "G-theta" method developed by Destuynder and Djaoua (1981). Their work did not reveal any non-linear geometrical effects, despite the investigation of rather strong heterogeneities.

Here we design an experimental such that :

- The toughness contrast of the obstacles will be measured independently using force measurement so that comparison between theory and experiment can be done without any adjustable parameter.

- The experimental setup will allow to tune continuously the toughness contrast from small to large values in order to explore the transition from linear to non-linear front deformations.

In order to fulfil this aspiration, we take inspiration from the work of Xia *et al.* (2012) and use thin film peeling as a model system to study the problem of crack propagation in heterogeneous materials. This chapter is organized as follows:

- Section 5.1 presents why and to which extent thin film peeling is appropriate to investigate problems of perturbed planar crack propagation analyzed theoretically in the previous chapters 3 and 4.

- We then present, in Section 5.2, the experimental procedure by describing the different tasks used to realize the experiments. Sub-section 5.2.1 describes the procedure used to prepare samples. In sub-section 5.2.2, we present the geometry used for the peeling test experiment. In sub-section 5.2.3, we explain how to characterize the adhesion energy and measure the toughness contrast. Sub-section 5.2.4 presents procedure to measure the deformed front shape and its amplitude.

- As a first set of experiments, in Section 5.3, we study peeling of thin films from rigid substrate patterned with a sinusoidal distribution of fracture energy along the front direction.

- As a second set of experiments, in Section 5.4 we study peeling of thin films from rigid substrate patterned with a single obstacle of infinite length in the direction of propagation.

- Finally, we use these experiments to infer the range of validity of the first- and second-order theory of crack perturbation and discuss some previous experimental results (Patinet *et al.*, 2013).

5.1 Context of the study: Thin film peeling as a model system for the study of planar crack propagation

We choose here thin film peeling (see *e.g.* Xia *et al.* (2011), Xia *et al.* (2012)) as a model system to explore experimentally fracture mechanics problem. Aim of this section is to explain why and to which extent it might be appropriate to investigate problems of perturbed planar crack propagation analyzed theoretically in previous chapters 3 and 4. Fig. 5.1 compares a peeling and a planar crack geometry. Fig. 5.1 (a) shows a schematic of a planar crack problem where a crack $\mathcal{F}$ of size a, is embedded in some arbitrary isotropic elastic infinite medium, subjected to some mode I loading through an imposed force F. And Fig. 5.1 (b) shows a schematic representation of the peeling of a thin film from a rigid substrate. The peeling front Γ separates the released portion of the film from the portion of the film still bonded to the substrate. It propagates as thin film is peeled off from rigid substrate upon applied peeling force F_p at peeling angle θ_p. Fig. 5.1 (c) represents the 2D view of the thin film model on the Oxy plane. We compare both

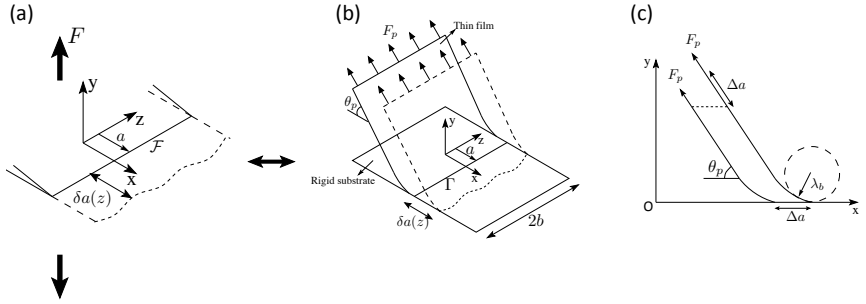

Figure 5.1: Schematic representation of (a) a semi-infinite crack embedded in an infinite medium, and (b) thin film peeled from a rigid substrate, (c) 2D view of the thin film at two different instants during the peeling process.

geometries in terms of front perturbations and perturbed driving force.

- **Perturbation of the front :**

  In peeling geometry, the peeling front is confined to the interface plane between the film and the substrate. As a result, it gets perturbed only in-plane within Oxz. This makes peeling geometry appropriate to study the problem of planar crack propagation.

- **Driving force :**

  – *Straight crack configuration :* For a planar crack with the straight configuration, at Griffith's equilibrium of energy, the driving force is proportional to square of applied force F and is given (Irwin, 1958) in the following form,

  $$G^0 \simeq F^2 g^0(a) \tag{5.1}$$

  where $g^0(a)$ describes the effect of the geometry of the straight crack $\mathcal{F}$ on the value of the ERR. For the peeling of an inextensible thin film from a rigid substrate, Rivlin (1944) has proposed like in fracture theory, an energy approach to derive the relation between the applied peeling force F_p and the driving force G^0. *i.e.*,

  $$G^0 \simeq \frac{F_p}{2b}(1 - \cos\theta_p) \tag{5.2}$$

where b denotes the half-width of the film. However, in the limit where the peeling angle approaches zero, large stretching deformations may occur that dominate over the bending mode of deformation of the film considered here. Kendall (1973) has derived an alternative, more refined equation by incorporating the elasticity of the thin film. This transition from a peeling mode governed by stretching to a mode governed by bending occurs for a peeling angle $\theta_p^c \simeq \sqrt[4]{G^0/Eh}$, where h is the thickness of the thin film. As a result, to have the domination of the bending mode over the deformation of the film in the sequel, we use a large enough peel angle such that $\theta_p > \theta_p^c$.

– *Perturbed crack configuration :* Let's now assume that during their propagation, crack $\mathcal{F}$ and peeling front Γ get perturbed within their plane Oxz by a small amount $\delta a(z)$. Rice (1985) has derived the expression of the variations in driving force induced by coplanar perturbation of the semi-infinite planar crack embedded in an infinite medium :

$$\frac{\widehat{\delta G}(a;k)}{G^0(a)} = \left[\frac{1}{\mathcal{L}} - |k|\right] \widehat{\delta a}(k) \tag{5.3}$$

where k is the wavenumber along the crack front and $\mathcal{L}$ is a characteristic length scale of the geometry and the loading system given by $G^0/(dG^0/da)$. In the case of thin film peeling that corresponds to the problem of an elastic plate clamped to some rigid body with perturbed clamped boundary, the driving force has been calculated using Von Karman plate theory that take into account both bending and stretching of the plate (Ponson *et al.*, 2014). When the deformation of the plate is governed by bending deformations only (for $\theta_p > \theta_p^c$), the variations of driving force read in Fourier's space,

$$\frac{\widehat{\delta G^p}(a;k)}{G^0} = -4\sqrt{1 + \frac{1}{4(\lambda_b k)^2}}\ |k|\widehat{\delta a}(k) \tag{5.4}$$

where λ_b is a characteristic bending length that corresponds about the radius of curvature at peeling front (see Fig. 5.1(c)) that follows,

$$\lambda_b = \sqrt{\frac{Eh^3}{24(1-\nu^2)G^0}}. \tag{5.5}$$

Depending on the wavelength $\lambda = 2\pi/k$ of the peeling front perturbations, one shall distinguish two asymptotic behaviours,

$$\begin{cases} \dfrac{\widehat{\delta G^p}(a;k)}{G^0} & \simeq & -4|k|\widehat{\delta a}(k) \ \text{ if } \lambda \ll 4\pi\lambda_b \\ \dfrac{\widehat{\delta G^p}(a;k)}{G^0} & \simeq & \dfrac{2}{\lambda_b}\widehat{\delta a}(k) \ \text{ if } \lambda \gg 4\pi\lambda_b. \end{cases} \tag{5.6}$$

In the case of small wavelength of the peeling front perturbations, the formula converges to the same form as the second term of Eq.(5.3) of one for a planar crack embedded in an infinite medium. The only difference is that now the variations in the driving force are increase by the factor of 4. From a pure bending plate theory, Legrand *et al.* (2011) found the same result using Love-Kirchhoff plate theory. In the case of large wavelength of the peeling front perturbations, the variations in the

driving force, just like in the case of a planar crack perturbation, is proportional to front perturbations. The only difference is the cut-off lengths, $\mathcal{L}$ and λ_b, of the regime $(\widehat{\delta G^p}(a;k)/G^0 \sim -|k|\widehat{\delta a}(k))$ displaying a non-local driving force that are specific to each geometry.

Conclusively, in the sequel experimental investigation, toughness fluctuations will be chosen such that wavelengths λ of the induced front perturbations remain small with respect to the characteristic bending length, *i.e.* $\lambda \ll 4\pi\lambda_b$, but large enough so that $\lambda \gtrsim h$. The first condition ensures that the cut-off effects arising for large wavelengths of the film perturbation can be neglected and that LEFM approach developed in the previous chapters 3 and 4, applies. The second condition ensures that the geometry of the detachment front can be described by the previous calculations made in the limit $h/d \to 0$. It is now necessary to explain why, in the limit of very thin plates $h/d \to 0$, the LEFM analysis of a crack lying at the interface between two *elastic* plates (see Fig. 4.2) applies to the peeling of an elastic plate from a *rigid* substrate. It so occurs that for the problem considered in Fig. 4.2, the replacement of the bottom elastic plate by a rigid one does not affect the calculation, as long as the limit $h/d \to 0$ is considered. Indeed in this limit, as a result of the Love-Kirchhoff theory of thin plates, all components of the displacement are identically zero on the unbroken part of the interface between the two plates, irrespectively of the elasticity of the bottom plate; hence the boundary conditions imposed onto the top plate by the bottom one are exactly the same as if the latter were rigid[1]. Note that for a given front geometry, the perturbation δG of the elastic energy-release-rate is twice larger when the upper plate is bonded onto another elastic plate rather than on some rigid substrate, since the same amount of elastic energy is released from both plates; but since the same argument also holds for the elastic energy-release-rate G^0 for a straight crack front, Eqs. (4.33) derived above using only the value of the *ratio* $\delta G/G^0$ apply indifferently to both cases.

5.2 Experimental setup

The experimental setup consists of a thin film (F) made of polydimethylsiloxane (PDMS), and a substrate (S) made of a transparency with some printed ink pattern, as represented schematically in Fig. 5.2.

5.2.1 Sample preparation

The specimen preparation follows the procedure detailed in Xia *et al.* (2012). Basic steps are:

- **Substrate with controlled heterogeneities:** To introduce obstacles of controlled geometry and toughness and permit a quantitative comparison with the predictions of Section 4.4, an obstacle aligned with the peeling direction is printed on the transparency using a standard commercial printer. The neat side of the transparency is subsequently glued onto a glass plate.
- **Preparation of PDMS:** The SYLGARD Âő184 silicone elastomer kit is used for the experiments. The curing agent is thoroughly mixed with the base at 1:10 ratio. The mixture is then kept inside a desiccator for about 30 minutes. Inside the desiccator, the mixture undergoes degassation under vacuum provided by a vacuum pump.

[1]This does not remain true for elastic plates of finite thickness, because as a result of the theory of 3D elasticity, the horizontal components of the displacement are no longer zero on the unbroken part of the interface.

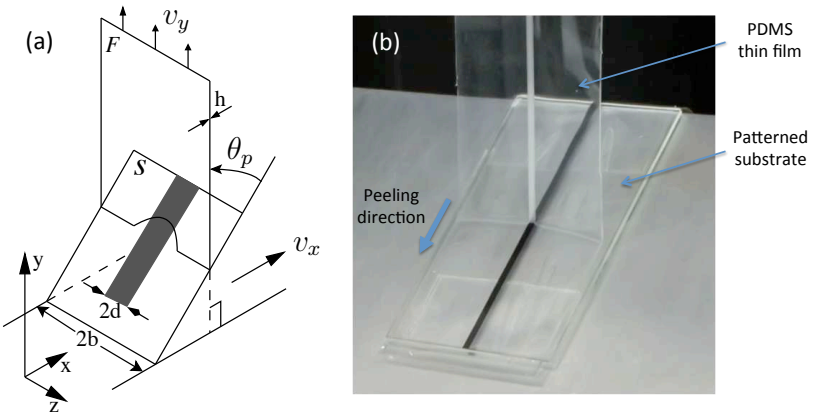

Figure 5.2: Experimental setup: (a) Schematic representation of the peeling test. The substrate is translated horizontally at the velocity v_x in order to maintain a constant peeling angle θ_p. (b) Snapshot of the experiment.

- **Spin coating of PDMS thin films:** The PDMS premix is spin-coated over the rigidly supported transparency by spinning the machine at a rate of 300 rpm during 20 s. This procedure produces homogeneous thin films with thickness $h = 400$ μm.
- **Curing of Sample:** This phase is followed by a curing of the thin film and its substrate at a temperature of 60°C for two hours. The curing temperature and time control the cross linking and lead to a Young modulus E and a Poisson ratio ν of PDMS of 1.2 MPa and 0.5 (a value characteristic of incompressible elastomers), respectively. The heat treated samples are then kept at room temperature for 48 hours prior to the test. This two-stage curing treatment is used to minimize the residual stress in cured PDMS.

5.2.2 Peeling test

A standard peel test configuration is employed to measure the peel force required to peel off the PDMS thin film. As shown in Fig. 5.2, the free end of the PDMS thin film is peeled off at a constant speed, $v_y = 1.65$ mm.s^{-1}, and at a peel angle $\theta_p = 45°$, from the ink-patterned rigid substrate. For ease of experimental implementation, the film is always peeled upwards, and the rigid substrate is rotated about its hinge to obtain any desired peel angle. In order to maintain a constant peel angle θ_p during the test, the substrate is moved in the horizontal direction at a speed $v_x = v_y \sin\theta_p/(1-\cos\theta_p)$. In this way, a stationary regime of propagation is reached.

5.2.3 Characterization of the adhesion energies

To introduce defects pinning the detachment front, we take advantage of strong adhesion of PDMS on ink, characterized by the high interfacial fracture energy G_c^{O}, as compared to that on neat transparency, characterized by the lower energy G_c^{M}. To vary the strength of these defects, we tune their grayscale c_{gray} ($c_{\mathrm{gray}} = 0$ without any obstacle and $c_{\mathrm{gray}} = 1$ for a black obstacle).

The first task is to measure the interfacial fracture energies of PDMS with the transparency (G_c^{M}), and with the printed obstacle (G_c^{O}) as a function of c_{gray}. To do so, we first deduce the mean interfacial fracture energy $\overline{G_c}$ from Rivlin (1944)'s equation (5.2) with the half-width[1]

[1]This width is kept constant during the first set of experiments discussed here, but will be varied in a second

$b = 24$mm of the adhesive (see Fig. 5.2). An alternative, more refined equation due to Kendall (1973) incorporating the elasticity of the film is also used, without significantly changing the results obtained (see Fig. 5.3) due to the large peeling angle taken here. The inset (a) of Fig. 5.3 shows the peel force F_p as a function of the peel displacement, for various values of the width $2d$ of the obstacle. One sees that the force quickly increases to reach a stationary value. This reflects the stationary loading conditions imposed to the adhesive that is peeled with an angle maintained constant during the experiment.

To now deduce the values of G_c^{M} and G_c^{O} from that of $\overline{G_c}$, we perform peel strength measurements of samples with defects with the same gray level c_{gray} but various widths $2d$, and use the equation

$$\overline{G_c} = \left(1 - \frac{d}{b}\right) G_c^{\mathrm{M}} + \frac{d}{b}\, G_c^{\mathrm{O}} \tag{5.7}$$

expressing the "mixture rule'" for the effective fracture energy of heterogeneous interfaces invariant along the propagation direction. This procedure is illustrated in Fig. 5.3 where the best linear fit of the experimental curve is used to determine the values of G_c^{M} and G_c^{O}. The adhesion energy of the PDMS-transparency interface found, $G_c^{\mathrm{M}} = 2.2 \pm 0.1$ J.m^{-2}, is confirmed independently through additional peel tests performed on homogeneous specimens. Note that the values of fracture energy are found to slightly vary with the velocity of the peeling front. In the experiments reported in this paper, the velocity is therefore fixed to a value of $v_p = 1.65$ mm.s^{-1}.

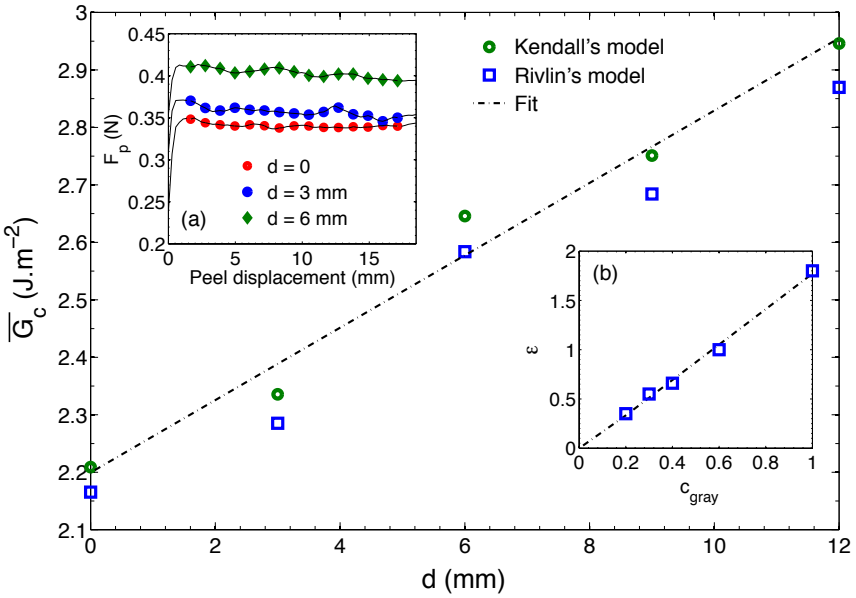

Figure 5.3: Effective adhesion energy of the interface as a function of the half-width d of the obstacle, for $c_{\mathrm{gray}} = 0.4$. Inset (a): Peel force versus displacement curves for the same grayscale but different obstacle half-widths. Inset (b): Contrast of interfacial fracture energy versus grayscale of the obstacle.

This procedure provides accurate values of the normalized toughness contrast. The contrast defined by

$$\epsilon(c_{\mathrm{gray}}) = [G_c^{\mathrm{O}}(c_{\mathrm{gray}}) - G_c^{\mathrm{M}}]/\overline{G}_c$$

set discussed in Section 5.4.2.

is represented as a function of c_{gray} in the inset (b) of Fig. 5.3. One observes that $\epsilon(c_{\text{gray}})$ evolves linearly with c_{gray}, according to the law $\epsilon(c_{\text{gray}}) = 1.8\, c_{\text{gray}}$. The maximum value of 1.8 corresponding to black ink permits to explore crack pinning by rather strong obstacles, beyond the range of validity $\epsilon \lesssim 0.2$ of the first-order theory determined previously.

5.2.4 Image Acquisition

In parallel to measuring the peel force required to peel off the PDMS thin film during peeling test, a Nikon DSLR 800E equipped with a high-magnification lens of the Zeiss Makro-Planar T* 100mm f/2 ZF.2 lens is positioned above the substrate surface, perpendicularly to it, and used to record *in situ* t 4,800×2,704 pixel size images of the peel-front configuration. The characteristic features of the camera like the shutter speed and the exposure time are chosen in order to obtain a good contrast between the peeled part of the film and the part of the film that is still bonded to the substrate. Typical pictures are shown in Figs. 5.4 (c) and 5.6 (c). Using a proper lighting device, the front shape appears as a thin bright line. The other, thicker bright line that appears on the raw image results from the reflection of the light on the curvy part of the debonded thin film and is discarded in the analysis. Image processing is then used to enhance the contrast and discrete positions of the front are obtained by manual selection on a zoomed image.

5.3 Sinusoidal perturbations of the peeling front: Effect of contrast

As mentioned in its title, the aim of this section is to quantify the crack propagation in the sinusoidal toughness map defined by Eq. (3.66) and represented schematically in Fig. 5.4 (b). In the stationary regime, G_0 does not depend on the crack size a, hence it is not possible to define a mean position using Eq. (3.29). Instead, from now on, we take as reference the straight line which intersects the front in $z = 0$ and denote δa the front perturbation from this new reference in agreement with Eq. (3.75). The first- and second-order approximations, corresponding to

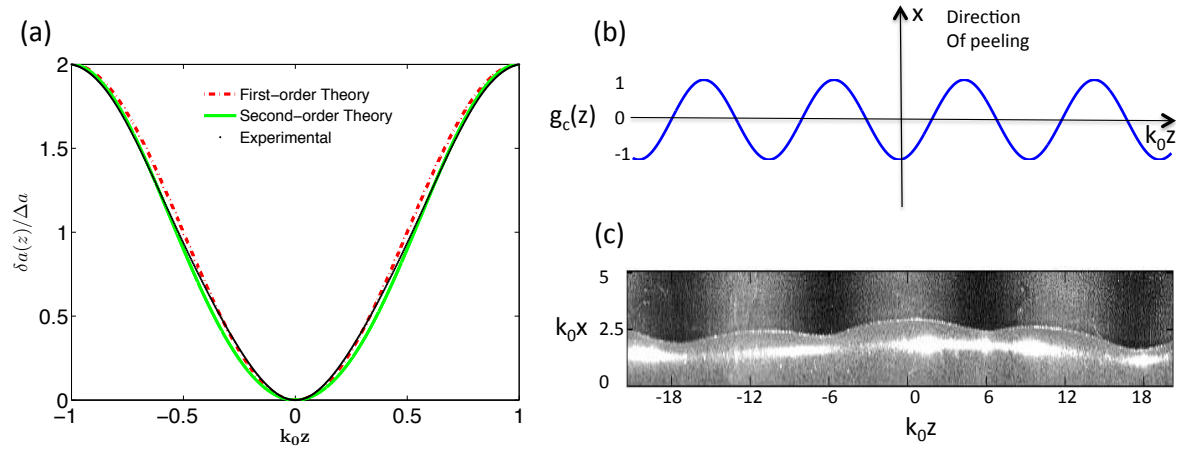

Figure 5.4: (a) Equilibrium shape of crack front at contrast $\epsilon = 0.2$ and wavelength $\lambda_0 = 12$mm; (b) Representation of the sinusoidal distribution of the toughness; (c) Typical snapshot of the peeling front as it propagates in sinusoidal toughness map.

the limit $h/d \to 0$ that is same Eq. (3.75) but divided by 4, are also plotted in Fig. 5.4(a) using the contrast value $\epsilon = 0.2$ measured independently from peel force measurements and wavelength $\lambda_0 = 12$ mm. It is observed that the second-order theory brings correction only to the shape of the perturbed front but it doesn't affect the amplitude of the perturbed front. The "tunability" of the printed ink distribution may be exploited to explore other contrasts. Fig. 5.5 shows the measured normalized amplitude of the crack front perturbations as a function of toughness contrast for given wavelength of the toughness fluctuations $\lambda_0 = 12$ mm. This value of wavelength is smaller that the cut-off length $4\pi\lambda_b$. As shown analytically in Eq. (3.76), we expect then the front deformation to vary linearly with the toughness contrast, even taking into account the secod-order correction. This is in rather good agreement with our experimental measurement within the range of toughness contrast investigated here. Despite the correct

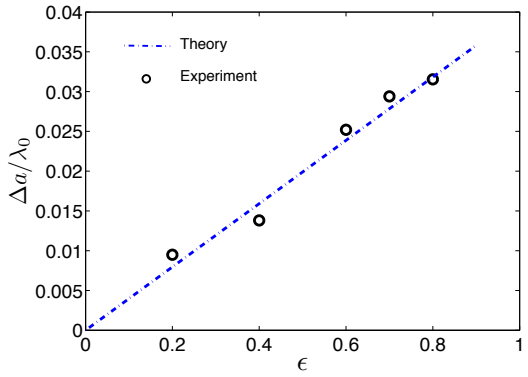

Figure 5.5: Effect of toughness contrast on amplitude of front deformation for wavelength $\lambda_0 = 12$ mm.

agreement between analytical and experimental results in the case of sinusoidal pattern of obstacles, one shall notice that exploration of effects due to second-order corrections are still missing since :

- second-order contribution does not affect the deformation amplitude up to rather large toughness contrasts that would require high order corrections.
- with our experimental setup, the maximum contrast value one can get is about 0.9.

Therefore, to explore effects due to second-order corrections, we move to the study of crack front pinning by a single obstacle.

5.4 Deformation of the front pinned by a strong obstacle

Again in this case, in the stationary regime, G_0 does not depend on the crack size a, hence it is not possible to define a mean position using Eq. (3.29). Instead, from now on, we take as reference the straight line which intersects the front in $z = 0$ and denote δa the front perturbation from this new reference in agreement with Eq. (3.59). The result is plotted on Fig. 5.6(a) with an amplification in the $y-$direction. One immediately recognizes the characteristic shape of a crack front pinned by an isolated obstacle of larger toughness, as has been observed by Dalmas *et al.* (2008); Patinet *et al.* (2013); Budzik *et al.* (2013); Chopin *et al.* (2011).

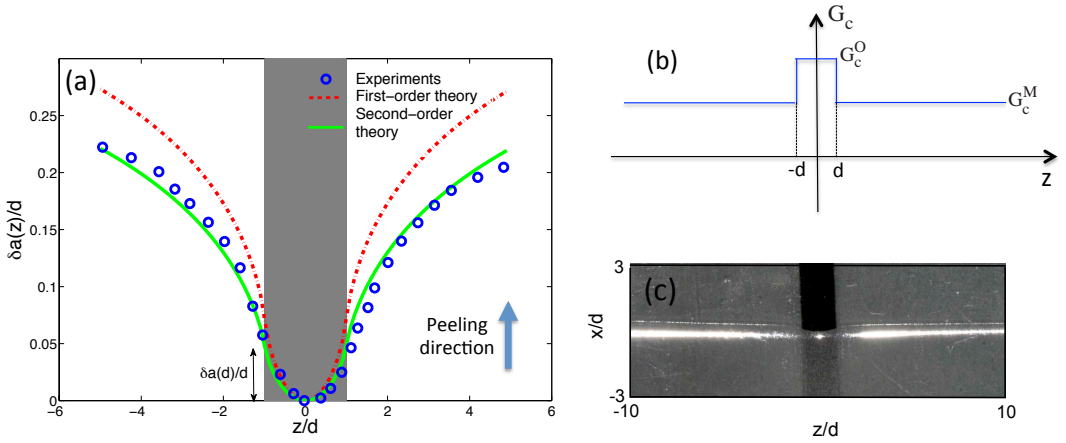

Figure 5.6: (a) Equilibrium shape of a crack front pinned by a single obstacle of contrast $\epsilon = 0.66$ with $b/d = 24$, and comparison with the first- and second-order theoretical predictions (Eqs. (4.33))); (b) Representation of distribution of the toughness corresponding to single obstacle with width of $2d$; (c) Typical snapshot of the peeling front as it crosses an obstacle. Here, the toughness contrast is $\epsilon = 1.0$ in order to highlight the front deformation;

The first- and second-order approximations (Eqs. (4.33)),corresponding to the limit $h/d \to 0$, are also plotted in Fig. 5.6(a) using the contrast value $\epsilon = 0.66$ measured independently from peel force measurements. It is observed that the second-order theory brings a significant correction to the first-order one, by predicting a less deformed ("stiffer") crack front, and considerably improves the agreement between experiment and theory. Experimentally, we limited our analysis to the region $|z/d| \leq 5$. Beyond this domain, accurate measure of the front shape becomes extremely difficult because we could not avoid the presence of unwanted heterogeneities which deform the front. Hence it is difficult to measure up to which value of z/d the theoretical predictions remain valid.

5.4.1 Effect of the toughness contrast

The "tunability" of the printed obstacles may be exploited to explore other contrasts. Fig. 5.7 shows the normalized amplitude of the crack front perturbation, defined as the amplitude of this deformation within the obstacle, that is the difference of position $\delta a(d)$ of the front at the edge and center of this obstacle, normalized by the defect half-width d. The range of explored toughness contrasts here varies from negative ($G_c^O < G_c^M$) to positive ($G_c^O > G_c^M$). The quantity $\delta a(d)/d$ depends only on the contrast, and varies linearly with it according to the first-order theory. In contrast, the experiments exhibit some "saturation" of the amplitude as the contrast increases. These saturation and divergence are correctly predicted by the second-order theory.

This quantitative comparison with experiments permits to define the practical limits of the first- and second-order theories. We retrieve experimentally that the first-order calculation provides an accurate prediction (within 10%) of the deformation of the front of a pinned crack for low contrasts, $\epsilon \lesssim 0.2$ (see Section 4.4.2). The second-order calculation extends this range of validity to at least $\epsilon = 0.7$, as shown experimentally (Fig. 5.7). For larger contrasts, the second-order theory underestimates the deformation of the front; either a higher-order development or a numerical approach (see Bower and Ortiz (1991); Lazarus (2003)) would be needed to

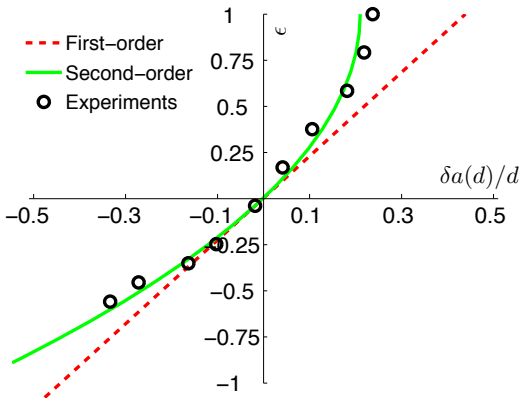

Figure 5.7: Variations of the amplitude $\delta a(d)/d$ of the crack front deformation as a function of toughness contrast, and comparison with the predictions of the first- and second-order theories.

accurately describe the geometry of the crack front in such situations.

5.4.2 Effect of the sample width on the deformation of the front

To investigate question of the effect of the sample width, we measure the crack front deformation for a fixed contrast $\epsilon = 0.66$ and a fixed defect half-width $d = 1\,\text{mm}$, but various specimen widths $2b$. Fig. 5.8(a) shows the results obtained[1]. The comparison with the first- and second-order theories (strictly valid in the limit $b/d \to +\infty$) displayed in Fig. 5.8(a) shows that the specimen width has a negligible effect on the crack front deformation if $b/d \gtrsim 12$ in the peeling test geometry used in this study. Provided this condition is met, the second-order expansion captures the front geometry fairly well, confirming the results of the previous section and the relevance of the second-order correction for strong obstacles.

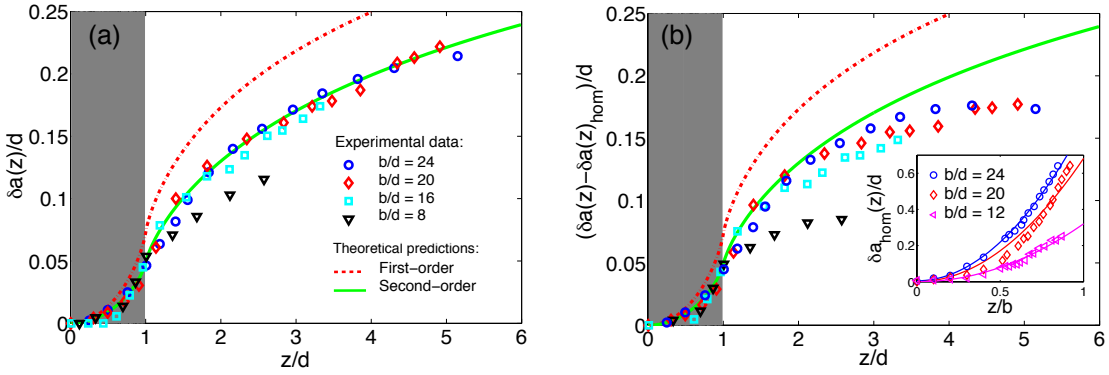

Figure 5.8: Effect of the specimen widths on the front perturbation: (a) Geometry of the pinned front for $\epsilon = 0.66$ for various specimen widths b. (b) Geometry of the pinned front after correction by the front geometry without defect.

For the smallest sample having $b/d = 8$, the crack front geometry is clearly influenced by

[1]Because of the symmetry ($z \to -z$) of the peeling test geometry, we only show one half of the front and represent the mean value of the deformations $\delta a(z)$ measured in the regions $z < 0$ and $z > 0$

the finite width of the specimen. To account for this effect, Patinet *et al.* (2013) proposed to correct the crack front deformation $\delta a(z)$ observed by subtracting the deformation $\delta a_{\rm hom}(z)$ measured for a homogeneous interface, before comparing it to that predicted theoretically for an infinitely wide specimen. This procedure is tentatively applied to our experiments: first, the crack front geometry was measured in homogeneous specimens of various widths $2b$, as shown by the discrete points in the inset of Fig. 5.8(b). The parabolas $\delta a_{\rm hom}(z) = 0.037\, z^2/b$ also represented there by straight lines provide a good description of the experimental points. Then this deformation was subtracted from the original deformation and the corrected crack front geometry was compared to the theoretical predictions in Fig. 5.8(b). One observes that this procedure degrades the agreement between experimental and theoretical values.

The apparent inappropriateness of this procedure might be due to the fact that it makes the implicit assumption that the zeroth-order crack front shape (for a homogeneous interface) *is* influenced by the finite width of the specimen, but that the first- and second-order corrections (due to the presence of the obstacle) are *less*, since the corrected crack front deformation $\delta a(z) - \delta a_{\rm hom}(z)$ is compared to the sum of these corrections *calculated in the limit* $b/d \to +\infty$. There is no clear reason why this assumption should be correct, especially considering the large influence of the thickness $2h$ of the specimen upon the first- and second-order corrections.

A discussion of the results of Patinet *et al.* (2013) is finally possible. These authors performed similar measurements of the crack front deformation when pinned by a single obstacle, and concluded that the predictions of the first-order theory were quantitatively correct *over a much larger range of values of the contrast than found here*. Since this range of validity was shown to be independent of the specimen thickness, we might attribute this discrepancy to the finite width of the specimen: Patinet *et al.* (2013) used specimen widths in the range $9 \lesssim b/d \lesssim 13$, for which the effect of the finite width of the specimen was significant in our setup, and used the procedure of correction of the observed crack front geometries depicted above. Now in the double cantilever beam they used, the sign of the curvature of the crack front for a homogeneous interface was opposite to that of the same curvature in our peeling test. As a result, the subtraction of $\delta a_{\rm hom}(z)$ from $\delta a(z)$ resulted in an *increase* of the crack front deformation instead of a *decrease* like in our case (see Figs. 5.8(a) and (b)). *If*, as suggested by the above results, the procedure of correction of the observed crack front shapes was in reality inappropriate, it might have led to an overestimation of the crack front deformation bringing it closer to the predictions of the first-order theory, and thus giving the impression of correctness of this theory beyond its real range of applicability.

While the effect of the specimen thickness on the pinning of crack fronts can now be quantitatively taken into account, the role played by the specimen width is less obvious and deserves further investigations. To circumvent this difficulty in our experiments, we used thin films of sufficiently large width $b \gtrsim 12d$ with respect to the heterogeneity size d. Note however that this range of validity might vary with the employed test geometry.

5.5 Concluding remarks

The aim of this chapter focused on experiments performed in the limit of infinitesimal thickness of a infinite-plate, using peeling test with fully controlled fields of local fracture energy. Two different distribution of the toughness were explored; (i) crack propagating in a sinusoidal distributed obstacles, and (ii) crack crossing a single obstacle. In both cases, the distribution is invariant along the crack propagation direction.

This experimental work interpretes the following generic features of crack pinning in samples of finite size:

- The experimental crack front deformations were observed to be in good agreement with the theoretical formulas and the second order term to (i) greatly improve the agreement and (ii) broaden their range of applicability in terms of admissible values of the toughness contrast.
- Although the effect of specimen thickness can now be quantitatively taken into account, the finite width of the specimen might play a significant role and deserve further investigations. In practice, we found that in peeling tests, films at least 12 times wider than the defect size are necessary in order to apply the theory developed in previous chapters 3 and 4 under the hypothesis of infinite width.
- Generally speaking, the non-linear correction arising from large contrasts of toughness is expected (Delaplace *et al.*, 1999; Xia *et al.*, 2012) to play a significant role in various experimental situations and should be taken into account to predict the failure behavior of engineered heterogeneous materials with new and improved properties. We have shown that the second order approximation is useful to increase the accuracy. However numerical methods which will be described in the part II, become unavoidable to consider strong heterogeneities.

Part II

A numerical study for an arbitrary toughness contrast

Introduction

For a moderate toughness contrast, first order (Rice, 1985; Bonamy, 2009; Lazarus, 2011) and second order (Leblond *et al.*, 2012; Vasoya *et al.*, 2013; Willis, 2013) perturbation approaches are valid so that it becomes possible to derive some analytical results (Part I). As still discussed in chapter 1 at first order approximation, it has been shown that two situations may occur depending on the spatial toughness distribution (Roux *et al.*, 2003): (1) if the variations of toughness in the propagation direction are small (or negligible), the crack front deforms so that the stress intensity factor reaches the local toughness at each position along the crack front ($K = K_c$ everywhere). It is in particular the case when the toughness map is invariant in the direction of propagation; (2) in contrast, if the spatial fluctuations along the propagation direction are strong, some parts of the front remain pinned on higher toughness positions ($K < K_c$ at some places). Using terminology defined in Gao and Rice (1989), the first situation is coined *regular* and the second *irregular* process in the sequel. In the case of *regular* crack propagation, heterogeneous material can safely be replaced by an equivalent homogeneous one with effective toughness equal to its mean value $< K_c >$ (Roux *et al.*, 2003; Patinet *et al.*, 2013). But in the case of *irregular* crack propagation, the equivalent toughness can no more be obtained by a simple average and the effective toughness is governed by the pinned zones hence is larger than the spatial average along crack front (Patinet *et al.*, 2013; Demery *et al.*, 2014).

The study of a crack propagating in a heterogeneous toughness with an arbitrary toughness contrast, is still lacking in literature. Here, we address the problem in some, as simple as possible, situations. In particular, we take into account the effect of large crack front deformations induced by large toughness contrasts, and investigate the influence of local toughness map on the crack propagation problem and on the macroscopic effective toughness during crack propagation. We restrict to in-plane propagation of a flat crack. In order to focus on the crack front deformations without introducing any boundary effects, we use the finite perturbation method proposed by Rice (1989) and developed numerically by Bower and Ortiz (1990); Lazarus (2003). Moreover we study a circular crack front rather than a straight one to avoid any inevitable truncation effects of the discretization. As of now, we keep the toughness map $K_c(M)$ in a general scalar form which includes contrast effects along crack front as well a spatial variation of toughness field in the propagation direction:

$$K_c(M) = \overline{K}_c \left[1 + \Delta\, \eta(M)\right] \tag{5.8}$$

The quantity $\overline{K}_c$ corresponds to the mean value of the toughness over crack plane, Δ to the relative toughness contrast, the function $\eta(M)$ describes the toughness fluctuations at point M. Aim is then to study the influence of the toughness contrast Δ and the toughness fluctuations $\eta(M)$ on the crack propagation. This part is organised in two chapters:

Chapter 6

In this chapter, we propose an homogenization method to bridge micro to macro scales. At the micro scale the crack front is deformed by the local toughness map. At the macro scale, we define some approximate undeformed geometry and apparent toughness. We present a numerical procedure devoted to this problem. This procedure is based on large numerical iterations of first-order approximation expounded in chapter 2.

Chapter 7

As an application, this chapter involves the study of a crack propagating in some model toughness field which gives invariance of the problem along crack propagation direction. In detail, we explore effects of different toughness field parameters in terms of toughness contrast Δ and intrinsic length ξ of the heterogeneity. We find that depending on Δ and ξ, the propagation is regular (for small enough Δ and ξ) or irregular (for larger Δ and ξ). In the regular case, the crack reaches a stationary shape, whereas in the irregular case, some fingering occurs. Correspondingly, the effective toughness is shown to decrease with Δ and ξ than average value of the local toughness up to its minimum one.

Chapter 6

Problem definition and numerical method

6.1 Problem definition

We consider a planar crack $\mathcal{F}$ with initial local radius $a(M)$, embedded in an infinite isotropic elastic medium with heterogeneous fracture toughness properties and loaded in pure mode I through some uniform remote stress applied at infinity σ (see Fig. 6.1).

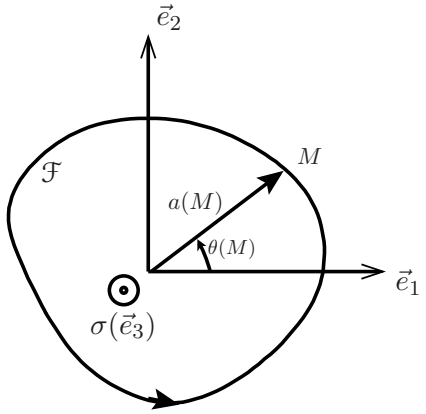

Figure 6.1: A tensile planar crack in an infinite body under uniform stress σ

We assume a quasi static propagation of the crack front, so that the crack advance at a point M of the front is governed by Irwin's criterion (1.8):

$$\begin{cases} K(M) < K_c(M) & : \quad \text{no crack advance} \\ K(M) = K_c(M) & : \quad \text{possible crack advance} \end{cases} \tag{6.1}$$

where $K(M)$ is the SIF and $K_c(M)$ the toughness at point M given by equation (5.8).

We suppose that the remote loading σ adapts in order to stay in the quasi static regime and to ensure crack propagation at least, on some part of the front. This implies that at each

moment:

$$\max_{M\in\mathcal{F}} \frac{K(M)}{K_c(M)} = 1 \tag{6.2}$$

Under the assumption of quasi static propagation and for a given toughness map $K_c(M)$, the problem is to find the successive positions of the crack front and the corresponding loading σ.

6.2 Homogenization: Macroscopic apparent fracture properties

Aim of this section is to address possible ways to do homogenization for determining the effective toughness. The main difficulty of the problem is that due to heterogeneous toughness, the front will not preserve a circular geometry as the crack advances. Rather it will roughen due to the facing toughness heterogeneity. Hence the geometry of the crack front has to be accounted for. Due to such interaction of the front with the local toughness, the local stress intensity factor will be modulated. In an homogenization process, we shall replace such complex problem at smaller scales by an equivalent circular crack of mean radius a:

$$a = \sqrt{\frac{S}{\pi}} \tag{6.3}$$

where S is a crack surface area. Correspondingly by applied stress, a first natural definition of apparent effective fracture toughness would be,

$$K_{\text{eff}} = \frac{2}{\sqrt{\pi}}\sigma\sqrt{a}. \tag{6.4}$$

where σ is defined by Eq. (6.2).

On the other hand, such homogenized quantities may be defined by statistical means over local elastic fields instead of just looking at applied loading alone. For example, the simplest way is to integrate local fields along the crack front, either the stress intensity factor,

$$K_{\text{m}} = \frac{1}{L}\int_{\mathcal{F}} K(M)\mathrm{d}M \tag{6.5}$$

or the energy release rate field,

$$G_{\text{m}} = \frac{1}{L}\int_{\mathcal{F}} G(M)\mathrm{d}M \tag{6.6}$$

where L is total length of the crack front.

From aspects of physical energy dissipation during crack propagation, a more interesting and important quantity would be a mean ERR defined by averaging local ERR over advanced crack area,

$$G_{\text{A}} = \frac{\int_{\mathcal{F}} G(M)\delta a(M)\mathrm{d}M}{\int_{\mathcal{F}} \delta a(M)\mathrm{d}M} \tag{6.7}$$

where $\delta a(M)$ is a small advance of crack front position ($\delta a(M) > 0$).

All these four macroscopic quantities ($K_{\text{eff}}, K_{\text{m}}, G_{\text{m}}, G_{\text{A}}$) may serve as an equivalent macroscopic toughness value writing an Irwin or a Griffith type criteria at the macro-scale. As the

crack front is being deformed due to heterogeneity, all these macroscopic quantities are supposed to evolve during propagation with mean crack size a. Thus in order to define a single valued apparent effective property, one shall define the equivalent macroscopic quantities as an integration of these evolving quantities over mean crack size. That is:

$$F_c^{\infty} = \left\langle \overline{F} \right\rangle_a = \lim_{a\to\infty} \frac{1}{a} \int_{a_0}^{a} \overline{F}(a')\mathrm{d}a' \tag{6.8}$$

where, $\overline{F}$ is equal to either K_{eff}, K_{m}, G_{m}, G_{A}.

For the geometrical deformation of the crack front, we introduce the following macroscopic quantities:

- A normalized amplitude of perturbed crack front defined by:

$$\frac{\Delta a}{a} = \frac{\max_{M\in\mathcal{F}}[a(M)] - \min_{M\in\mathcal{F}}[a(M)]}{a}. \tag{6.9}$$

- An integral along the perturbed crack front of the local deformations:

$$I(a) = \int_0^{2\pi} \left| \frac{1}{a(M)} \frac{\partial a}{\partial \theta}(M) \right| \mathrm{d}\theta(M). \tag{6.10}$$

6.3 Numerical Procedure

Knowing the local toughness map, it is in particular possible to obtain the global quantities a, K_{eff}, K_{m}, G_{m}, G_{A}, $\Delta a/a$ and $I(a)$ if one is able to solve the propagation problem. Bower and Ortiz (1990) followed by Lazarus (2003), developed a powerful method based on the iteration of Rice (1989)'s linear schemes given by Eqs. (2.11 and 2.13). The efficiency of this method arises from the need for the sole 1D meshing of the crack front. The basic difference in these methods is that, the method is *implicit* in Bower and Ortiz (1990)'s work in the sense they update the local front geometry by inverting the linear elastic kernels at each iteration, whereas Lazarus (2003)'s method is *explicit*, in the sense she updates the front geometry using some Paris type propagation law. Here, we adapt the method of Lazarus (2003) to our problem. In particular, we are taking care of numerical instability that might arise due to inappropriate discretization [Appendix C.1] and develop a new step to calculate homogenized effective failure properties during propagation. In practice, we introduce the dimensionless SIF $\widehat{K}$ by :

$$K(M) = \sigma\sqrt{a_0}\,\widehat{K}(M). \tag{6.11}$$

It depends on the crack front shape and size but by linearity of the elasticity problem, is independent of applied loading. As discuss below, we calculate this quantity by numerical means, the loading being derived from it. We start from an initial circular crack of radius a_0 for which $\widehat{K}(M) = \widehat{K_0}$ with

$$\widehat{K_0}(M) = \frac{2}{\sqrt{\pi}} \text{ and } W = 1. \tag{6.12}$$

The problem is then solved iteratively by successive small perturbations $\delta a(M)$ of the crack front in the following main four steps:

1. Irwin-Griffith propagation law (6.1) is regularized by some Paris' law with a large Paris exponent β (Lazarus, 2003) that is:

$$\delta a(M) = \delta a_{\max} \left(\frac{\widehat{K}(M)/K_c(M)}{\max_{M\in\mathcal{F}} \widehat{K}(M)/K_c(M)} \right)^{\beta}, \quad \beta \gg 1 \tag{6.13}$$

it ensures to retrieve Irwin's threshold behaviour (6.1), since:

$$\begin{cases} \delta a(M) \sim 0 \text{ if } K(M) < K_c(M) \\ \delta a(M) \sim \delta a_{\max} \text{ if } K(M) = K_c(M). \end{cases} \tag{6.14}$$

Here $\delta a_{\max}$ is a numerical parameter which is supposed to be small enough such that first, Rice (1989)'s linear scheme can be applicable and second, such that numerical results are stable. Advantage of using Paris's law is that the crack advance at all steps is directly provided in some explicit way. Disadvantages is, as for Euler's explicit scheme, that numerical instability may appear for some discretization parameters. This issue is discussed in more details in the appendix C.1.

2. the dimensionless SIF $\widehat{K}$ and FK W are updated by using Rice (1989) first order perturbation formulae (2.11) and (2.13).

3. the critical loading is then obtained by introducing (6.11) in (6.2):

$$\frac{\sigma\sqrt{a_0}}{\overline{K}_c} = \left[\max_{M\in\mathcal{F}} \frac{\widehat{K}(M)}{1+\Delta\,\eta(M)} \right]^{-1} \tag{6.15}$$

where $\overline{K}_c$, Δ and $\eta(M)$ are defined in (5.8).

4. the global effective toughness defined in previous section re-read in terms of $\widehat{K}$;

   - Mean SIF K_m:

$$K_{\mathrm{m}} = \frac{\sigma\sqrt{a_0}}{L} \int_{\mathcal{F}} \widehat{K}(M)\mathrm{d}M \tag{6.16}$$

   - Mean ERR G_m:

$$G_{\mathrm{m}} = \left(\frac{1-\nu^2}{E} \right) \frac{\sigma^2 a_0}{L} \int_{\mathcal{F}} \widehat{K}^2(M)\mathrm{d}M \tag{6.17}$$

   - Mean ERR over advanced crack area:

$$G_{\mathrm{A}} = \left(\frac{1-\nu^2}{E} \right) \sigma^2 a_0 \;\; \frac{\int_{\mathcal{F}} \widehat{K}^2(M)\delta a(M)\mathrm{d}M}{\int_{\mathcal{F}} \delta a(M)\mathrm{d}M} \tag{6.18}$$

where σ is given by Eq. (6.15)

6.4 Numerical code

The numerical code of Lazarus (2003) is written in C-language. Its aim is to predict the mode I propagation of any shaped planar embedded in an homogeneous media. It was found that for any initial shape (heart, elliptical, rectangular) the crack always retrieves a circular shape. We have extended this code to deal with heterogeneous fracture properties. In particular, we have been handling the large crack front deformations induced by strong heterogeneity. In some particular case of heterogeneous fracture properties, we have implemented the symmetric and periodic boundary conditions while calculating two integrals (2.11) and (2.13) that update the SIF $\widehat{K}$ and FK W. As a result, it reduces the total computational CPU time. Per one numerical iteration, the CPU time is reduced by factor of $(1/2k)^3$, where k denotes the periodicity.

Let us discuss on the choice of different numerical parameters. On the one hand, to have better predictions of effects due to heterogeneities, the length of the segment (between two nodes) l_N must be smaller than the size ξ of heterogeneity that defined by toughness map. For example, in a case of periodic toughness map with the wavelength λ of fluctuations in the toughness, l_N must be smaller than λ. On the other hand, as wanted, value of β must be large enough so that brittle fracture framework works perfectly. However, this must be balanced by the fact that increasing β implies higher constraint on N, $\delta_{\max}$ due to the diminution of the numerical stability region (see Appendix C.1, fig. C.2). In practice, we have chosen the value of β equal to 25 which gives the well converged results. Accordingly, we have chosen number of nodes N and maximum possible front advance $\delta_{\max}$ using (i) stability curve presented on Fig. C.2 and (ii) constraint that $l_N \ll \lambda$.

6.5 Concluding remarks

To bridge information from micro to macro scales, an homogenization of the problem is introduced through several definitions of macroscopic quantities defining an apparent toughness and an apparent geometry of the crack front during propagation. We propose to solve the problem numerically by adapting the *iterative-perturbation* numerical method of Lazarus (2003), based on the perturbation approach described in chapter 1. This method uses as input the toughness map and an initial circular crack shape and yields as output:

(i) the evolution of the critical loading corresponding to quasi-static propagation and

(ii) the corresponding evolution of the crack shape.

We apply it in the next chapter to an invariant toughness map along the propagation direction.

Chapter 7

Circular cracks propagating in an invariant toughness field along the propagation direction

Aim of this chapter is to explore crack propagation in the following toughness map:

$$K_c(\theta) = \overline{K}_c \left[1 + \Delta \cos(k\theta)\right]. \tag{7.1}$$

By Irwin's relation (1.7) corresponding critical ERR reads,

$$G_c(\theta) = \frac{\overline{G}_c}{1 + \frac{\Delta^2}{2}} \left[1 + 2\Delta \cos(k\theta) + \Delta^2 \cos^2(k\theta)\right] \tag{7.2}$$

where,

$$\overline{G}_c \equiv \frac{1}{2\pi} \int_0^{2\pi} G_c(\theta) \mathrm{d}\theta = \frac{1-\nu^2}{E} \overline{K}_c^2 \left(1 + \frac{\Delta^2}{2}\right) \tag{7.3}$$

In this way, toughness map (5.8) depends on the position only through the polar angle θ of M so that the toughness is invariant in the directional of propagation. k is the wave-number of toughness fluctuations the corresponding size of the heterogeneity being $\xi = \dfrac{2\pi}{k} a$. This choice of toughness map allows us to focus, as wanted, on the large toughness contrasts effects (or effect of large front perturbations). In the case of weak heterogeneity ($\Delta \ll 1$), it corresponds moreover to the weak pinning case described by Roux *et al.* (2003), for which a regular regime is reached ($K = K_c$ everywhere along front) and the macroscopic toughness has been shown to be equal to the mean toughness map $\overline{K}_c$. The aim here is to discuss the possible effects of larger toughness contrast on this behavior: Is a regular regime still reached ? what about the definition and evolution of the macroscopic toughness ? To answer to these questions, we study several configurations of the toughness map introduced above, corresponding to various combinations of wave-number k or equivalently on the heterogeneity size and toughness contrast Δ.

For given wave-number k of toughness fluctuations, we retrieve that in the case of small contrast Δ, a crack propagation coins the *regular* propagation whereas in the case of large enough toughness contrast, despite the spatial invariance of the toughness in the propagation direction, a regular regime is never reached and a fingering instability occurs. The study of

such fingering process and its implication on the macroscopic effective fracture properties are central key points to be discussed in the sequel.

7.1 First-order approximation: Analytical results

Consider a planar circular crack embedded in some arbitrary isotropic elastic body symmetric about the crack plane, loaded in pure mode I through some remote constant loading. Assume that the crack is perturbed, by a small distance within its plane. The position O of the center of the circular crack remains unchanged after perturbation (Fig. 7.1), and any point M of it is described by its radius $a(\theta)$. Under such conditions, Gao and Rice (1987) provides the

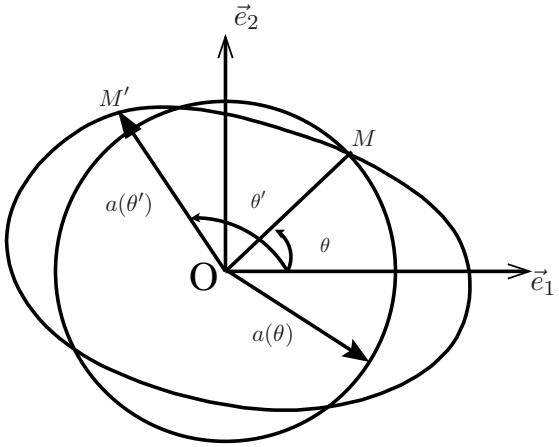

Figure 7.1: A slightly perturbed planar crack in an infinite body under uniform stress σ

infinitesimal variation $\delta\widehat{K}$ of the local elasticity in the following form,

$$\delta\widehat{K}(\theta) = \frac{\widehat{K}^0[a(\theta)]}{8\pi} PV \int_0^{2\pi} \frac{a(\theta')/a(\theta) - 1}{\sin^2[(\theta - \theta')/2]} \mathrm{d}\theta' \tag{7.4}$$

where $\widehat{K}^0[a(\theta)]$ is the unperturbed SIF corresponding to the circular crack with radius of $a(\theta)$ which passes through point M. In the case of an harmonic perturbation of a circular front with radius a, *i.e.*

$$a(\theta) - a \sim D\cos(k\theta) \tag{7.5}$$

where D is a constant with $D/a \ll 1$, one gets, with a few transformations, the SIF along perturbed crack front:

$$K(\theta) = \frac{2}{\sqrt{\pi}} \sigma\sqrt{a} \left[1 - \frac{D}{2a}(k-1)\cos(k\theta)\right]. \tag{7.6}$$

It will be useful in sequel to make note on stability of circular crack front shape upon such harmonic perturbations. Linear stability analysis provides that SIF at most advanced point of front to be less than SIF at most retard point. By Eq. (7.5) most advanced point, let denote it

by A, is corresponding to $\theta = 0$ and most retarded point, let denote it by B, is corresponding to $\theta = \pi/k$. By Eq. (7.6) then it reads,

$$K(B) > K(A) \tag{7.7}$$

which means that B will advance faster than A so that the circular shape will be retrieved in the absence of any other heterogeneity.

7.1.1 The equilibrium shape of the crack front

We shall now apply the preceding Eq. (7.6) to the study of co-planar propagation of the crack governed by Irwin-Griffith equilibrium $(6.1)_2$. For a given loading, provided that K equal to K_c at every point of the crack front, the heterogeneous toughness map (7.1) determines the geometry of crack front given by Eq. (7.5). By equating Eq. (7.6) to the Eq. (7.1), one gets,

- corresponding to the unperturbed configuration :

$$\frac{2}{\sqrt{\pi}}\sigma\sqrt{a} = \overline{K}_c. \tag{7.8}$$

- corresponding to the cosine perturbation :

$$\frac{D}{a} = -\frac{2\Delta}{k-1}. \tag{7.9}$$

With this analytical solution at first-order for small front perturbation, we have verify results from our numerical code [see Appendix D.1]. It shall also be remarked that for $k = 1$, Eq. 7.9 is diverging which means that there is no solution to the equation $K = K_c$ along all the front; the propagation can only be irregular.

7.1.2 Macroscopic quantities

Using local solutions of zeroth and first order derived in previous section, the different quantities introduced in Section 6.2 read :

- From definition (6.4) and zero-order solution (7.8):

$$K_{\text{eff}} = \overline{K}_c. \tag{7.10}$$

- Upon use of $K(\theta) = K_c(\theta)$ in definition (6.5):

$$K_{\text{m}} = \overline{K}_c. \tag{7.11}$$

- Similarly, upon use of $G(\theta) = G_c(\theta)$ in definition (6.6) and first order expression $G_c(\theta) = \overline{G}_c\,[1 + 2\Delta\cos(k\theta)]$ of $G_c(\theta)$ derived from Eq. (7.2), one gets:

$$G_{\text{m}} = \overline{G}_c \tag{7.12}$$

and by definition (6.7) G_{A} reads,

$$G_{\text{A}} = \frac{\int_{\mathcal{F}} G_c(\theta)\delta a(\theta)\mathrm{d}\theta}{\int_{\mathcal{F}} \delta a(\theta)\mathrm{d}\theta} \tag{7.13}$$

where positive advance of front $\delta a(\theta)$ has to be determined by the front perturbation given by Eq. (7.5) and reads,

$$\delta a(\theta) = D\left[1 + \cos(k\theta)\right] \tag{7.14}$$

so that upon use of this equation in integral (7.13), one gets,

$$G_{\mathrm{A}} = \overline{G}_c. \tag{7.15}$$

In all above calculations for global quantities we have used $\int_0^{2\pi} \cos(k\theta)\mathrm{d}\theta = 0$. One shall notice that in the limit $\Delta \ll 1$, all potential definitions (6.4-6.7) of an equivalent toughness are equivalent and equal to the mean value of K_c or G_c along crack plane.

For geometrical quantities, from Eq. (7.9) one obtains that the normalized amplitude of deformed front $\Delta a/a$ reaches a stationary value given by:

$$\frac{\Delta a^{\infty}}{a} = \frac{4\Delta}{k-1}. \tag{7.16}$$

A stationary value I^{∞} of integral $I(a)$ reads upon use of Eqs. (7.5) and (7.9) in Eq. (6.10),

$$I^{\infty} = k\left(\frac{2\Delta}{k-1}\right)\int_0^{2\pi}\left|\frac{\sin(k\theta)}{1-\frac{2\Delta}{k-1}\cos(k\theta)}\right|\mathrm{d}\theta.$$

As front shape is symmetric and periodic in polar coordinate, the domain $[0, 2\pi]$ of integral simply made of $2k$ equal domains $[0, 2\pi/k]$. Thus above integral reads,

$$I^{\infty} = k\left(\frac{2\Delta}{k-1}\right)2k\int_0^{\frac{\pi}{k}}\left|\frac{\sin(k\theta)}{1-\frac{2\Delta}{k-1}\cos(k\theta)}\right|\mathrm{d}\theta.$$

Upon use of Taylor expansion $\dfrac{1}{1-\frac{2\Delta}{k-1}\cos(k\theta)} \sim 1 + O(\Delta)$ and $\int_0^{\pi}\sin x\ \mathrm{d}x = 2$, one gets:

$$I^{\infty} = 8\Delta\left(\frac{k}{k-1}\right). \tag{7.17}$$

7.2 Higher order resolution: Two regimes depending on (k, Δ)

Aim of this section is to explore crack propagation behavior at all orders using numerical method described in previous chapter.

7.2.1 (k, Δ) phase-diagram

For exploring all possible results, we have run numerical simulations for several toughness maps (7.1) with different wave numbers k and toughness contrasts Δ. Results from these simulations are showing two kinds of crack propagation behavior depending on k and Δ:

- for small toughness contrast $\Delta < \Delta_c(k)$ (Fig. 7.2a):

  At initial stage, only zones of the front where the toughness is weaker start advancing whereas the tougher parts remain pinned. But after this transient phase, the whole front reached Irwin criteria, then remains in a stationary shape. This situation corresponds to a regular process in the nomenclature introduced in the introduction.

- for large contrast $\Delta > \Delta_c(k)$ (Fig. 7.2b):

  The parts of the front where the toughness is higher never reach the threshold and remain pinned. The crack front never attains a stationary shape. Instead it develops a flower like shape with infinitely growing petals or fingers. It corresponds to an irregular propagation process.

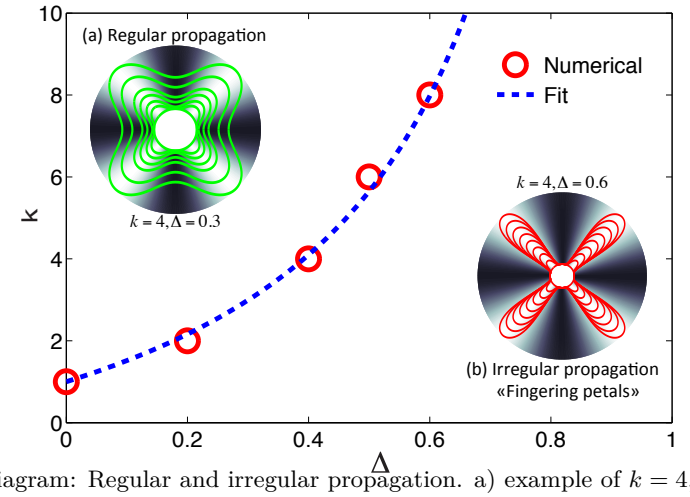

Figure 7.2: Phase diagram: Regular and irregular propagation. a) example of $k = 4$, $\Delta = 0.3$, b) example of $k = 4$, $\Delta = 0.6$.

Fig. 7.2 represents these two propagation behaviors on a $k - \Delta$ phase diagram. One shall make remark that, *as the value of wave-number k of toughness fluctuations increases, the range of toughness contrasts for which crack propagation is regular, increases.* Regions for both behaviors are separated by well fitted relation between wave-number and toughness contrast, that is

$$\Delta_c(k) = \frac{k-1}{3.65+k} \tag{7.18}$$

where $\Delta_c(k)$ represents corresponding critical value of contrast. That means $\Delta_c \to 0$ when $k \to 1$ (in agreement with first-order results described in §7.1) and $\Delta_c \to 1$ when $k \to \infty$. The stability boundary that has been found here also covers the stability boundary ($k > 1$, $\Delta = 0$) that has been constructed by Gao and Rice (1987) based on linear stability analysis of crack front perturbation in the homogeneous media. In the sequel both behaviors will be studied more precisely.

7.2.2 Regular propagation

In this section we present evolution of the local elasticity and geometry of crack front during regular propagation. As typical examples, the results for cases with toughness contrast of $\Delta = 0.3$ with $k = 4$ and $k = 6$ are considered. Figs. 7.3(a) and 7.3(b), show the evolution of the successive equilibrium positions of crack fronts and Figs. 7.3(c) and 7.3(d) the evolution of the corresponding local SIF K normalized by $\overline{K}_c$. Abscissa in Figs. 7.3(c) and 7.3(d) is the normalized polar co-ordinate θ/θ_0 along crack front, where θ_0 is the period of toughness map :

$$\theta_0 = 2\pi/k. \tag{7.19}$$

The different colored curves corresponding to different stages during propagation are in correspondence with each other. Red dashed curve is corresponding to normalized fracture toughness $K_c/\overline{K}_c$ along crack front. Let denote A ($\theta = \pi/k$) a point along the crack front where the toughness is minimum and B ($\theta = 0$) where it is maximum.

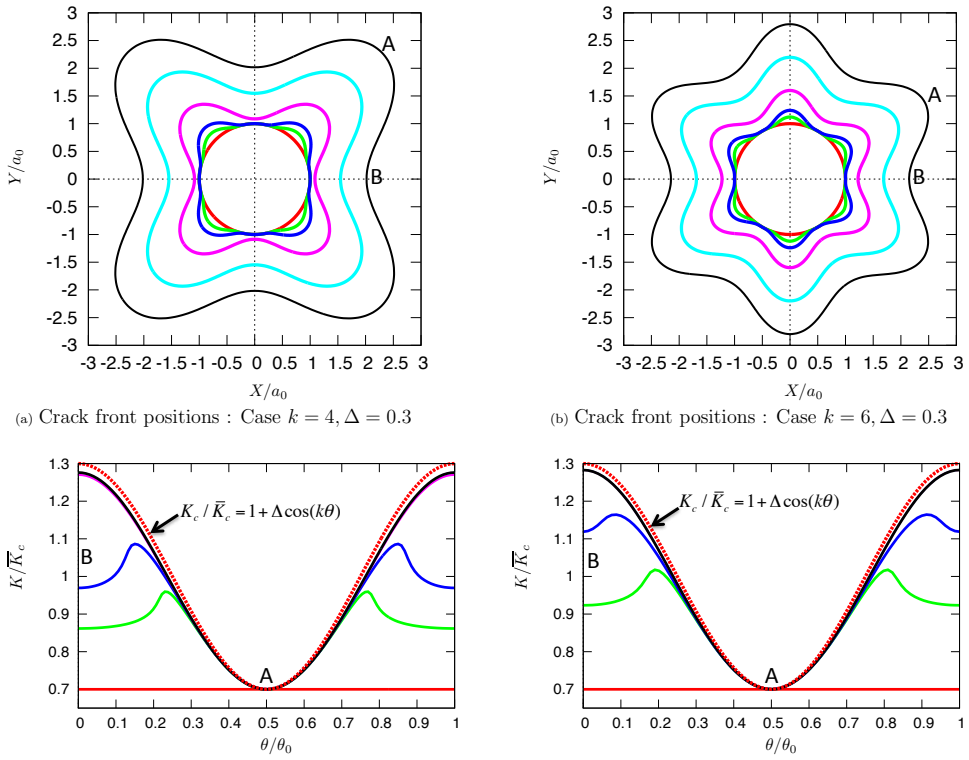

(a) Crack front positions : Case $k = 4, \Delta = 0.3$

(b) Crack front positions : Case $k = 6, \Delta = 0.3$

(c) Evolution of $K/\overline{K}_c$: Case $k = 4, \Delta = 0.3$

(d) Evolution of $K/\overline{K}_c$: Case $k = 6, \Delta = 0.3$

Figure 7.3: Evolution of local quantities: Regular crack propagation

On Figs. 7.3(a) and 7.3(b) we observe that the propagation is continuous without jumps, showing that the pinning is weak. One can notice that first the crack front deforms from a circular crack to a k-petals flower shape, which then, remains the same.

It can be explained by looking at Figs. 7.3(c) and (d). In the initial stage, the configuration of crack front is circular, so that only the points where K_c is minimum reach the threshold (dashed red curve) and propagate (around point A). Then, during a transient phase more and more points reach the threshold and start propagate. For example see some front positions during this initial stage, depicted in green and blue curves in Figs. 7.3(a) and (b): only the points around weakest point A advance while points around toughest point B remain pinned by surround tough heterogeneity. Correspondingly SIFs at tough points B then increase (see Figs. 7.3(c) and (d)), in agreement with the result (7.6) of Gao and Rice (1987), until reaching the maximum toughness. At this point the Irwin's criteria $K = K_c$ is, and further remains, verified all along the crack front. By propagation law (6.13) crack front attains and then remains in a stationary shape, *i.e.* crack just propagates with homothetical scaling of '*k-petal*' front shape (see last three front shapes denoted in magenta, cyan and black: all these three shapes are the same and corresponding SIFs along these crack fronts are the same and equal

everywhere to K_c).

Let us now focus at the evolution during propagation of macroscopic quantities, normalized amplitude of front deformations $\Delta a/a$, integral of local deformations $I(a)$ and normalized SIF $K/\overline{K}_c$ at weak point A and tough point B. Fig. 7.4 shows the evolution of normalized geometric quantities, $\Delta a/a_0$ and $I(a)$, describing front deformations. It can be seen that both quantities start with zero value corresponding to the initial circular crack configuration and increase until a plateau is reached. The plateau corresponds to the stationary regime. In this regime the shape of the crack doesn't change, only its size is growing in proportional to crack mean size, *i.e.* $\Delta a^{\infty} \propto a$.

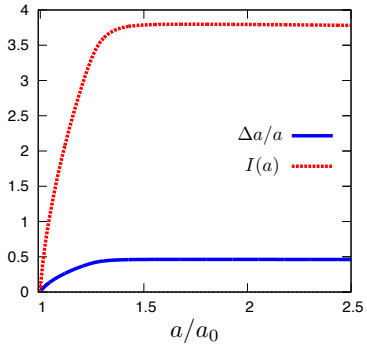

Figure 7.4: Evolution of macroscopic geometrical quantities : $k = 4,\ \Delta = 0.3$

Correspondingly, Fig. 7.5 shows the evolution of $K/\overline{K}_c$ at points A and B, as a function of normalized amplitude of front deformations $\Delta a/a_0$. Fig. 7.5(a) is corresponding to the cases of $k = 4, \Delta = 0.3$ and Fig. 7.5(b) to $k = 6, \Delta = 0.3$. The red cross marks are in correspondence to the minimum fracture toughness, *i.e.* $K_c^{min}/\overline{K}_c = 1 - \Delta$ and the black cross marks are in correspondence to the maximum fracture toughness, *i.e.* $K_c^{max}/\overline{K}_c = 1 + \Delta$.

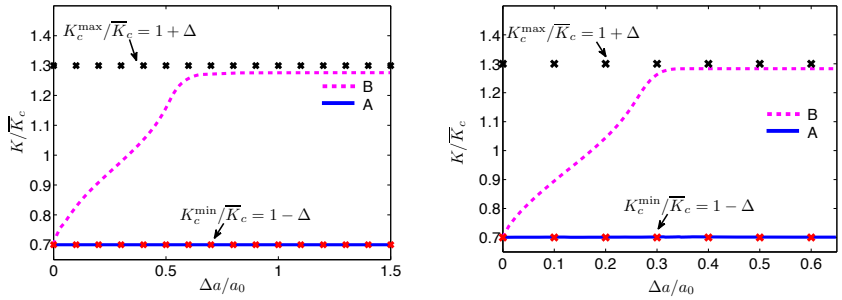

(a) Case $k = 4, \Delta = 0.3$ (b) Case $k = 6, \Delta = 0.3$

Figure 7.5: Evolution of normalized $K/\overline{K}_c$ at weak point A and tough point B: Regular crack propagation

Therefore as still discussed previously, from starting threshold is always reached at weak point A: both plain curve corresponding to the evaluation of the SIF and the crossed curve, correspondingly to the value of $1 - \Delta$ of $K/\overline{K}_c$ can not be distinguished. At tough point B, $K/\overline{K}_c$ increases during a transient zone, until it reached its threshold (*i.e.* $K_c(B)/\overline{K}_c = 1 + \Delta$) and then it remains same during stationary regime.

7.2.3 Irregular propagation

Aim of this section is to look at the evolution of local quantities during irregular crack propagation. As typical examples, the results for cases with large enough toughness contrast of $\Delta = 0.6$ with $k = 4$ and $k = 6$ are considered. Figs. 7.6(a) and 7.6(b), show successive equilibrium positions of crack fronts in these cases. Tough parts of crack front B remain pinned while weak parts A remain in advanced: large "fingers" develop. One shall also notice that although the

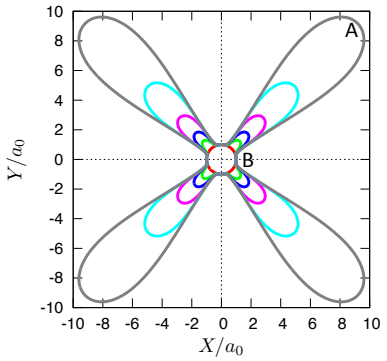

(a) Crack front positions: Case $k = 4, \Delta = 0.6$

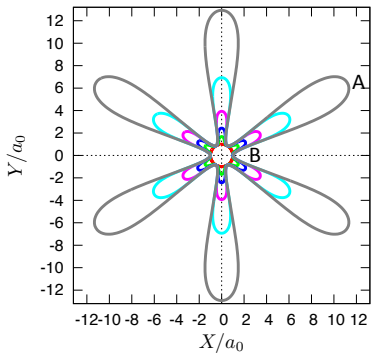

(b) Crack front positions: Case $k = 6, \Delta = 0.6$

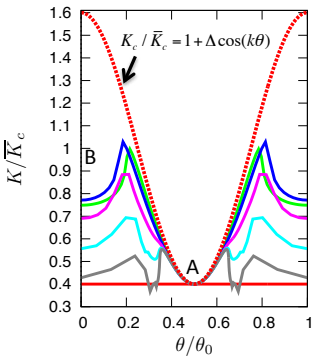

(c) Evolution of $K/\overline{K}_c$: Case $k = 4, \Delta = 0.6$

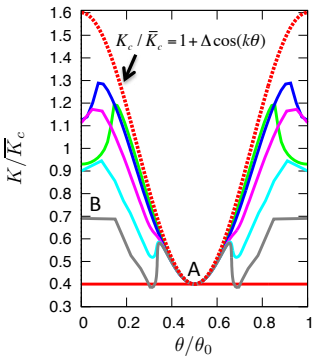

(d) Evolution of $K/\overline{K}_c$: Case $k = 6, \Delta = 0.6$

Figure 7.6: Evolution of local quantities: Irregular propagation

whole shape is not stationary, the shape at the top of the petals, around A, is always stationary.

It can be explained by looking at Figs. 7.6 (c) and (d). Similarly as it has been observed in the case of regular propagation, in the initial stage, only the points where K_c is minimum reach the threshold (dashed red curve) and propagate (around point A). A front part around point A advances while points around toughest point B remain pinned by surround tough heterogeneity (see curves till curve coloured with dark blue). Correspondingly SIFs at tough points B then increase (see Figs. 7.6 (c) and (d)), in agreement with the result (7.6) of Gao and Rice (1987). But before it reaches to the maximum toughness, $K(B)/\overline{K}_c$ starts to decrease and point B remains pinned forever. At this point amplitude of front perturbations becomes of same order of initial crack size, *i.e.* $\Delta a \propto a_0$. This will be cleared more during discussion on Figs. 7.8. Finally, it can be noticed that, as observed in Fig. 7.6 the front part around point A is always stationary, corresponding SIFs along this part of the crack are the same and equal everywhere to K_c.

Fig. 7.7 shows the evolution of macroscopic geometric quantities $\Delta a/a$ and $I(a)$ during propagation. They both increase with a/a_0 since the deformations of the crack always increases. The increase in $\Delta a/a$ however slows down with a. This can be rationalized by the fact that a stationary shape exists around point A and becomes dominant in the calculation of the mean size a in the comparison to the initial crack.

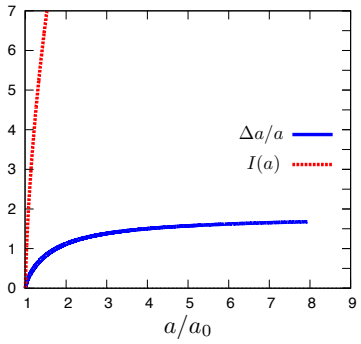

Figure 7.7: Evolution of macroscopic geometrical quantities : $k = 4,\ \Delta = 0.3$

Figs. 7.8 shows the evolution of the normalized SIF $K/\overline{K}_c$ at weak A and tough B points. Again, as linear perturbation theory predicted, at initial stage, the normalized SIF $K/\overline{K}_c$ increases at point B but, in contrary to regular propagation, before it attains Irwin's threshold, it reached some peak value and then starts to decrease. Point B therefore, get disconnected from loading and remains pinned forever and thus whole system remains in an eternal transient regime with increasing in finger size.

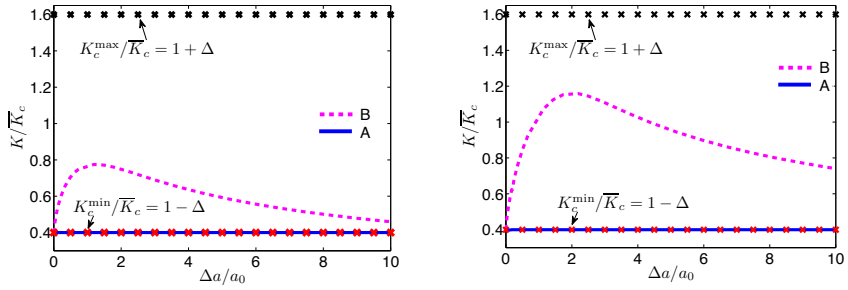

(a) Case $k = 4, \Delta = 0.6$ (b) Case $k = 6, \Delta = 0.6$

Figure 7.8: Evolution of normalized $K/\overline{K}_c$ at weak point A and tough point B : Irregular crack propagation

For other values of k, results are presented in Appendix D.4.

7.2.4 Physical mechanism for the fingering instability

Here, we explain the basic physical mechanism of the fingering instability by looking at the evolution of the local elasticity of crack front. To remove the loading effect, we have introduced the normalized local SIF by $K(M)/K_0$, where $K_0 = \dfrac{2}{\sqrt{\pi}}\sigma\sqrt{a_0}$ (SIF corresponding to circular

crack with radius of a_0). This quantity only depends on the crack shape and size. Fig. 7.9(a) shows a typical evolution of this quantity at weak point A and at tough point B as a function of the normalized petal size $\Delta a/a_0$. One shall notice that, at initial stage, K/K_0 increases at point

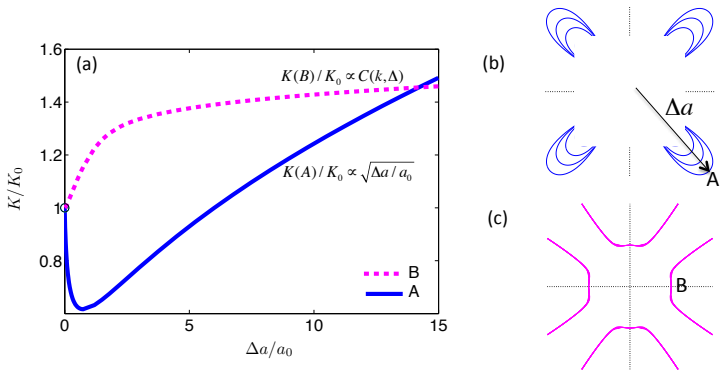

Figure 7.9: Irregular crack propagation: (a) evolution of K/K_0 at weak point A and tough point B; (b) successive front positions in vicinity of weak point A; (c) successive front positions in vicinity of weak point B (case $k = 4, \Delta = 0.6$)

B and decreases at point A, in agreement with small perturbation theory developed by Gao and Rice (1987). After the petal becomes of the size of the initial crack size a_0 (*i.e.* $\Delta a/a_0 \sim 1$),

- A part of the front around point B is trapped in some limit geometry, see Fig. 7.9 (c). Corresponding evolution of $K(B)/K_0$, slows down and seems to converge to some plateau value, *i.e.* $K(B)/K_0 \propto Cst.$
- A part of the front around point A evolves with some stationary shape (see Fig. 7.9(b)). Correspondingly, $K(A)/K_0$ evolves, like square root of petal size, *i.e.* $K(A)/K_0 \propto \sqrt{\Delta a/a_0}$.

Conclusively, it shall be noticed that due to such large front perturbations, even though the elasticity of the crack front depends on the whole crack front geometry, local elasticity around point A and B evolve differently and become disconnected. It'll be seen in Appendix D.3.2 that:

(i) At point A, the SIF evolves as the square-root of the radius of the local curvature.

(ii) At point B, the SIF is approximately equal to the one of the small initial circle of size a_0.

7.3 Evolution of the global quantities

For the initial circular crack of radius a_0, $K(M) = K_0$ all along the front, so that *onset* of propagation given by Eq. (6.2) verifies

$$\frac{2}{\sqrt{\pi}} \frac{\sigma\sqrt{a_0}}{K_c} = \frac{K_c^{\min}}{K_c} = 1 - \Delta. \tag{7.20}$$

It follows that for $a = a_0$,

$$\frac{K_{\text{eff}}}{\overline{K}_c} = \frac{K_{\text{m}}}{\overline{K}_c} = 1 - \Delta \tag{7.21}$$

and

$$\frac{G_{\text{A}}}{\overline{G}_c} = \frac{G_{\text{m}}}{\overline{G}_c} = \frac{G_c^{\min}}{\overline{G}_c} = \frac{(1-\Delta)^2}{1+\frac{\Delta^2}{2}}. \tag{7.22}$$

Below we present the evolution of these quantities when a increases in both cases: regular and irregular propagation.

7.3.1 Evolution of the loading

Fig. 7.10 (a) shows the evolution of the normalized loading as a function of normalized mean radius a/a_0 for two values of the contrast Δ equal to 0.3 and 0.6 in corresponding to cases of regular and irregular for $k = 4$. In both cases, initial evolution of the normalized loading starts with value ($\sim (1-\Delta)$) corresponding to the initial circular crack geometry and during initial stage it increases from this value until a peak value. In the case of regular propagation,

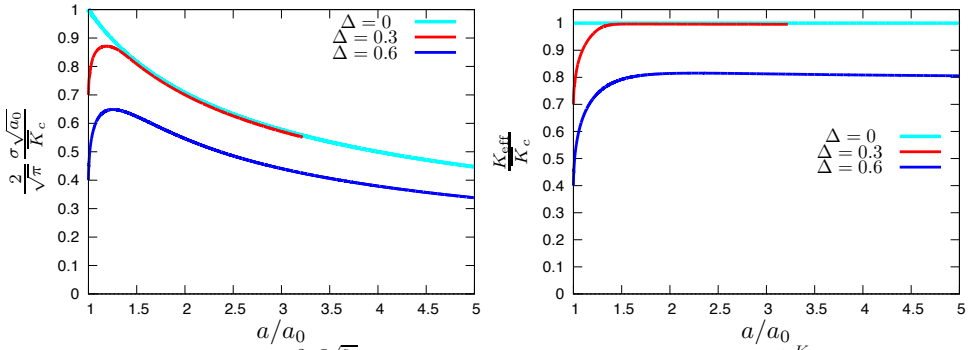

(a) Evolution of $\frac{2}{\sqrt{\pi}}\frac{\sigma\sqrt{a_0}}{\overline{K}_c}$ (b) Evolution of $\frac{K_{\text{eff}}}{\overline{K}_c}$

Figure 7.10: Evolution of loading during propagation: Case $k = 4$

after this point (where tough point B get breaks and start to propagate), stationary regime is reached and it starts to decay with mean crack size in the same decay form as it follows in case of homogeneous toughness field ($\Delta = 0$) that is $\frac{2}{\sqrt{\pi}}\frac{\sigma\sqrt{a_0}}{\overline{K}_c} \sim \sqrt{\frac{a_0}{a}}$. This indicates that $K_{\text{eff}}/\overline{K}_c = 1$ (Fig. 7.10 (b)).

In the case of irregular propagation, still point B doesn't get break at this point, but the loading starts to decay in same form of inverse square root of mean crack size and correspondingly K_{eff} reaches to some plateau value (Fig. 7.10 (b)). The only difference is in proportionality constant, now in the case of irregular propagation this proportional constant is smaller, so that K_{eff} remains smaller than $\overline{K}_c$ (Fig. 7.10 (b)).

7.3.2 Evolution of the macroscopic SIF and ERR

Fig. 7.11 (a) shows evolution of the quantities G_{A}, G_{m}, K_{m} as a function of crack mean size a in the case of regular propagation. They start with the corresponding minimum values of the

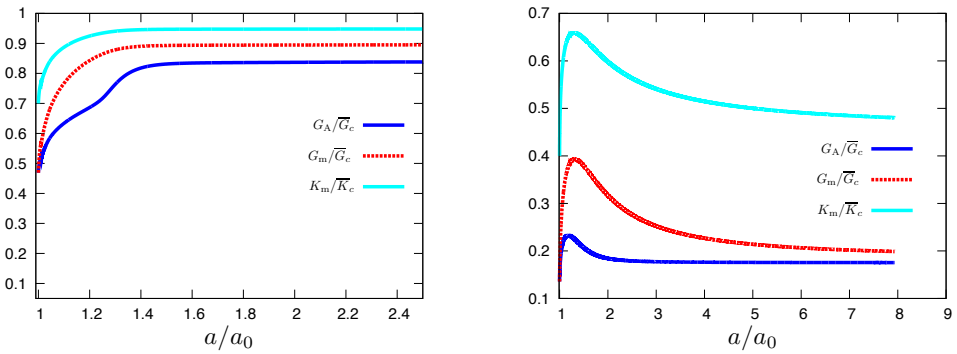

(a) Case : $k = 4, \Delta = 0.3$ (b) Case:$k = 4, \Delta = 0.6$

Figure 7.11: Evolution of global quantities during (a) regular propagation, and (b) irregular propagation.

toughness, and increase until a plateau is reached, once in the stationary regime.

Fig. 7.11 (b) shows evolution of the same quantities as a function of crack mean size a during irregular propagation. Their evolution starts with their onset values, it increases at initial stage of propagation, attains a peak value, decrease and after a while drop it seems to tend toward some stationary plateau value. Due to limit on computational cost, it is difficult to pursue the calculation further to verify the existence of this plateau. We have also tried to interpolate the decrease with some simple functions but without success. Also, instead of discussing each case of (k, Δ), we decide to report the discussion in the next section where the values of the plateau are studied as a function of k and Δ.

7.3.3 Influence of the geometrical parameters (k, Δ) of the toughness field on the asymptotic macroscopic values

As named the section title, aim of this section is to look at the influence of the toughness contrast Δ and toughness spatial re-partition k on the asymptotic macroscopic values $G_{\mathrm{A}}^{\infty}, G_{\mathrm{m}}^{\infty}, K_{\mathrm{m}}^{\infty}$ and $K_{\mathrm{eff}}^{\infty}$ corresponding to stationary plateau regime of the macroscopic quantities. Figs. 7.12(a) and (b) describe the influence on the asymptotic macroscopic values G_{A}^{∞} and G_{m}^{∞} and Figs. 7.12(c) and (d) describe the influence on the asymptotic macroscopic values K_{m}^{∞} and $K_{\mathrm{eff}}^{\infty}$. The points corresponding to the regular case (*empty symbol*) correspond to the well defined plateau of Figs. 7.10 (b) and 7.11 (a). The points corresponding to the irregular case (*filled symbol*) are choose to correspond to the values of the quantities for $a/a_0 = 7$. They are hence greater than the asymptotic values which are numerically difficult to catch.

For small enough toughness contrast $\Delta \ll 1$, the first-order approximations (Section 7.1) are retrieved. Corresponding all the quantities are equivalent and equal to toughness average value along crack plane. Appendix D.2 presents when first-order approximation starts to make error.

For larger toughness contrast, all quantities are no more equivalent and they are always lower than toughness average value. They decrease with increase in toughness contrast Δ and with decrease in toughness re-partition k. The decrease is slower in the case of regular propagation regime than in the irregular one. Let us discuss further both behaviours separately.

In the case of regular propagation, since $K = K_c$ everywhere, the SIF along the crack front

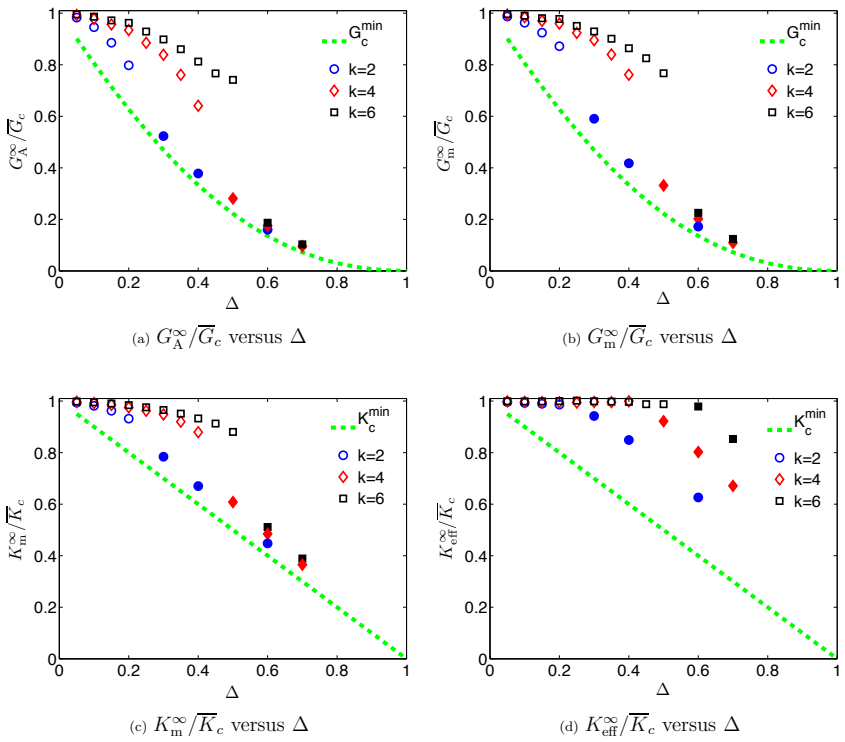

(a) $G_{\mathrm{A}}^{\infty}/\overline{G}_c$ versus Δ (b) $G_{\mathrm{m}}^{\infty}/\overline{G}_c$ versus Δ

(c) $K_{\mathrm{m}}^{\infty}/\overline{K}_c$ versus Δ (d) $K_{\mathrm{eff}}^{\infty}/\overline{K}_c$ versus Δ

Figure 7.12: Influence of toughness map parameters k and Δ on the equivalent fracture properties. *Empty* symbols are correspond to regular propagation and *filled* one are correspond to irregular propagation.

is given by :

$$K(\theta) = \frac{2}{\sqrt{\pi}}\sigma\sqrt{a}\left(\widetilde{K}_m + \Delta\widetilde{K}\cos(k\theta)\right) \tag{7.23}$$

with $\Delta\widetilde{K} = \Delta$. We have moreover obtained numerically that the mean value of $\widetilde{K}$ verifies $\widetilde{K}_{\mathrm{m}} = 1$ (see Appendix D.3.1). Then since $K = K_c$ all along crack front, one gets in particular for $\theta = \pi/2k$:

$$\frac{2}{\sqrt{\pi}}\sigma\sqrt{a}\widetilde{K}_m = \overline{K}_c \Rightarrow \frac{2}{\sqrt{\pi}}\frac{\sigma\sqrt{a}}{\overline{K}_c} = \frac{1}{\widetilde{K}_m}$$

Since $\widetilde{K}_m = 1$ and definition (6.4), one gets

$$\frac{K_{\mathrm{eff}}^{\infty}}{\overline{K}_c} = 1 \tag{7.24}$$

for any toughness map parameters within regime of regular propagation[1].

For the asymptotic values of other macroscopic quantities, let takes K_{m}^{∞} as an example, by definition (6.5) one shall write,

$$\frac{K_{\mathrm{m}}^{\infty}}{\overline{K}_c} = \frac{1}{2\pi}\int_0^{2\pi}(1 + \Delta\cos(k\theta))\,\mathrm{d}s(\theta)$$

[1]By following same procedure in section 3.5 calculating effective fracture toughness in the case of half-plane crack, it can be noticed that $G_{\mathrm{eff}} < \overline{G}_c$ since $\mathrm{d}G^0/\mathrm{d}a < 0$.

$$= 1 + \frac{k\Delta}{\pi} \int_0^{\pi/k} \cos(k\theta) \mathrm{d}s(\theta). \tag{7.25}$$

The integration in second term of above equation can be split in following two terms,

$$\int_0^{\pi/k} \cos(k\theta) \mathrm{d}s(\theta) = \int_0^{\pi/2k} \cos(k\theta) \mathrm{d}s(\theta) + \int_{\pi/2k}^{\pi/k} \cos(k\theta) \mathrm{d}s(\theta).$$

Since $\cos(k\theta)$ changes sign at $\theta = \pi/2k$, first integration on $[0, \pi/2k]$ is positive and second integration on $[\pi/2k, \pi/k]$ is negative and since the front deformed more in weak part of toughness map the length of domain $[\pi/2k, \pi/k]$ is larger than $[0, \pi/2k]$ which gives the overall $\int_0^{\pi/k} \cos(k\theta) \mathrm{d}\theta < 0$ and thus

$$K_{\mathrm{m}}^{\infty} < \overline{K}_c. \tag{7.26}$$

Similarly, one can demonstrate that $G_{\mathrm{m}}^{\infty} < \overline{G}_c$, $G_{\mathrm{A}}^{\infty} < \overline{G}_c$.

Finally one shall notice that, for a given values of k, these values decrease, whereas quantities corresponding to front deformation $\Delta a^{\infty}/a$ and I^{∞} increase (Fig. 7.13), with Δ. Physically, it looks obvious, that in case of higher contrast, the crack front deforms more, hence propagates more in weaker regions and therefore, the mean toughness along the front is decreasing as the contrast increases. Now for a given value of Δ, they increase, whereas $\Delta a^{\infty}/a$ and I^{∞} decrease with the heterogeneity wavenumber k, that is when the number of defects increases along the crack front. Physically, it is due to the fact that when k increases, the amplitude of the deformation has less space to develop, and so the front becomes more straight. Indeed, from fit which has been shown in Fig. 7.2, it can bee seen that in the limit of $k \to \infty$ the propagation of a crack always remains within regular regime. Top of it, a correlated fact is that for this limit case all the quantities are simply equal to $\overline{K}_c$.

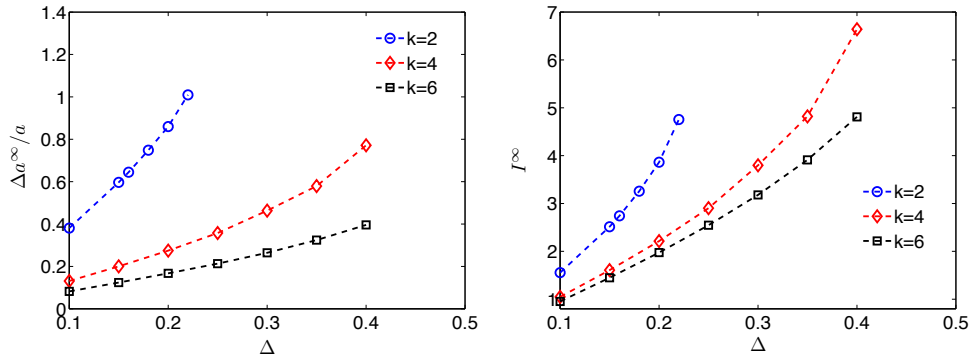

(a) $\Delta a^{\infty}/a$ versus Δ (b) I^{∞} versus Δ

Figure 7.13: Influence of toughness map parameters k and Δ on the equivalent front deformations.

In the case of irregular propagation, the effective toughness seems to be governed by the sole minimum toughness values. For example, see Fig. 7.12 (a), G_{A}^{∞} follows the minimum of G_c curve. It is slightly above but it may be due to the fact that we take values at a finite value of a ($a/a_0 = 7$). If one looks at the definition (6.7) of G_{A}, the integrals are zero nearly

everywhere along the front since $\delta a \sim 0$, except in the vicinity of point A where $G \sim G_c^{\min}$ so that $G_{\mathrm{A}}^{\infty} \sim G_c^{\min}$.

On the values of K_{m}^{∞} and G_{m}^{∞}, from Fig. 7.6, it seems that the SIF K becomes nearly constant along the front so that $K \sim K_c^{\min}$ nearly everywhere so that K_{m}^{∞}, G_{m}^{∞} are approximately equal to their minimum values.

For the values of $K_{\mathrm{eff}}^{\infty}$, threshold is reached around point A, *i.e.*:

$$K(A) = \frac{2}{\sqrt{\pi}}\sigma\sqrt{a}\widetilde{K}(A) = K_c^{\min} \Rightarrow K_{\mathrm{eff}} \sim \frac{K_c^{\min}}{\widetilde{K}(A)}. \tag{7.27}$$

And it has been shown in Appendix D.3.2 that $\widetilde{K}(A)$ is linked to the radius $R_c(A)$ of curvature at A, *i.e.* $\widetilde{K}(A) \sim \sqrt{R_c(A)/a}$. Since $R_c(A)/a \sim Ctc < 1$, one gets that,

$$K_{\mathrm{eff}}^{\infty} > K_c^{\min}. \tag{7.28}$$

The decrease of $K_{\mathrm{eff}}^{\infty}$ with increase in toughness contrast Δ and with decrease in toughness repartition k is linked to the behaviour of $\widetilde{K}(A)$ with k, Δ which could only be find by numerical ways.

7.4 Concluding remarks

In this chapter, the influence of large toughness contrasts on the crack shape has been explored numerically. In order to focus on the effect of the large crack front deformations, we studied the case of a circular crack propagating in an invariant toughness map along the propagation direction. This allows us to observe whether crack front reaches a stationary shape regime in which Irwin's threshold is reached at each point of the front or not. In case of small contrasts, a stationary flower shape is always reached for which $K = K_c$ all along the front (regular propagation). For larger contrasts, some zones of the front remains pinned on the higher toughness regions so that the petals or fingers grow infinitely (irregular propagation). By performing systematic simulations for several configurations of the toughness map, corresponding to various combinations of wave-number k and toughness contrast Δ, the well defined boundary $\Delta_c(k)$ between the two behaviors was found: *regular crack propagation* regime for small contrast $\Delta < \Delta_c(k)$ and *irregular crack propagation* regime for large contrast $\Delta > \Delta_c(k)$.

In order to do homogenization over the heterogeneous fracture properties, different macroscopic quantities are introduced. All these quantities are equivalent to the average value of the toughness map for $\Delta \ll 1$ but it no more remains true for larger values of toughness contrast Δ. They are smaller than the average value and decrease with Δ. The decrease becomes dramatic in the fingering regime. The propagation is then governed only by the weakest part of the toughness map. On other hand, for a given value of the toughness contrast, these quantities increase with k. In the limit when $k \to \infty$, (i) propagation remains in the regime of regular propagation (Fig. 7.2), (ii) equivalent fracture properties are simply equal to the average value of toughness. The next interesting step would be to extend this study of large crack front deformations to the case of strong pinning (where heterogeneous toughness map also varies along crack propagation direction).

General conclusion

The primary objective of this thesis was to provide a quantitative description of effective toughness variations due to large deformations in the crack front geometry that can be induced by strong toughness heterogeneities. Before pursuing the detailed discussion on main results, let us remind the context of this work. For weak heterogeneities, Roux *et al.* (2003), Patinet *et al.* (2013) and Demery *et al.* (2014) have shown that (i) an increase in effective toughness may be reached only if some parts of the part remain pinned by some tougher material and (ii) this situation may occur only if the material is heterogeneous in the propagation direction, when it is homogeneous in this direction, the front shape deforms to reach a situation where $G = G_c$ all over the front and the effective toughness is equal to the average value of the local toughness on the crack plane. Here we want to see if even when the material is invariant in the propagation direction, some impact on the effective toughness may be induced by strong heterogeneities. Hence we made the following hypothesis. First, we studied the problem under the assumption of brittle quasi-static crack propagation ($G \leq G_c$). The propagation medium has been considered to be heterogeneous in the toughness field only, the elasticity constants have been assumed to be uniform. In order to focus on large toughness contrasts, the toughness map has been chosen to be invariant in the propagation direction. We have considered several problem configurations; (a) planar half-plane cracks located (i) in some infinite body, or (ii) on the mid-plane of a plate, subjected to mode I loading conditions, (b) planar circular crack located in some infinite body subjected to remote mode I stress loading. With this framework, we have studied the influence of the toughness map – its level and shape – on the planar crack propagation and its implication on the effective fracture toughness. Based on the basic questions we had raised while describing the objectives of this thesis work, the main results can be summarized in the following three points.

First, this study has proven to be useful to calculate the equilibrium front deformations and for measuring at least the range of toughness contrast values that validate the first-order approximation. This range has been summarized in the Table Cnl. Range of second-order approximation has been explored on the model peeling experiments in the case of half plane cracks. In the special case of pinning by a single infinitely elongated obstacle, the first-order approximation is sufficient for contrasts up to 0.2, whereas the second-order one correctly predicts the crack front deformation up to 0.7. The limit value has been shown to depend on the heterogeneity size, on the crack geometry: for instance in the case of half-plane cracks, it is 0.1 in the case of a single obstacle and 0.2 for a periodic array of obstacles. In the case of a circular crack, it varies from 0.14 to 0.24 when k varies from 2 to 6. To summarize, it shall be noticed that this range of validaty depends on the toughness map, the geometry of the crack, the type of loading since the deformation of the front depends on these parameters.

Table Cnl: Range of toughness contrast[a] Δ validating the first-order approximation.

Analytical – half plane cracks		Numerical – circular crack
		Toughness map: $K_c = \overline{K}_c\,[1 + \Delta\cos(k\theta)]$.
Single obstacle	0 – 0.1	$k = 2$; 0 – 0.14
Periodic obstacles	0 – 0.2	$k = 4$; 0 – 0.19
		$k = 6$; 0 – 0.24

[a] In part I, we defined it as G_c contrast and noted it as ϵ; In part II, we defined it as K_c contrast and noted it as Δ. Both definitions are related by $\epsilon = 2\Delta$.

Second, let us discuss whether Griffith's equilibrium condition $G = G_c$ all along the crack front can always be reached (*regular*) or not (*irregular*). Numerical study that has been done on the planar circular crack has shown that for small enough toughness contrast, the crack propagation always reaches a regular regime but for larger toughness contrasts, some situations exist where the regular regime is never reached even when the toughness field is invariant in the propagation direction. Some parts of the front remain pinned which results in crack propagation with growing fingers. On the other hand, for a half-plane crack front, we have shown using analytical results corresponding to second-order developments, that the second-order development is not enough to catch some irregular regime. Use of numerical tools is necessary to verify if such a transition exists for a half-plane crack. However, such a transition cannot be obtained for the half-plane crack without introducing a structural length scale that can be compared to an intrinsic length scale of the heterogeneous toughness field: for instance a length that is governed by the loading in the problem as in chapter 3, or a finite body size as in chapter 4, or a finite crack size as in Part II.

Third, for capturing the implication of such crack propagation on the effective response, different definitions of effective fracture properties have been introduced. Mainly two definitions are most relevant from engineering and physical point of views. One is to define it by replacing the deformed crack front by a straight/circular line configuration (G_{eff} in the case of half-plane crack, K_{eff} in the case of circular crack) and by considering the critical loading. This definition seems most useful in engineering applications. The other one is defined by the quantity of energy that is being dissipated per unit cracked surface area (G_0 in the case of circular crack). This definition gives more physical insight by quantifying small scale dissipations at macro scale. Both these quantities are – as found analytically – equivalent to the average value of the toughness map at the first-order approximations but this does not remain true for large front deformations induced by larger values of the toughness contrasts.

Let first discuss the behaviour of effective fracture toughness that has been defined from the engineering point of view. The second-order approximation of the half-plane crack propagating in the sinusoidal toughness field has shown that the effective fracture toughness is less than the average value of the local material toughness on the crack plane. However, in the case when a typical wavelength of the toughness field is smaller that the typical distance over which the loading varies significantly ($\mathrm{d}G^0/\mathrm{d}a \sim 0$), the weakening effect is rather limited and the effective fracture toughness is simply equal to the average value of the local material toughness. Therefore, the second-order correction has highlighted that the effective fracture toughness is

dependent on the loading condition. This phenomena is missed in the first-order approximation. In the case of circular crack, this effective fracture toughness K_{eff} has been found always equal to the average value of the local material toughness in the regular regime. We have seen that this surprisingly result is linked to the fact that the mean value of the SIF along the flower shaped crack front is equal to the SIF of an equivalent circular crack of the same area. This result however does not remain true for the half-plane crack submitted to uniform line traction forces ($\mathrm{d}G^0/\mathrm{d}a < 0$) for which G_{eff} was found to be smaller than $\overline{G}_c$.

On the other hand, it has been shown that the effective fracture toughness, defined from the energy dissipation at small scale, is smaller than the average value and decreases with the toughness contrast and the size of heterogeneity. This is linked to the fact that for given size of heterogeneity, as the contrast increases the crack front explores mainly the weak part of the toughness map. Therefore, the contribution of the minimum value of toughness map is dominant in the effective fracture toughness. On the other side, for a given toughness contrast, as the size of heterogeneity decreases (equivalently number of heterogeneity spot increases) the crack front has less space to deform and thus the effective fracture toughness remains equal to the average value of the local toughness. In the irregular regime, the decrease in the effective fracture toughness becomes dramatic. The propagation is then governed only by the weakest part of the toughness map.

Regarding perspectives of this work, both the theoretical and numerical frameworks that have been developed in this work are general for any given material toughness distribution. This means that these frameworks are useful to understand weak as well strong pinning effects on the apparent effective properties of heterogeneous materials. First, the influence of the heterogeneity variations in the propagation direction shall be investigated. Second, an interesting perspective would be to extend the numerical method to the half-plane crack. Such an extension would be useful to explore the transition from the regular to the irregular regime that have been explored here in the case of circular crack. Third, it would be interesting to explore the transition from regular to irregular propagation in experiments. From the optimization point of view, it would be interesting to use such frameworks, theoretical and numerical, to devise an optimization tool to design material systems with a tailored microstructure topology providing increased toughness.

Appendices

Appendix A

Appendix of chapter 3

A.1 Calculation of the integral $J(\alpha, \beta, \gamma)$

The well-known trigonometric relations

$$\begin{cases} \cos a \cos b &= \dfrac{1}{2}\left[\cos(a+b) + \cos(a-b)\right] \\ \sin a \sin b &= \dfrac{1}{2}\left[-\cos(a+b) + \cos(a-b)\right] \end{cases}$$

imply that

$$\begin{aligned} \sin(\alpha x)\sin(\beta x)\cos(\gamma x) &= \frac{1}{2}\left\{-\cos\left[(\alpha+\beta)x\right] + \cos\left[(\alpha-\beta)x\right]\right\}\cos(\gamma x) \\ &= \frac{1}{4}\left\{-\cos\left[(\alpha+\beta+\gamma)x\right] - \cos\left[(\alpha+\beta-\gamma)x\right]\right. \\ &\quad \left. + \cos\left[(\alpha-\beta+\gamma)x\right] + \cos\left[(\alpha-\beta-\gamma)x\right]\right\}. \end{aligned}$$

It then follows from equation (4.31) that

$$\begin{aligned} J(\alpha,\beta,\gamma) &= \frac{1}{4}\int_0^{+\infty}\left\{-\cos\left[(\alpha+\beta+\gamma)x\right] - \cos\left[(\alpha+\beta-\gamma)x\right]\right. \\ &\qquad \left. + \cos\left[(\alpha-\beta+\gamma)x\right] + \cos\left[(\alpha-\beta-\gamma)x\right]\right\}\frac{\mathrm{d}x}{x^2} \\ &= \frac{1}{4}\left[I(\alpha+\beta+\gamma) + I(\alpha+\beta-\gamma) - I(\alpha-\beta+\gamma) - I(\alpha-\beta-\gamma)\right], \\ I(\lambda) &\equiv \int_0^{+\infty}\frac{1-\cos(\lambda x)}{x^2}\,\mathrm{d}x. \end{aligned}$$

The integral $I(\lambda)$ is given by formula (3.782.2) of Gradshteyn and Ryzhik (1980):

$$I(\lambda) = \frac{\pi}{2}\,|\lambda|.$$

Inserting this result into the preceding expression of $J(\alpha, \beta, \gamma)$, one gets equation (3.56) of the text.

Appendix B

Appendix of chapter 4

B.1 Cracked Love-Kirchhoff plate with boundary subjected to prescribed forces

The aim here is to illustrate the fact that in the limit $A \to \infty$ (infinite-plate), no matter the boundary conditions on the boundary of the plate, the loading becomes equivalent to a prescribed bending moment. As a result, the corresponding FK always converges to the same FK given by Eq. (4.2). In order to show that, we first derive the FK in the case of a prescribed force on the boundary of a semi-infinite plate, and in a second step we take the limit $A \to \infty$ on FK obtained.

Let us consider the same geometry as in Legrand *et al.* (2011) and chapter 4, that is a semi-infinite plate of thickness $2h$ (Fig. B.1). Choose the coordinate axes in such a way that this plate occupies the domain $0 \leq x < +\infty, -h \leq y \leq h, -\infty < z < +\infty$ in 3D space. Assume that there is an emerging crack on the mid-plane of the plate, occupying the region $0 \leq x \leq a(z), y = 0, -\infty < z < +\infty$, where the distance $a(z)$ specifies the position of the crack front from the Oz axis. The plate is made of some isotropic elastic material with Young's modulus E and Poisson's ratio ν. The loading now consists of uniform, opposite line forces F_0, $-F_0$ in the y direction imposed on the upper and lower halves of the left boundary. The crack is thus loaded in a state of pure mode I at all points of its front.

In comparison to the work of Legrand *et al.* (2011), the views of the *exterior* problem (with variables $x, y/h, z$) and the *interior* problem (with variables $x/h, y/h, z$) remain similar. However, due to prescribed forces, the boundary conditions of the *exterior* problem with a perturbed crack front are changed. In particular boundary condition at $x = 0$ is changed into

$$V_x(0, z) = -F_0; M_{xx}(0, z) = 0 \tag{B.1}$$

where $V_x = Q_x + \dfrac{\partial M_{xz}}{\partial z}$ denotes the total shear force in the y direction; Q_x, M_{xz} and M_{xx} are the resultant shear forces and moments respectively as described in Fig. B.1 (d). For an isotropic Love-Kirchhoff plate

$$\begin{aligned} &V_x(0, z) = -D\frac{\partial}{\partial x}\left(\frac{\partial^2}{\partial x^2} + (2-\nu)\frac{\partial^2}{\partial z^2}\right) v(0, z) = -F_0 \\ &\Rightarrow \frac{\partial}{\partial x}\left(\frac{\partial^2}{\partial x^2} + (2-\nu)\frac{\partial^2}{\partial z^2}\right) v(0, z) = \frac{F_0}{D} \end{aligned} \tag{B.2}$$

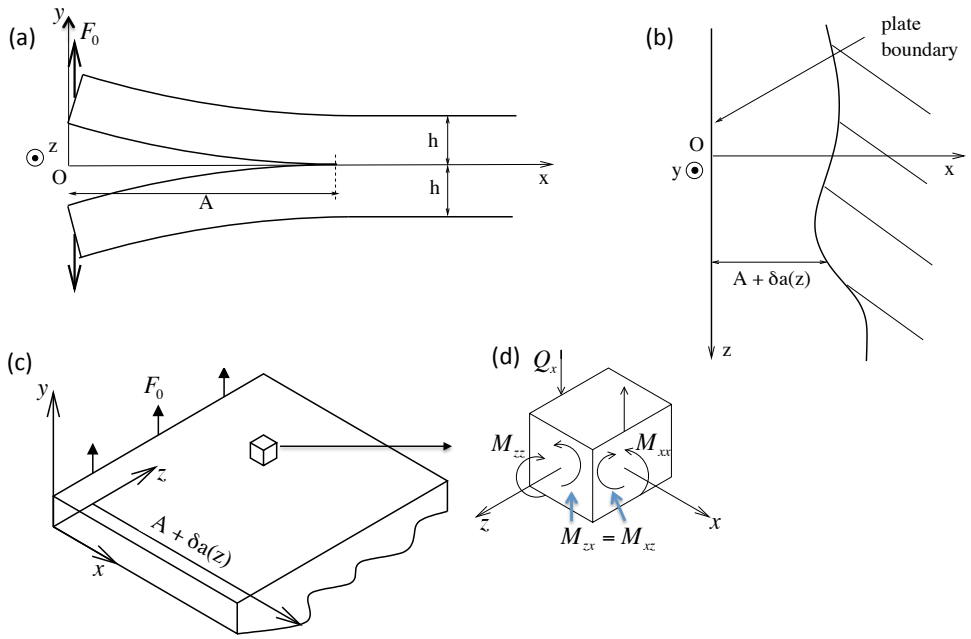

Figure B.1: A slightly perturbed emerging crack lying on the mid-plane of a semi-infinite plate subjected to constant line force $\pm F_0$ at its left boundary: (a) View of the original crack in the Oxy plane; (b) View of the perturbed crack in the Ozx plane; (c) Equivalent Kirchhoff plate model of upper plate with applied force at $x = 0$ and clamped condition at $x = A + \delta a(z)$; (d) Representation of the different moments and transverse shear stress acting.

and

$$\begin{aligned} &M_{xx}(0,z) = -D\left(\frac{\partial^2}{\partial x^2} + \nu\frac{\partial^2}{\partial z^2}\right) v(0,z) = 0 \\ &\Rightarrow \left(\frac{\partial^2}{\partial x^2} + \nu\frac{\partial^2}{\partial z^2}\right) v(0,z) = 0. \end{aligned} \tag{B.3}$$

The clamped condition at $x = a(z)$ remains the same as of described in the work of Legrand *et al.* (2011). As a result, the equations of Love-Kirchhoff's plate theory on the upper plate now reads,

$$\left\{ \begin{array}{l} \left(\dfrac{\partial^2}{\partial x^2} + \dfrac{\partial^2}{\partial z^2}\right)^2 v(x,z) = 0 \text{ for } 0 \le x \le a(z), -\infty < z < +\infty \\ \left.\begin{array}{l} \dfrac{\partial}{\partial x}\left(\dfrac{\partial^2}{\partial x^2} + (2-\nu)\dfrac{\partial^2}{\partial z^2}\right) v(0,z) = \dfrac{F_0}{D} \\ \left(\dfrac{\partial^2}{\partial x^2} + \nu\dfrac{\partial^2}{\partial z^2}\right) v(0,z) = 0 \end{array}\right\} \text{ for } -\infty < z < +\infty \\ \left.\begin{array}{l} v(a(z),z) = 0 \\ \dfrac{\partial v}{\partial n}(a(z),z) = 0 \end{array}\right\} \text{ for } -\infty < z < +\infty. \end{array} \right. \tag{B.4}$$

Consider now a perturbation of the crack front of small amplitude, and denote $\delta v(x,z)$ the variation, under constant loading, of the normal displacement of the upper plate arising from the variation of position $\delta a(z)$ of the crack front around the mean value A. The equilibrium

equation and boundary conditions of the left side satisfied by $\delta v(x,z)$ are readily obtained through differentiation of Eqs. (B.4) at constant force F_0:

$$\left\{\begin{array}{l} \left(\dfrac{\partial^2}{\partial x^2}+\dfrac{\partial^2}{\partial z^2}\right)^2 \delta v(x,z)=0 \text{ for } 0\le x\le A, -\infty<z<+\infty \\ \left.\begin{array}{l} \dfrac{\partial}{\partial x}\left(\dfrac{\partial^2}{\partial x^2}+(2-\nu)\dfrac{\partial^2}{\partial z^2}\right)\delta v(0,z)=0 \\ \left(\dfrac{\partial^2}{\partial x^2}+\nu\dfrac{\partial^2}{\partial z^2}\right)\delta v(0,z)=0 \end{array}\right\} \text{ for } -\infty<z<+\infty \\ \left.\begin{array}{l} \delta v(A,z)=0 \\ \dfrac{\partial \delta v}{\partial x}(A,z)=-2\gamma K^0\delta a(z) \end{array}\right\} \text{ for } -\infty<z<+\infty \end{array}\right. \tag{B.5}$$

where γ denotes the constant connecting the SIF $K(P)$ in the interior problem to the component $C_{11}(P)$ of Love-Kirchhoff's deformation tensor in the exterior problem (see Section 4.2 for its definition and Section 4.3 for its calculation in the paper of Legrand *et al.* (2011)).

In order to solve this problem, let us take its Fourier transform in the direction z; we get

$$\left\{\begin{array}{l} \left(\dfrac{\partial^2}{\partial x^2}-k^2\right)^2 \widehat{\delta v}(x,k)=0 \text{ for } 0\le x\le A, -\infty<k<+\infty \\ \left.\begin{array}{l} \dfrac{\partial}{\partial x}\left(\dfrac{\partial^2}{\partial x^2}-(2-\nu)k^2\right)\widehat{\delta v}(0,k)=0 \\ \left(\dfrac{\partial^2}{\partial x^2}-\nu k^2\right)\widehat{\delta v}(0,k)=0 \end{array}\right\} \text{ for } -\infty<k<+\infty \\ \left.\begin{array}{l} \widehat{\delta v}(A,k)=0 \\ \dfrac{\partial \widehat{\delta v}}{\partial x}(A,k)=-2\gamma K^0\widehat{\delta a}(k) \end{array}\right\} \text{ for } -\infty<k<+\infty. \end{array}\right. \tag{B.6}$$

The solution of Eq. $(B.6)_1$ must be looked the form of an exponential $e^{\xi x}$. Then ξ satisfies the characteristic equation $\left(\xi^2-k^2\right)^2=0$, which admits two double solutions, $\xi=k$ and $\xi=-k$. Thus $\widehat{\delta v}(x,k)$ must be of the form

$$\widehat{\delta v}(x,k)=(Px+Q)\sinh(kx)+(Rx+S)\cosh(kx) \tag{B.7}$$

where P,Q,R and S are constants to be determined. Now, by Eqs. $(B.6)_{2,3}$ one gets,

$$kQ=\frac{1+\nu}{1-\nu}R; \quad kS=-\frac{2P}{1-\nu}. \tag{B.8}$$

With these relations and Eqs. $(B.6)_{4,5}$, finally one gets,

$$\left\{\begin{array}{rcl} P &=& -2\gamma(1-\nu)K^0\widehat{\delta a}(k)\dfrac{kA(1-\nu)\cosh(kA)+(1+\nu)\sinh(kA)}{k^2A^2(1-\nu)^2+4\cosh^2(kA)-(1+\nu)^2\sinh^2(kA)} \\ Q &=& -2\gamma(1+\nu)K^0\dfrac{\widehat{\delta a}(k)}{k}\dfrac{2\cosh(kA)-kA(1-\nu)\sinh(kA)}{k^2A^2(1-\nu)^2+4\cosh^2(kA)-(1+\nu)^2\sinh^2(kA)} \\ R &=& -2\gamma(1-\nu)K^0\widehat{\delta a}(k)\dfrac{2\cosh(kA)-kA(1-\nu)\sinh(kA)}{k^2A^2(1-\nu)^2+4\cosh^2(kA)-(1+\nu)^2\sinh^2(kA)} \\ S &=& 4\gamma K^0\dfrac{\widehat{\delta a}(k)}{k}\dfrac{kA(1-\nu)\cosh(kA)+(1+\nu)\sinh(kA)}{k^2A^2(1-\nu)^2+4\cosh^2(kA)-(1+\nu)^2\sinh^2(kA)}. \end{array}\right. \tag{B.9}$$

The variation of the SIF in Fourier's space is given by Eq. (30) of Legrand *et al.* (2011) :

$$\frac{\widehat{\delta K}(k)}{K^0} = \frac{1}{2\gamma K^0}\frac{\partial^2 \widehat{\delta v}}{\partial x^2}(A,k) - \frac{3\chi}{\gamma K^0}\widehat{\delta a}(k),\ \chi \equiv -\frac{1}{6}\frac{\mathrm{d}^3 v}{\mathrm{d}x^3}(A) \tag{B.10}$$

where $v(x)$ is the solution in the upper plate for a uniform perturbation of the crack front, $a(z) \equiv A$:

$$v(x) = -\frac{F_0}{D}\left[\frac{A^3}{3} - \frac{A^2}{2}x + \frac{1}{6}x^3\right] \tag{B.11}$$

so that

$$\frac{F_0}{D} = -2\frac{\gamma K^0}{A};\ \chi = -\frac{\gamma K^0}{3A}. \tag{B.12}$$

By Eqs. (B.7) and (B.9),

$$\frac{1}{2\gamma K^0}\frac{\partial^2 \widehat{\delta v}}{\partial x^2}(A,k) = -\frac{k\left[(3+\nu)(1-\nu)\sinh(2kA) + 2kA(1-\nu)^2\right]}{k^2A^2(1-\nu)^2 + 4 + (3+\nu)(1-\nu)\sinh^2(kA)}. \tag{B.13}$$

Combining Eqs. (B.10), $(B.12)_2$ and (B.13), one gets

$$\frac{\widehat{\delta K}(k)}{K} = F(kA)\frac{\widehat{\delta a}(k)}{A}. \tag{B.14}$$

$F(p)$ is a function of the "reduced wavenumber" $p = kA$ defined by

$$F(p) \equiv 1 - p\,\frac{(3+\nu)(1-\nu)\sinh(2p) + 2p(1-\nu)^2}{p^2(1-\nu)^2 + 4 + (3+\nu)(1-\nu)\sinh^2(p)}. \tag{B.15}$$

Note the important limit $p \to \pm\infty$ of the function $F(p)$:

$$F(p) = 1 - 2|p| + O\left(p^2 e^{-2|p|}\right) \text{ for } p \to \pm\infty. \tag{B.16}$$

This result means that when the distance A from the left boundary to the crack front goes to infinity, the FK of the cracked plate goes to the limit described by Eq. (4.2) of text.

B.2 Calculation of integrals I_1 and I_2

B.2.1 Integral I_1

This integral is given by

$$\begin{aligned} I_1(h;k,k';z_1) &= PV\int_{-\infty}^{+\infty}\int_{-\infty}^{+\infty}\frac{f(\frac{z-z_1}{h})f(\frac{z'-z}{h})}{(z-z_1)^2(z'-z)^2} \\ &\quad\times\left(e^{ik(z-z_1)}-1\right)\left(e^{ik'(z'-z)}-1\right)e^{ik'(z-z_1)}\mathrm{d}z\mathrm{d}z'. \end{aligned}$$

Quite remarkably, one may express it in terms of the sole function X defined by Eq. (4.4). To do so, the first step consists in performing the changes of variables $z - z_1 = \zeta$, $z' - z = \xi$; one thus gets

$$\begin{aligned} I_1(h;k,k';z_1) &\equiv I_1(h;k,k') = PV\int_{-\infty}^{+\infty}\int_{-\infty}^{+\infty}\frac{f(\frac{\zeta}{h})f(\frac{\xi}{h})}{\zeta^2\xi^2}\left(e^{ik\zeta}-1\right)\left(e^{ik'\xi}-1\right)e^{ik'\zeta}\mathrm{d}\zeta\mathrm{d}\xi \\ &= PV\int_{-\infty}^{+\infty}\frac{f(\frac{\zeta}{h})}{\zeta^2}\left(e^{i(k+k')\zeta}-e^{ik'\zeta}\right)\mathrm{d}\zeta\ .\ PV\int_{-\infty}^{+\infty}\frac{f(\frac{\xi}{h})}{\xi^2}\left(e^{ik'\xi}-1\right)\mathrm{d}\xi. \end{aligned}$$

Writing then $e^{i(k+k')\zeta} - e^{ik'\zeta}$ as $e^{i(k+k')\zeta} - 1 + 1 - e^{ik'\zeta}$, performing the changes of variables $\zeta/h = u$ and $\xi/h = v$, and using the definition (4.4) of X, one gets Eq. $(4.14)_1$ of the text.

B.2.2 Integral I_2

This integral is given by

$$I_2(h;k,k';z_1) = PV\int_{-\infty}^{+\infty}\int_{-\infty}^{+\infty}\frac{f(\frac{z'-z_1}{h})f(\frac{z'-z}{h})}{(z'-z_1)^2(z'-z)^2}\times \left[e^{ik(z'-z_1)} - 1 - \frac{e^{ik(z-z_1)}-1}{z-z_1}(z'-z_1)\right]\left[e^{ik'(z-z_1)}-1\right]\mathrm{d}z\mathrm{d}z'.$$

Again, one may express it in terms of the sole function X. Indeed, one may first perform the changes of variables $z'-z_1=\zeta$, $z-z'=\xi$; one gets

$$I_2(h;k,k';z_1) \equiv I_2(h;k,k') = PV\int_{-\infty}^{+\infty}\int_{-\infty}^{+\infty}\frac{f(\frac{\zeta}{h})f(\frac{\xi}{h})}{\zeta^2\xi^2} \times\left(e^{ik\zeta}-1-\frac{e^{ik(\zeta+\xi)}-1}{\zeta+\xi}\zeta\right)\left(e^{ik'(\zeta+\xi)}-1\right)\mathrm{d}\zeta\mathrm{d}\xi.$$

Now, "symmetrizing" the integrand with respect to the variables of integration ζ and ξ, one gets

$$\begin{aligned}
I_2(h;k,k') &= \frac{1}{2}PV\int_{-\infty}^{+\infty}\int_{-\infty}^{+\infty}\frac{f(\frac{\zeta}{h})f(\frac{\xi}{h})}{\zeta^2\xi^2}\left(e^{ik\zeta}+e^{ik\xi}-1-e^{ik(\zeta+\xi)}\right)\left(e^{ik'(\zeta+\xi)}-1\right)\mathrm{d}\zeta\mathrm{d}\xi\\
&= \frac{1}{2}PV\int_{-\infty}^{+\infty}\int_{-\infty}^{+\infty}\frac{f(\frac{\zeta}{h})f(\frac{\xi}{h})}{\zeta^2\xi^2}\left(e^{ik\zeta}-1\right)\left(e^{ik\xi}-1\right)\left(1-e^{ik'(\zeta+\xi)}\right)\mathrm{d}\zeta\mathrm{d}\xi\\
&= \frac{1}{2}PV\int_{-\infty}^{+\infty}\frac{f(\frac{\zeta}{h})}{\zeta^2}\left(e^{ik\zeta}-1\right)\mathrm{d}\zeta\ .\ PV\int_{-\infty}^{+\infty}\frac{f(\frac{\xi}{h})}{\xi^2}\left(e^{ik\xi}-1\right)\mathrm{d}\xi\\
&\quad -\frac{1}{2}PV\int_{-\infty}^{+\infty}\frac{f(\frac{\zeta}{h})}{\zeta^2}\left(e^{i(k+k')\zeta}-e^{ik'\zeta}\right)\mathrm{d}\zeta\ .\ PV\int_{-\infty}^{+\infty}\frac{f(\frac{\xi}{h})}{\xi^2}\left(e^{i(k+k')\xi}-e^{ik'\xi}\right)\mathrm{d}\xi.
\end{aligned}$$

Reasoning then like for integral I_1, one gets Eq. $(4.14)_2$ of the text.

Appendix C

Appendix of chapter 6

C.1 Stability study for numerical computations

Aim of this appendix is to describe a basic analysis of the numerical stability for explicit numerical method which is used in Part II: for which values of N and $\delta a_{\max}$, is the numerical scheme stable ?s

C.1.1 Problem Statement

We consider a planar circular crack with radius of a_0, embedded in an infinite isotropic elastic medium with homogeneous fracture toughness properties and loaded in pure mode I through some uniform remote stress σ applied at infinity (see Fig. C.1).

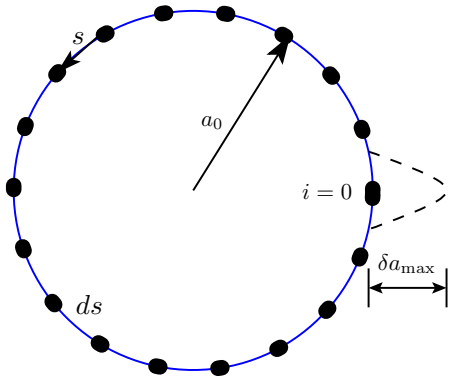

Figure C.1: Initial crack configuration with artificial perturbation δ_0

We perturbed then the front by advancing only the initial node ($i = 0$) by distance of $\delta a_{\max}$ in the following way:

$$\delta_i = \begin{cases} \delta a_{max} & \text{if i=0} \\ 0 & \text{if i} \neq 0. \end{cases} \tag{C.1}$$

Thanks to Gao and Rice (1987)'s stability analysis this perturbation must disappear if the material is homogeneous since the circular shape is stable. Hence we are looking for which values of $\delta a_{\max}, N$, it is indeed the case when solved with our scheme. To check whether the

artificial perturbation δ_i disappears or not, we check the uniformity of the distribution of SIF along the crack front when the mean size of the crack is twice the initial one (*i.e.*$a = 2a_0$). In order to do that, we have defined a standard deviation σ^2 of SIF distribution,

$$\sigma^2 \equiv \sqrt{\frac{1}{N}\sum_{i=1}^{N}\left[K[i] - \bar{K}\right]^2} \tag{C.2}$$

where $\overline{K}$ denotes statistical mean of the SIF distribution along the crack front that is:

$$\overline{K} \equiv \frac{1}{N}\sum_{i=1}^{N} K[i]. \tag{C.3}$$

We then look whether σ^2 is smaller (*stable*) or not (*unstable*) than a given precision p. In the sequel we will keep $p = 5\%$.

C.1.2 Result and discussion

We have run the simulations under different values of $N, \delta a_{\max}$. Fig. C.2 gives the satiability diagram for given values of β. There are region noted *stable* and *unstable* on the plots separated by a well defined boundary. Stable region means under any combination of N and $\delta_{\max}$ within this region perturbation δ_0 always demises as crack propagates while their combination within unstable region δ_0 is not going to demise. One notice that for a given value of β and num-

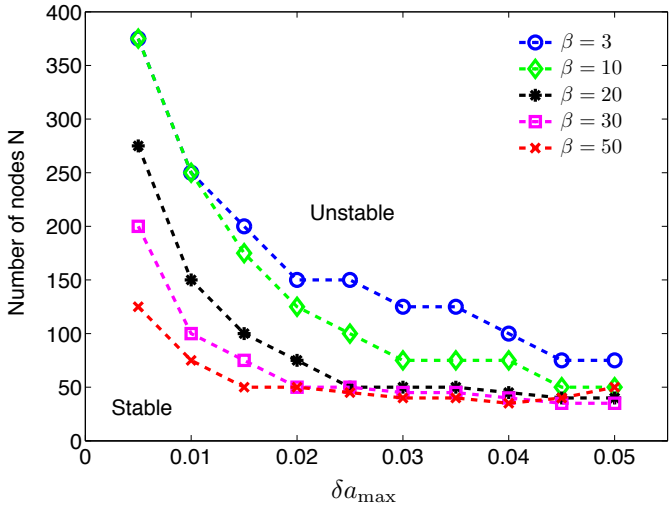

Figure C.2: Stability diagram of the numerical scheme.

ber of nodes N, the value of the temporal discretization has to be the small enough to ensure the numerical stability. We observe that when β increase the stability domain is considerably shrinking so that the calculation may be very time consuming (small time steps for large numbers of nodes). A compromise has to be found between high enough β (brittle case), and an acceptable number of nodes and crack advance. In the report, we choose $\beta = 25$ which has been verified to be enough to find a converged result.

Appendix D

Appendix of chapter 7

D.1 Verification of numerical results at first-order approximation

Main interests of this section is to verify the numerical results with first-order analytical results at small toughness contrasts. Fig. D.1 shows a comparison between the front geometries obtained numerically and analytically at first-order in the case of toughness map with $k = 4$ and $\Delta = 0.2$. Fig. D.1 (a) plots a stationary geometry of the perturbed crack front. Background colormap is showing a representation of the corresponding toughness map for $k = 4$. The already broken part of the map is denoted by the light colormap and unbroken part is denoted by the dark colormap. The interface between these colormaps denotes the crack front. One shall notice that the agreement between numerical and analytical results is very good with a negligible error. As can bee seen in see Fig. D.1 (b), the maximum relative error is only 1.4% despite the not so small value of Δ.

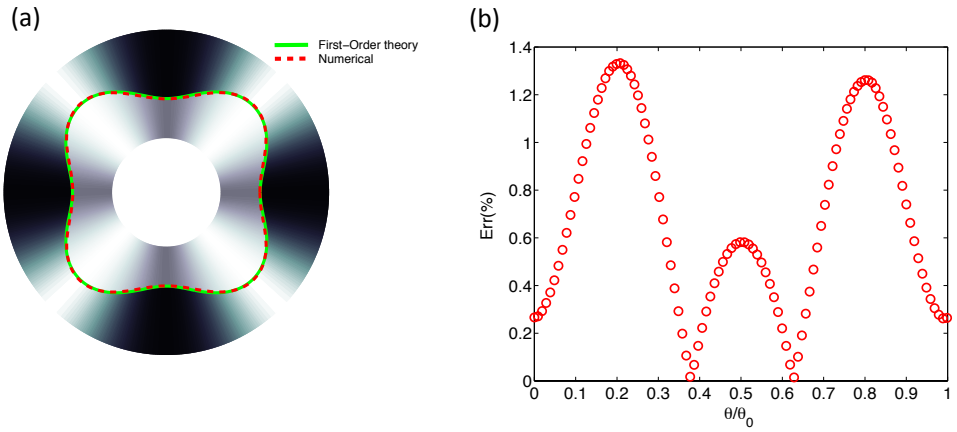

Figure D.1: Comparison with first-order approximation for $k = 4, \Delta = 0.2$: (a) Front geometry during stationary regime *i.e.* $K(\theta) = K_c(\theta)$, (b) Error between the results along crack front.

D.2 Range of toughness contrasts validating the first-order approximation

As mentioned in the main text, aim of this appendix to look at the range of toughness contrast that validates the first-order approximation. For same we have calculated the relative error of numerical results from their first-order approximations. We have performed these calculations on results during stationary regime of crack propagation. For example let say error in the numerical value of G_{A}^{∞} from its first order approximation, *i.e.*:

$$Err(\%) = \frac{G_{\mathrm{A}}^{\infty} - \overline{G}_c}{\overline{G}_c} \times 100. \tag{D.1}$$

Fig. D.2 (a) plots this error as a function of toughness contrast Δ for given wavenumber k. Similarly, relative errors in other global quantities like G_{m}^{∞} and K_{m}^{∞} are plotted in Figs. D.2 (b) and D.2 (c) respectively.

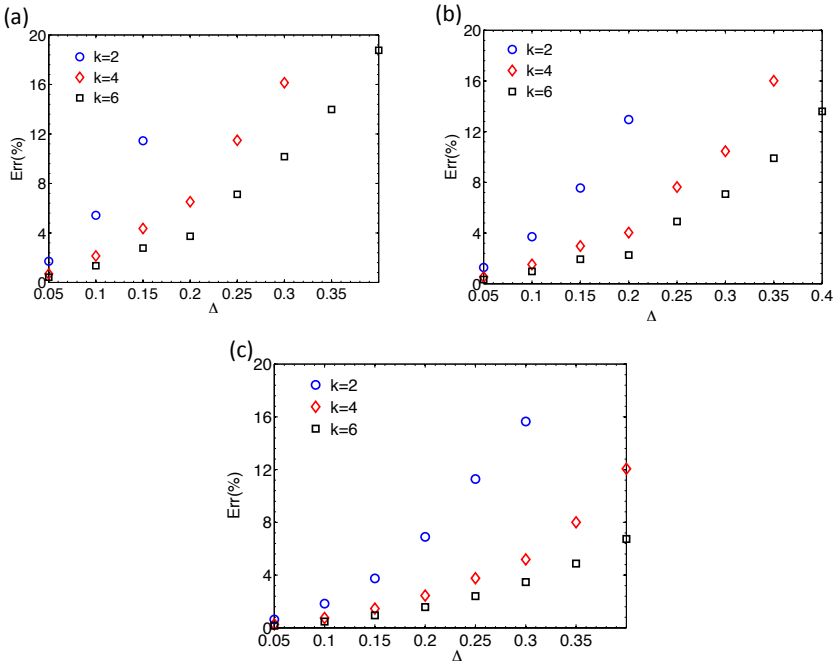

Figure D.2: Relative error made by their *first-order* approximations of ; (a) G_{A}^{∞}, (b) G_{m}^{∞}, and (c) K_{m}^{∞}.

For small values of the toughness contrast these quantities evolve exactly as their first-order approximations within some small error but as contrast increases the error made using first-order approximation starts to increase.

It can be noticed that a range of the toughness contrasts that validates the first-order approximation increases as value of k increases. This means that the more the material has irregular fracture properties, the more it responses linearly.

D.3 SIF along the obtained flower shape cracks

In addition to the propagation, the numerical code provides the values of the SIF along the flower shapes we obtain. We now discuss these values in corresponding to these shapes independently from any advance law. In order to do that we remove by linearity, the loading from the SIF and concentrate at functions $\widetilde{K}$ and $\widehat{K}$ defined by

$$K(\theta) = \frac{2}{\sqrt{\pi}}\sigma\sqrt{a}\widetilde{K}(\theta) = \frac{2}{\sqrt{\pi}}\sigma\sqrt{a_0}\widehat{K}(\theta), \tag{D.2}$$

so that $\widetilde{K} = 1$ if circular crack of radius a and $\widehat{K} = 1$ if circular crack of radius a_0. Both $\widetilde{K}$ and $\widehat{K}$ depend on θ, k, Δ and $\Delta a/a_0$ but not on the loading. Whereas $\widehat{K}$ depends on the shape and size of the crack, $\widetilde{K}$ depends only on its shape.

D.3.1 Regular propagation

Because of the evolution of front shape always attains a stationary regime in the case of regular propagation, we focus here on function $\widetilde{K}$.

As an example we have plotted in Fig. D.3, the evolution of the normalized $\widetilde{K}$ during crack propagation in the case of toughness map with $k = 4$ and $\Delta = 0.3$. Fig. D.3(a) shows the evolution along crack front as crack propagates, different colored curves are in corresponding to different positions of crack front shown in Fig. 7.3(a).

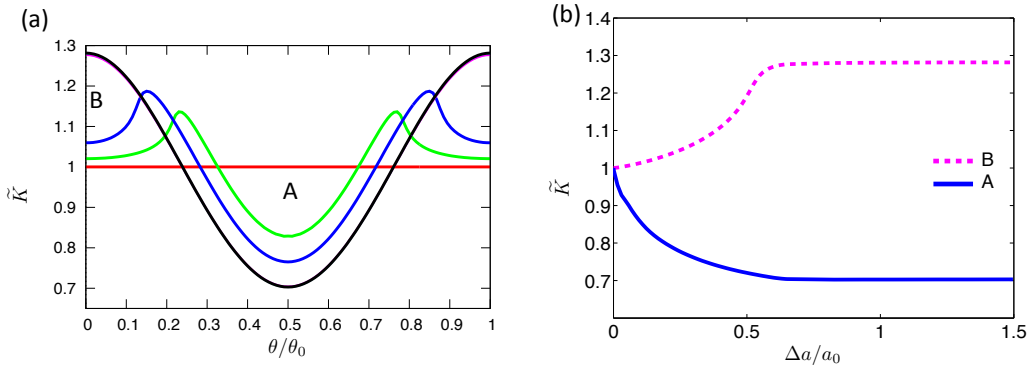

Figure D.3: Evolution of the normalized $\widetilde{K}$ during crack propagation in the case of $k = 4, \Delta = 0.3$; (a) distribution along crack front, and (b) evolution at weak point A and at tough point B with normalize amplitude $\Delta a/a_0$ of front deformation.

One shall notice that during transient regime, this quantity evolves with front deformations and then during stationary regime, it attains some stationary value which depends only on the front shape. For example, let's look at the evolution of this quantity at points A and B as a function of the normalized amplitude of the front deformations (Fig. D.3(b)). As described first-order approximation in section 7.2.2, at initial stage $\widetilde{K}(A)$ decreases while $\widetilde{K}(B)$ increases and then both attain plateau values.

Next step, we look at the dependency of these stationary values on the toughness map (k, Δ). Fig. D.4(a) shows $\widetilde{K}$ as function of θ/θ_0 for different values of k and a given value of Δ. One shall notice that, with such re-scaling, all curves are collapsing, without surprise since

$K = K_c$ everywhere, on one master curve which is independent of wave-number k and depends only on toughness contrast Δ. Fig. D.4(b) give these values for different values of Δ. Re-scale these curves in following way,

$$\mathcal{K}\left(\frac{\theta}{\theta_0}\right) = \frac{\widetilde{K}\left(\theta/\theta_0\right) - \widetilde{K}_m}{\Delta\widetilde{K}} \tag{D.3}$$

where $\widetilde{K}_m$ is the mean value of $\widetilde{K}$ defined by:

$$\widetilde{K}_m \equiv \frac{\widetilde{K}_{max} + \widetilde{K}_{min}}{2} \tag{D.4}$$

and $\Delta\widetilde{K}$ is the amplitude of $\widetilde{K}$ defined by:

$$\Delta\widetilde{K} \equiv \frac{\widetilde{K}_{max} - \widetilde{K}_{min}}{2}. \tag{D.5}$$

All normalized $\widetilde{K}$ curves are then collapsed in single master $\mathcal{K} - curve$, see Fig. D.5. This $\mathcal{K} - curve$ is independent of both toughness field parameters, wave-number k and toughness contrast Δ and it is found that this function follows a cosine function, *i.e.*,

$$\mathcal{K}(\theta) = \frac{1}{2}\cos\left(2\pi\frac{\theta}{\theta_0}\right) \ \forall k, \Delta, \Delta a^{\infty}/a. \tag{D.6}$$

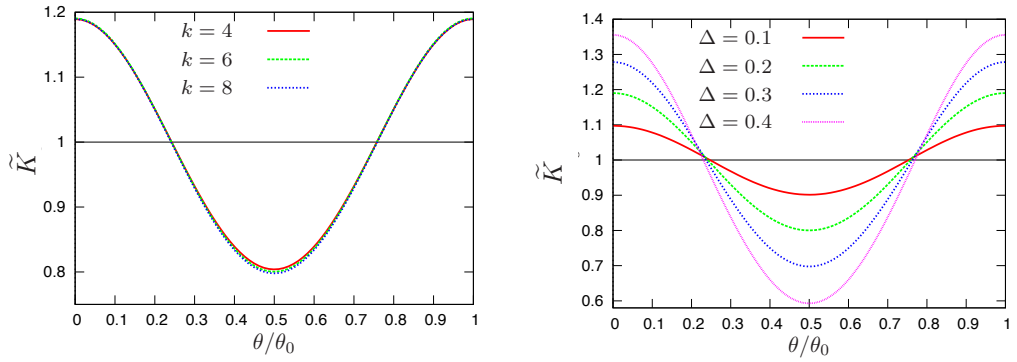

(a) $\widetilde{K}$ Vs θ/θ_0: Case $\Delta = 0.2$ (b) $\widetilde{K}$ Vs θ/θ_0: Case $k = 6$

Figure D.4: Local elastic field: Stationary regime

We verify that the value of $\Delta\widetilde{K}$ is given by:

$$\Delta\widetilde{K} \sim \Delta. \tag{D.7}$$

This results from $K = K_c$ everywhere. The value of $\widetilde{K}_m$ could however not be obtained from the criterion. It depends on the crack front shape and could only be obtained numerically. We show that it is independent of toughness map and is given by

$$\widetilde{K}_m = 1. \tag{D.8}$$

This value corresponds to the one of a circular crack of same area than the flower shape crack. This means that the average value of the SIF along our flower shape cracks is equal to the SIF of a circular crack of the same area. Is this a general property for any flower shape crack ? We will see in Appendix D.5 that it seems to be the case.

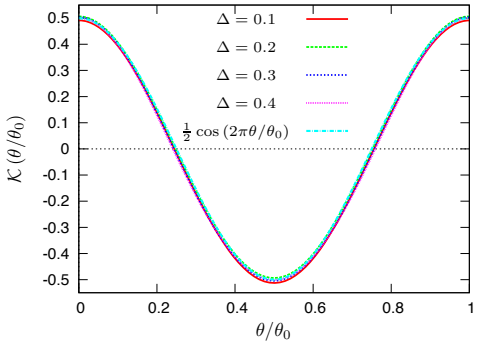

Figure D.5: Master curve for local elastic field in stationary regime

D.3.2 Irregular propagation

Fig. D.6 shows a typical distribution of dimensionless SIF $\widetilde{K}$ and $\widehat{K}$ along crack front. Different colored curves are in corresponding to different positions of crack front shown in Fig. 7.6(a). Fig. D.6(a) plots the distribution of $\widetilde{K}$ and Fig. D.6(b) plots the distribution of $\widehat{K}$. After some

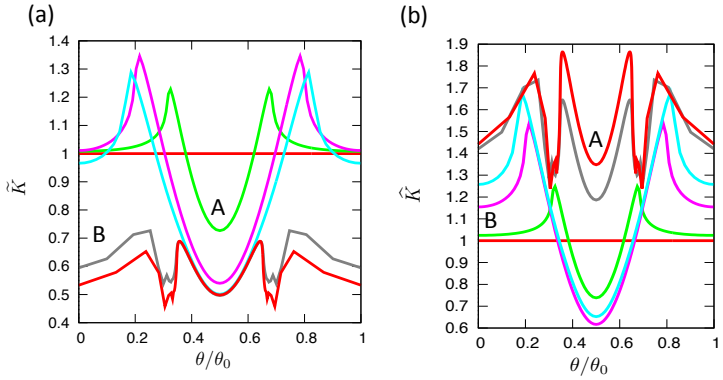

Figure D.6: Distribution of dimensionless SIF along crack front corresponding to different successive equlibrium positions of front in the case: $k = 4, \Delta = 0.6$; (a) $\widetilde{K}$ Vs θ/θ_0, (b) $\widehat{K}$ Vs θ/θ_0.

propagation, around point A, the distribution of $\widetilde{K}$ becomes invariant with propagation (last two curves, the red and grey are collapsed in a single curve). At point B, the distribution of $\widehat{K}$ becomes invariant with propagation (last two curves, coloured with the red and grey are collapsed).
Focus now at the evolution of $\widetilde{K}(A)$ at point A and $\widehat{K}(B)$ at point B as a function of normalized finger petal size $\Delta a/a_0$. As an example we have plotted in Fig. D.7, the evolution of these quantities in the case of toughness map with $k = 4$ and $\Delta = 0.6$. Fig. D.7(a) shows the evolution of $\widetilde{K}(A)$ and Fig. D.7(b) shows the evolution of $\widehat{K}(B)$. It can be noted that after a transient phase both $\widetilde{K}(A)$ and $\widehat{K}(B)$ attain some plateau values. Let denote these stationary values as $\widetilde{K}_A^\infty$ and $\widehat{K}_B^\infty$. They depend on (k, Δ) only.

Fig. D.8 shows $\widetilde{K}_A^\infty$ as a function of toughness contrast Δ for given toughness spatial re-

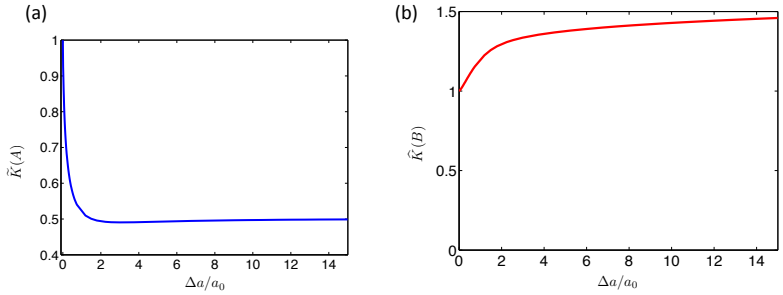

Figure D.7: Evolution of the normalized local SIF at points A and B during crack propagation in the case of $k = 4, \Delta = 0.6$; (a) evolution of $\widetilde{K}(A)$, and (b) evolution $\widehat{K}(B)$, with normalize amplitude $\Delta a/a_0$ of front deformation.

partition k. $\widetilde{K}_A^\infty$ decreases as toughness contrast Δ and toughness spatial re-partition k increase. Let us link this behaviour to the radius of local curvature around point A. Figs. D.9 (a) and

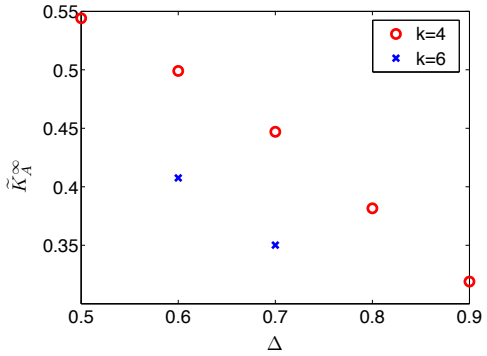

Figure D.8: Dependency of $\widetilde{K}_A^\infty$ on toughness map parameters (k, Δ).

(b) give the evolution of the shape $[a(\theta) - a_0]/a_0$ for values of k and Δ respectively. One can observe that the radius of curvature $R_c(A)$ around A decreases with k and Δ. To correlate this behaviour with the one of $\widetilde{K}_{\mathrm{A}}^\infty$ let us plot $\dfrac{\widetilde{K}_{\mathrm{A}}^\infty}{\sqrt{R_c(A)/a}}$ as a function of Δ (Fig. D.9 (c)). As Δ increases, the value of the SIF at point A becomes well approximated by the one of a circular crack of radius $R_c(A)$. One has $\widetilde{K}_{\mathrm{A}}^\infty \sim \sqrt{R_c(A)/a}$.

Similarly, Fig. D.10 plots the $\widehat{K}_B^\infty$ as a function of toughness contrast Δ for a given value of k. One shall notice that, $\widehat{K}_B^\infty$ converges to unity as contrast increases. This is linked to the fact that as toughness contrast increases more and more points around tough point B remain pinned and therefore the value of $\widehat{K}_B^\infty$ is dominated purely by the initial circular crack configuration even though very small part of front (around point A) has been broken and gone far away. Therefore, as contrast increases the evolution of the SIF around point B simply converges to the SIF corresponding to the circular crack with radius of a_0 (that is K_0). As a schematic representation of this explanation, Fig. D.11 shows front shapes around point B for different cases with contrast of 0.6, 0.8 and 0.9. It shall be seen that as contrast increases the front shape around the vicinity of point B converges to circular shape with size of a_0. To summarize, it

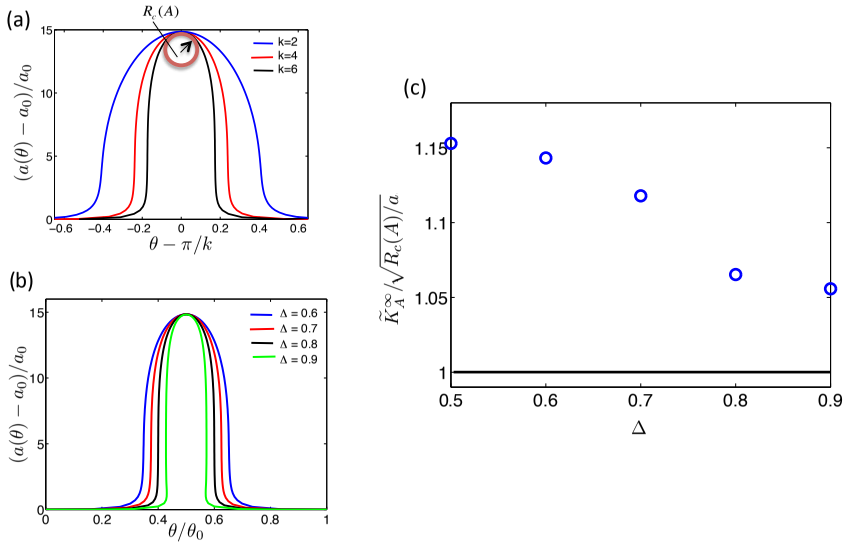

Figure D.9: Dependency of the local curvature around point A; (a) on toughness map parameter k for given Δ; (b) on toughness map parameter Δ for given k and (c) comparative ratio of $\widetilde{K}_A^{\infty}$ calculated numerically and from local curvature.

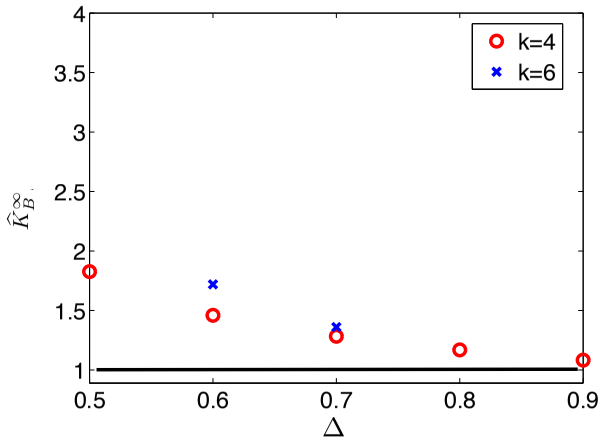

Figure D.10: Dependency of plateau value $\widehat{K}_B^{\infty}$ on toughness map parameters (k, Δ).

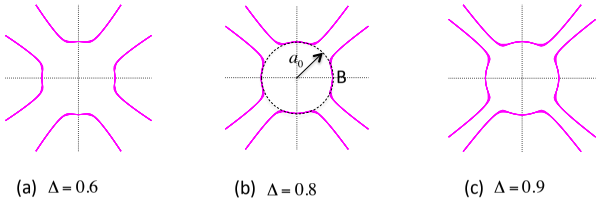

Figure D.11: Front shapes in vicinity of tough point B: $k = 4$

shall be noticed that at such large front perturbations, the local SIF at these points A and B depends on the whole shape of the front but approximate values can be found by considering the local curvatures :

- $\widetilde{K}(A) \sim \sqrt{\dfrac{R_c(A)}{a}} \Rightarrow K(A) \sim \dfrac{2}{\sqrt{\pi}}\sigma\sqrt{R_c(A)}.$
- $\widetilde{K}(B) \sim 1 \Rightarrow K(B) \sim \dfrac{2}{\sqrt{\pi}}\sigma\sqrt{a_0}.$

D.4 Numerical solutions for other values of k

D.4.1 Case $k = 1$

This is the special case of a toughness map for which, as remarked in §7.1 of main text, there is no solution to the equation $K = K_c$ along all the front except for $\Delta = 0$ (which is corresponding to the case of the crack propagating in a homogeneous media): The propagation is always irregular for any toughness contrast value other than zero ($\Delta > 0$). For instance, we have plotted the

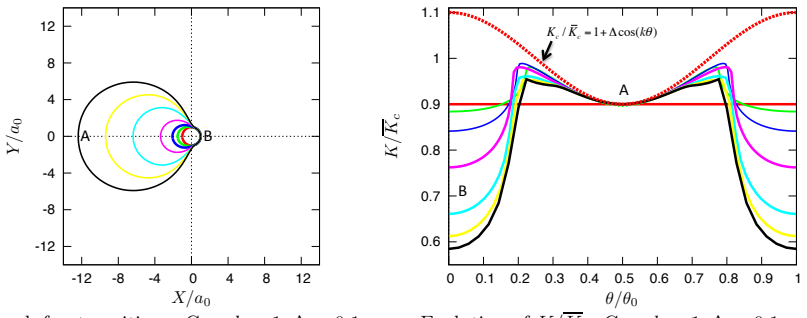

(a) Crack front positions: Case $k = 1, \Delta = 0.1$ (b) Evolution of $K/\overline{K_c}$: Case $k = 1, \Delta = 0.1$

Figure D.12: Evolution of local quantities in the special case of $k = 1$.

crack front position in Fig. D.12 (a) and corresponding evolution of $K/\overline{K}_c$ in Fig. D.12 (b) with tiny toughness contrast equal to 0.1. It shall be noticed that propagation is irregular: the crack advance only in the weakest zone.

D.4.2 Case $k = 2$

The results are similar to those commented in sections 7.2.2 and 7.2.3 of chapter 7 for cases $k = 4$ and $k = 6$. Figs. D.13 (a) and (c) are corresponding to a case of regular propagation ($\Delta = 0.1$) and Figs. D.13 (b) and (d) are corresponding to the case of irregular propagation ($\Delta = 0.4$).

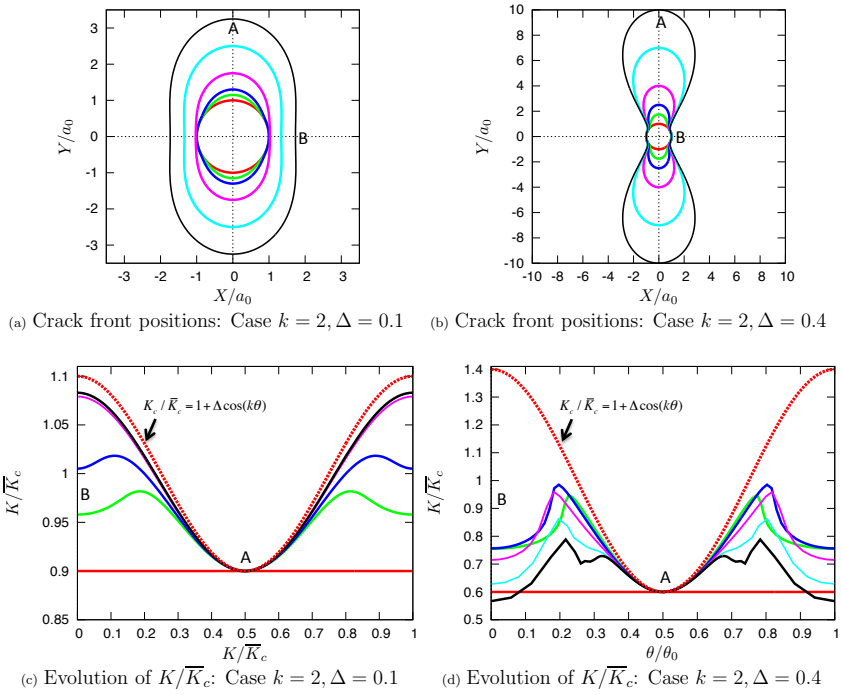

(a) Crack front positions: Case $k = 2, \Delta = 0.1$ (b) Crack front positions: Case $k = 2, \Delta = 0.4$

(c) Evolution of $K/\overline{K}_c$: Case $k = 2, \Delta = 0.1$ (d) Evolution of $K/\overline{K}_c$: Case $k = 2, \Delta = 0.4$

Figure D.13: Evolution of local quantities in the case of $k = 2$.

First, the front is pinned at the strongest part, so that SIF first increases there. In the regular case, it increases up to required threshold. But in the irregular case, it starts to decrease before, so that part of the crack front there remains pinned forever and fingering occurs.

D.5 Different examples of invariant toughness map along the propagation direction

As mentioned in Appendix D.3.1, aim of this appendix is to show how the master curves corresponding to stationary regime can be influenced by different map toughness configuration. As an example, here we study the following toughness map:

$$K_c(\theta) = \overline{K}_c \left[1 + \Delta \cos^3(k\theta)\right]. \tag{D.9}$$

For a typical results of this problem, Fig. D.14 plots the successive front positions and corresponding evolution of $K/\overline{K}_c$ for cases of $k = 2, \Delta = 0.15$ and $k = 4, \Delta = 0.25$. The discussion follows as commented previously for the case of regular propagation of previous toughness map. That is initial circular geometry of the crack front reaches some stationary shape after some transient zone. At this point the IrwinÕs criteria $K = K_c$ is, and further remains, verified all along the crack front as described by the evolution of the $K/\overline{K}_c$.

Next step is to study the influence of toughness map parameters on this stationary regime. Fig. D.15 plots the corresponding $\widetilde{K}$ along the crack front for different values of k and Δ. For given value of toughness contrast $\Delta = 0.15$, Fig. D.15 (a) shows the result for different values of $k = 2$ and 4. Again, it shall be noticed that, $\widetilde{K}$ is itself semi-master curve that is independent

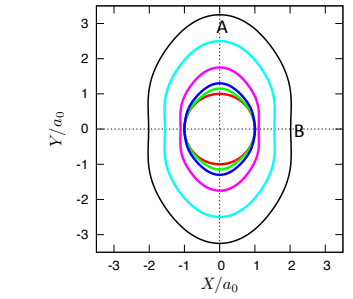

(a) Successive front position : $k = 2, \Delta = 0.15$

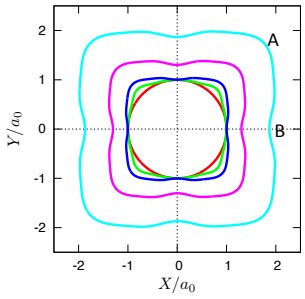

(b) Successive front position : $k = 4, \Delta = 0.25$

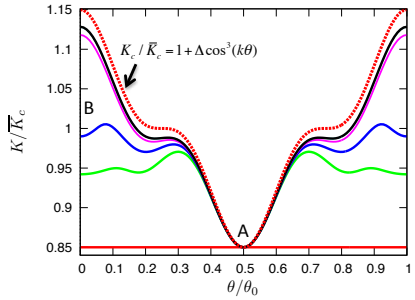

(c) Evolution of $K/\overline{K}_c$: $k = 2, \Delta = 0.15$

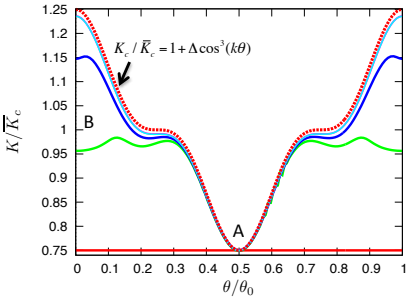

(d) Evolution of $K/\overline{K}_c$: $k = 4, \Delta = 0.25$

Figure D.14: Evolution of local quantities: Regular propagation.

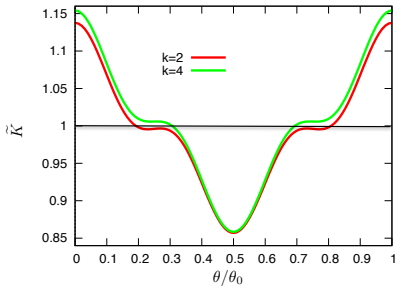

(a) Case : $\Delta = 0.15$

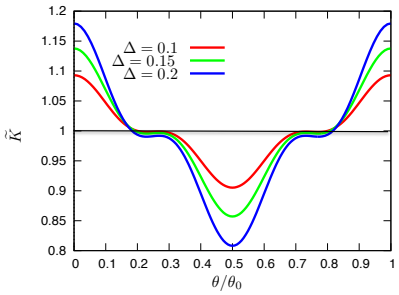

(b) Case: $k = 2$

Figure D.15: Local elastic field during stationary regime.

of k. Now, for given value of $k = 2$, Fig. D.15 (b) shows the result for different values of $\Delta = 0.1, 0.15$ and 0.2. Following same procedure as described in §D.3.1 one gets a master curve that presented in Fig. D.16 and follows, as awaited, a cubic of cosine, *i.e.*

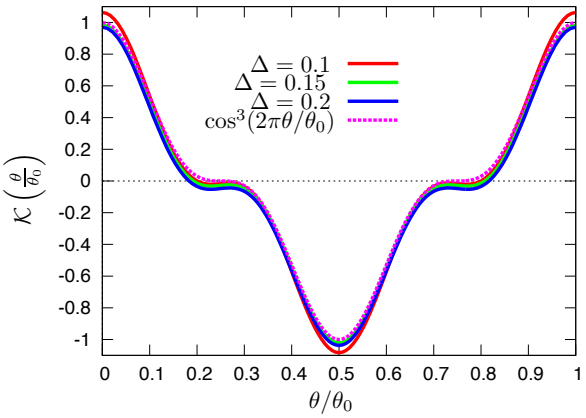

Figure D.16: Master curve for local elastic field during stationary regime.

$$\mathcal{K}(\theta) = \cos^3\left(2\pi\frac{\theta}{\theta_0}\right) \ \forall k, \Delta, \Delta a^\infty/a, \tag{D.10}$$

with $\Delta\widetilde{K} \sim \Delta$. Here as before, we find again

$$\widetilde{K}_m = 1 \tag{D.11}$$

which implies that $K_{\text{eff}} = \overline{K}_c$. With remotely loaded circular crack, Does this remain true for any invariant toughness map along the propagation direction is however still an open question? For sure for other loading conditions, it doesn't remain true as we have shown that for half-plane cracks, even for invariant toughness map along the propagation direction, $K_{\text{eff}} \neq \overline{K}_c$ as soon as $\mathrm{d}K^0/\mathrm{d}a < 0$ (refer §3.5).

Bibliography

Adda-Bedia M., Katzav E., Vandembroucq D. (2006). Second-order variation in elastic fields of a tensile planar crack with a curved front. *Phys. Rev. E*, 73, 035106.

Barenblatt G.I. (1962). The mathematical theory of equilibrium cracks in brittle fracture. *Adv. Appl. Mech.*, 7, 55-129.

Bonamy D. (2009). Intermittency and roughening in the failure of brittle heterogeneous materials. *J. Phys. D: Appl. Phys.*, 42, 214014.

Bonamy D., Bouchaud E. (2011). Failure of heterogeneous materials: a dynamic phase transition? *Phys. Reports*, 498, 1-44.

Bonamy D., Santucci S., Ponson L. (2008). Cracking dynamics in material failure as the signature of a self-organized dynamic phase transition. *Phys. Rev. Lett.*, 101, 045501.

Bower A. F., Ortiz M. (1990). Solution of three-dimensional crack problems by a finite perturbation method. *J. Mech. Phys. Solids*, 38, 443-480.

Bower A-F., Ortiz M. (1991). A three-dimensional analysis of crack trapping and bridging by tough particles. *J. Mech. Phys. Solids*, 39, 815-858.

Budzik M.K., Jumel J., Shanahan M. E. R. (2013). Adhesive fracture of heterogeneous interfaces. *Philos. Mag.*, 93:19, 2413-2427.

Bueckner H.F. (1970). A novel principle for the computation of stress intensity factors. *Zeitschrift für Angewandte Mathematik und Mechanik*, 50 (9), 529-546.

Cherepanov C.P. (1967). Crack propagation in continous media. *Appl. Math. Mech.*, 31, 476-488.

Chopin J. (2010). *Statique et dynamique d'un front de fissure en milieu hétérogène*. Ph.D. Thesis, Université Pierre et Marie Curie (Paris VI), France (in French).

Chopin J., Prevost A., Boudaoud A., Adda-Bedia M. (2011). Crack front dynamics across a single heterogeneity. *Phys. Rev. Lett.*, 107, 144301.

Daguier P., Bouchaud E., Lapasset G. (1995). Roughness of a crack front pinned by microstructural obstacles. *Euro. phys. Lett.*, 31, 367-372.

Dalmas D., Barthel E., Vandembroucq D. (2009). Crack front pinning by design in planar heterogeneous interfaces. *J. Mech. Phys. Solids*, 57, 446-457.

Dalmas D., Lelarge A., Vandembroucq D. (2008). Crack propagation through phase- separated glasses: effect of the characteristic size of disorder. *Phys. Rev. Lett.*, 101, 255501.

Delaplace A., Schmittbuhl J., Maloy K.J. (1999). High resolution description of a crack front in a heterogeneous plexiglas block. *Phys. Rev. E*, 60, 1337-1343.

Demery V., Rosso A., Ponson L. (2014). From microstructural features to effective toughness in disordered brittle solids. *Euro. phys. Lett.*, 105, 34003.

Destuynder P., Djaoua M. (1981). Sur une interprétation mathématique de lÕintégrale de rice en théorie de la rupture fragile. *Math. Methods Appl. Sci.*, 3, 70-87.

Davidge R.W., Tappin G. (1968).The effective surface energy of brittle materials. *J. Mat. Sci.*, 3:pp.165-173.

Favier E., Lazarus V., Leblond J.-B. (2006). Coplanar propagation paths of 3D cracks in infinite bodies loaded in shear. *Int. J. Solids Struct.*, 43 (7-8), 2091-2109.

Gao H., Rice J.R. (1989). A first-order perturbation analysis of crack trapping by arrays of obstacles. *ASME J. Appl. Mech.*, 56, 828-836.

Gao H., Rice J.R. (1987). Somewhat circular crack. *Int. J. Frac.*, 33:155-174.

Gao H., Rice J.R. (1986). Shear stress intensity factors for planar crack with slightly curved front. *ASME J. Appl. Mech.*, 53 (4), 774-778.

Gleizer A., Sherman D. (2014). The cleavage energy at initiation of (110) silicon. *Int. J. Frac.*, 187:1-14.

Gradshteyn I.S., Ryzhik I.M. (1980). *Table of Integrals, Series, and Products*, Academic Press.

Griffith A.A. (1920). The phenomena of rupture and flow in solids. *Phil. Trans. Roy. Soc. Lond.*, A221, 163-198.

Hartman P. J.(1980). The attachment energy as a habit controlling factor III. Application to corundum. *J. Cryst. Growth.*, 49, p. 166.

Hossain M.Z., Hsueh C.-J., Bourdin B., Bhattacharya K. (2014). Effective toughness of heterogeneous media. *J. Mech. Phys. Solids*, 71:15-32.

Inglis C. E. (1913). Stresses in a plate due to the presence of cracks and sharp corners. *Trans. Inst. Naval Arch.*, 55, 219-239.

Irwin G.R. (1957). Analysis of stresses and strain near the end of a crack traversing a plate. *ASME J. Appl. Mech.*, 24(3), 361-364; (1958) "Discussion". *ASME J. Appl. Mech.*, 25(2), 299-303.

Katzav E., Adda-Bedia M., Ben Amar M., Boudaoud A. (2007). Roughness of moving elastic lines: crack and wetting fronts. *Phys. Rev. E*, 76, 051601.

Kendall K., 1973. Thin film peeling-elastic term. *J. Phys. D*, 8, 105-117.

Lawn B. (1993). Fracture of brittle solids. *Cambridge University.*

Lazarus V. (2003). Brittle fracture and fatigue propagation paths of 3D plane cracks under uniform remote tensile loading. *Int. J. Frac.*, 122(1-2):23-46.

Lazarus V. (2011) Perturbation approaches of a planar crack in linear elastic fracture mechanics: a review. *J. Mech. Phys. Solids*, 59(2),121-144.

Lazarus V., Leblond J.-B. (2002). In-plane perturbation of the tunnel-crack under shear loading. I: bifurcation and stability of the straight configuration of the front. *Int. J. Solids Struct.*, 39 (17), 4421-4436.

Lazarus V., Leblond J.-B. (1998). Three-dimensional crack-face weight functions for the semi-infinite interface crack. I. Variation of the stress intensity factors due to some small perturbation of the crack front. *J. Mech. Phys. sol.*, 46 (3), 489-511.

Leblond J.-B., Lazarus V., Mouchrif S.-E. (1999). Crack paths in three-dimensional elastic solids. II. Three-term expansion of the stress intensity factors - Aapplications and perspectives. *Int. J. Solids Struct.*, 36 (1), 105-142.

Leblond J-B., Patinet S., Frelat J., and Lazarus V. (2012). Second-order coplanar perturbation of a semi-infinite crack in an infinite body. *Eng. Frac. Mech.*, 90: 129-142.

Leblond J.-B., Mouchrif S.-E., Perrin G. (1996). The tensile tunnel-crack with a slightly wavy front. *Int. J. Solids Struct.*, 33 (14),1995-2022.

Legrand L., Patinet S., Leblond J.B., Frelat J., Lazarus V. and Vandembroucq D. (2011). Coplanar perturbation of a crack lying on the mid-plane of a plate. *Int. J. Frac.*, 170, 67-82.

Li X., Keer L.M. (1992). The growth of pressurised planar cracks between barriers. *Int. J. Solids Struct.*, 29(1): 27-39.

Marder M., Fineberg J. (1996). How things break. *Physics today*, 49, 24-29.

Mower T. M., Argon A. S.(1995). Experimental investigations of crack trap- ping in britlle heterogeneous solids. *Mech. Mater.*, 19, 343Ð364.

Nemat-Nasser S., Hori M. (1999). Micromechanics: Overall Properties of Heterogeneous Materials. *Elsevier Science*, North-Holland, The Netherlands.

Orowan E. (1955). Energy criteria of fracture. *Weld J. Res. Suppl.*, 30:157-160.

Patinet S., Alzate L., Barthel E., Dalmas D., Vandembroucq D., Lazarus V. (2013.) Finite size effects on crack front pinning at heterogeneous planar interfaces: Experimental, finite elements and perturbation approaches. *J. Mech. Phys. Solids*, 61:311-324.

Patinet S., Vandembroucq D., Roux S. (2103). Quantitative prediction of effective toughness at random heterogeneous interface. *Phys. Rev. Lett.*, 110, 165507.

Pérez R., Gumbsch P. (2000). An ab initio study of the cleavage anisotropy in silicon. *Acta. Mater.*, 48:4517-4530.

Ponson L., Bonamy D. (2010). Crack propagation in brittle heterogeneous solids: material disorder and crack dynamics. *Int. J. Frac.*, 162, 21-31.

Ponson L. et al. Effect of peeling angle on the adhesion of heterogeneous thin films. *submitted to J. Mech. Phys. Solids.*

Rice J.R. (1968). A path independent integral and the approximate analysis of strain concentrations by notches and cracks. *ASME J. Appl. Mech.*, 35, 379-386.

Rice J.R. (1972). Some remarks on elastic crack-tip stress fields. *Int. J. Solids Struct.*, 8(6), 751-758.

Rice J.R. (1985). First-order variation in elastic fields due to variation in location of a planar crack front. *ASME J. Appl. Mech.*, 52, 571-579.

Rice J.R. (1989). Weight function theory for three-dimensional elastic crack analysis. In R. P. Wei and R. P. Gangloff, editors, *Fracture Mechanics : Perspectives and Directions (Twentieth Symposium)*, pages 29-57, Philadelphia, USA, American Society for Testing and Materials STP 1020.

Rivlin R. S., 1944. The effective work of adhesion. *Paint Technol.*, 9, 215-218.

Roux S., Vandembroucq D., Hild F. (2003). Effective toughness of heterogeneous brittle materials. *Euro. J. Mech. A / Solids*, 22(5):743-749.

Santucci S., Grob M., Toussaint R., Schmittbuhl J., Hansen A., Maloy K.J. (2010). Fracture roughness scaling: A case study on planar cracks. *Euro. phys. Lett.*, 92, 44001.

Schmittbuhl J., Roux S., Vilotte J.P., Maloy K.J. (1995). Interfacial crack pinning: effect of nonlocal interactions. *Phys. Rev. Lett.*, 74, 1787-1790.

Schmittbuhl J., Delaplace A., Maloy K.J., Perfettini H., Vilotte J.P. (2003). Slow crack propagation and slip correlations. *Pure Appl. Geophys.*, 160, 961-976.

Schmittbuhl J., Maloy K. J. (1997). Direct observation of a self-affine crack propagation. *Phys. Rev. Lett.*, 78, 3888-3891.

Vasoya M., Leblond J-B., Ponson L. (2013). A geometrically-nonlinear analysis of coplanar crack propagation in some heterogeneous medium. *Int. J. Solids Struct.*, 50: 371-378.

Vasoya M., Unni A.B., Leblond J-B., Lazarus V., Ponson L (2014). Finite size and geometrical non-linear effects during crack pinning by heterogeneities: An analytical and experimental study. *Submitted to J. Mech. Phy. Solids.*

Vinci L. D. (1940). I libri di Meccanica. Hoepli, Milano.

Weibull A (1939). Statistical theory of the strength of materials. *Proc. Roy. Swed. Inst. Eng. Res.*, 151, 1-45.

Westergaard H.M. (1939). Bearing pressures an cracks. *ASME. J. Appl. Mech.*, 6 (2):49-53.

Willis J.R. (2013). Crack front perturbations revisited. *Int. J. Frac.*, 184(1-2):17-24.

Xia S., Ponson L., Ravichandran G., Bhattacharya K. (2012). Toughening and asymmetry in peeling of heterogeneous adhesives. *Phys. Rev. Lett.*, 108, 196101.

Xia S., Ponson L., Ravichandran G., Bhattacharya K. (2011). Adhesive tape with adhesion enhancement and directionality by structural and adhesive heterogeneity. *International patent* 079322 and US patent 0159241.

Xia S., Ponson L., Ravichandran G., Bhattacharya K. (*in preparation*). Adhesion of heterogeneous thin films: II. Adhesive heterogeneity.

Yarema S. Y. (1995). On the contribution of G.R. Irwin to fracture mechanics. History of fracture mechanics. *Mat. science*, 31(5).

Résumé

Le développement d'outils prédictifs qui relient l'échelle microscopique à l'échelle macroscopique dans le cadre de la rupture fragile est le défi majeur de cette thèse. Dans le cas d'une fissure plane se propageant de façon quasistatique, en mode I, dans un matériau faiblement hétérogène et invariant dans la direction de propagation, on peut montrer à l'aide d'une approche perturbative utilisant les fonctions de poids, que le seuil de rupture de Griffith est toujours atteint en tout point du front et que par conséquent la ténacité effective est simplement égale à la moyenne des valeurs locales.

Nous abordons ici le même problème mais avec des hétérogénéités de ténacité plus élevées. Dans la première partie, nous considérons une fissure semi-infinie dans un corps infini ou dans une plaque d'épaisseur finie et nous étendons analytiquement l'approche du premier au second ordre. Nous montrons que, même si le critère de Griffith est atteint partout, les déformations du front peuvent induire une déviation de la ténacité efficace de sa valeur moyenne. Nous effectuons de plus des expériences de peeling afin de préciser le domaine de validité des approches.

Dans la deuxième partie, nous considérons une fissure circulaire se propageant dans un motif de ténacité invariant dans la direction de propagation, et résolvons le problème numériquement, quelquesoit le contraste de ténacité et la taille des hétérogénéités, en itérant sur les formules du premier ordre. Pour un contraste d'hétérogénéité suffisamment grand, le critère de la Griffith ne peut plus être atteint partout: certains points du front sont piégés par les zones plus tenaces, tandis que d'autres parties avancent indéfiniment. De ce fait, la ténacité diminue avec la taille et le contraste, à partir de sa valeur moyenne locale jusqu'à son minimum.

Mots-clés: Rupture fragile; Fissure plane en tension; Champ de ténacité hétérogène; Propriétés effectives de rupture; Approche perturbative; Piégeage d'une fissure; Instabilité de forme.

Abstract

The development of predictive tools that bridge microscopic to macroscopic scales in brittle fracture is the key challenge of this thesis.

In the context of quasi-static planar crack propagation under mode I loading, it has been shown, using first-order weight-function perturbation approaches that, for weak heterogeneities, when the material is homogeneous in the propagation direction, the Griffith's threshold is always reached for all points of the crack front so that the effective toughness is simply equal to the average of the local toughness.

Here, we address the same problem but with stronger toughness heterogeneities. In the first part, we consider a half-plane crack embedded in an infinite body or in a finite thickness plate and we extend analytically the first-order approaches to the second-order. We show that even if Griffith's criterion is reached all over the front, the deformations of the front may induce some second-order deviation of the effective toughness from its mean value. We also perform peeling experiments that define their range of applicability.

In the second part, we consider a circular crack propagating in an invariant toughness map along the propagation direction and solved the problem numerically, for any toughness contrast and heterogeneity size, by iterating the first-order formulas. For large enough heterogeneity contrast, the Griffith's criterion can no more be reached everywhere: some points of the front are pinned by strong impurities, while some other parts advances continuously. Correspondingly, the effective toughness is shown to decrease with size and strength of heterogeneity from the average value of the local toughness down to its minimum one.

Keywords: Brittle fracture; Tensile planar crack; Heterogeneous toughness field; Effective failure properties; Perturbation method; Crack pinning; Shape instability.